Molecular Characterization of the Olivocochlear Efferent System

HARVARD UNIVERSITY
Graduate School of Arts and Sciences

DISSERTATION ACCEPTANCE CERTIFICATE

The undersigned, appointed by the

Department of the Division of Medical Sciences

have examined a dissertation entitled

Molecular Characterization of the Olivocochlear Efferent System

presented by Michelle M. Frank

candidate for the degree of Doctor of Philosophy and hereby certify that it is worthy of acceptance.

Signature David Ginty Digitally signed by David Ginty DN: cn=David Ginty, o, ou, email=david_ginty@hms.harvard.edu, c=US Date: 2020.07.27 16:03:03 -05'00'

Typed name: Prof. David Ginty

Signature Stephen Liberles Stephen Liberles (Aug 13, 2020 09:34 EDT)

Typed name: Prof. Stephen Liberles

Signature _____

Typed name: Prof. Gordon Fishell

Signature Amanda M Lauer Amanda M Lauer (Aug 13, 2020 09:06 EDT)

Typed name: Prof. Amanda Lauer

Signature _____

Typed name: Prof.

Date: July 27, 2020

Molecular Characterization of the Olivocochlear Efferent System

A dissertation presented

by

Michelle M. Frank

to

The Division of Medical Sciences

in partial fulfillment of the requirements

for the degree of

Doctor of Philosophy

in the subject of

Neurobiology

Harvard University

Cambridge, Massachusetts

July 2020

Dissertation advisor: Lisa V. Goodrich Michelle M. Frank

Molecular Characterization of the Olivocochlear Efferent System

Abstract

Our sense of hearing relies on connections between diverse cell types to process acoustic information and guide behaviors. Incoming sounds are transduced by hair cells in the cochlea and transmitted into the brain by spiral ganglion neurons (SGNs). In turn, feedback circuits modulate this auditory information at every level of sensory processing, including the sensory periphery. In particular, the olivocochlear neurons (OCNs) send projections from the auditory brainstem into the ear, synapsing onto both hair cells and SGNs. These enigmatic cells have been implicated in numerous aspects of auditory processing, including attentional modulation, separating speech sounds from background noise, and protecting the cochlea from damage. Mammalian OCNs are typically classified into medial (MOC) and lateral (LOC) components, with MOCs projecting to hair cells and LOCs targeting SGNs. However, a robust understanding of the development and function of these cells has long been hampered by a lack of genetic access and poorly understood heterogeneity among OCNs.

We used high-throughput, single-nucleus sequencing to profile the transcriptomes of individual brainstem neurons from neonatal and mature animals. There are two main clusters of OCNs at each timepoint, corresponding to MOC and LOC neurons. OCN subtypes differ in their expression of guidance and adhesion molecules, ion channels, and neurotransmitters, providing insights into the distinct ways that MOCs and LOCs are integrated into auditory circuitry. Although many of these differences are present neonatally and persist into adulthood, other OCN attributes emerge during the course of postnatal development, as the expression of ion channels, receptors, and neurotransmitters all vary between neonatal and mature cells. In addition, I identified a subset of LOCs that express the neuropeptides Npy, CGRP-II, and Ucn. Peptidergic and non-peptidergic

LOCs also differ in their expression of the cell adhesion factor *Tenm3*, suggesting that they may have distinct targets. In order to investigate OCNs in even greater detail, I generated *Gata3-FlpO* and *Ucn-Cre* mouse lines, which together provide an intersectional strategy for manipulating LOC neurons without affecting MOCs. Collectively, this work addresses longstanding questions about how coordinated networks of feedforward and feedback cells develop and interact to influence sensory processing.

Table of Contents

List of Figures

List of Tables

Acknowledgements

"To speak in popular terms about a subject that has been dealt with largely in learned discourse, we might compare scientific facts to frozen fish."

— Bruno Latour, *We Have Never Been Modern*

"I call for the rest of my collection to join us. The whole rout. They will come. I am certain of it. I just need to be patient. They are snails. And it will, as everything does, take forever."

— Sabrina Orah Mark, *Wild Milk*

Over the years, various thinkers have proposed an array of metaphors to describe the practice of science. Science is a community, a trading zone, an assemblage; it is a borderland, or, perhaps, a frozen fish. Over the course of graduate school, however, doing science often felt like nothing so much as herding a large pack of very slow, very unruly snails: nothing ever works out quite the way you expect, and everything always seems to take longer than it should. Yet in spite of the many uncertainties, I could not have asked for a more rewarding topic to study during my PhD, and I am extremely grateful to the many people who helped bring this research to fruition.

The work I describe here would not have been possible without contributions from many other scientists and fellow snail-herders, all of whom helped push me and this project forward. The Goodrich Lab has been a scientific haven, in which every member is always eager to share advice, support, and—in the pre-pandemic era—artfully decorated baked goods. Lisa Goodrich constantly encouraged me to pursue whichever research questions inspired me, no matter how impossible the experiments may have seemed. I constantly aspire to match her high standards for both science and mentorship.

I could not have asked for a better bay mate than Andrea Yung, who not only taught me most of what I know about mouse work and molecular biology, but also delivered Cornish pasties

and cookies on demand. Chester Chia's discerning taste raised my standards for microscopy, travel, and shoes. Austen Sitko and I have sufficiently synergized that we can now communicate with only animal gifs and stickers—I could ask for nothing more in a collaborator, and this project is deeply indebted to her contributions. The entire Program in Neuroscience and Department of Neurobiology provided an ambitious and supportive environment for all of this work, and I'm grateful to the many people in the department who provided me with encouragement, advice, and protocols. Early in this project, Kee Wui Huang and Minsuk Hyun went above and beyond in helping me establish a working sequencing pipeline for cells in the auditory brainstem.

It was a joy to work with my collaborators on Team SOC, Benedikt Grothe, Mike Myoga, and Wenjun Yan, and to begin tackling efferent physiology with Kiera Grierson. I'm also very grateful to Catherine Weisz and the members of her group—Sian Kitcher, Lester Torres Cadenas, and Matt Fischl—for welcoming me into their lab, feeding me chocolate, and helping me to think about the efferent system from a different perspective.

Austen Sitko, Mackenzie Hunt, Cheuk Wong, and Sarah Yoder performed several of the experiments presented here. Andrea Yung and Noah Druckenbrod provided diagrams and images for figures. Sandy Nandagopal and Natasha O'Brown provided sequences for several HCR probes, as well as valuable suggestions for *in situ* protocols. Austen Sitko, Noah Druckenbrod, Donna Fekete, and Chris Brown offered insightful feedback on sections of this manuscript. Susan Dymecki, Gord Fishell, David Ginty, and Michael Greenberg provided mouse lines. Bernardo Sabatini provided equipment for single-cell collections using 10x Genomics. I am thankful for the staff at Harvard's many core facilities: the Genome Modification Facility, Immunology Flow Cytometry Core, Neurobiology Imaging Facility, Biopolymers Facility, and Bauer Core all contributed to this work. Many thanks to Susan Dymecki, David Ginty, and Charlie Liberman for all of the useful feedback they provided as my dissertation advisory committee and to Gord Fishell, David Ginty, Amanda Lauer, and Stephen Liberles for serving on my dissertation examination committee. This work was supported by 5R01DC015974 from the NIDCD.

CHAPTER ONE

Introduction

This chapter was previously published in a modified form in *Wiley Interdiscip Rev Dev Biol*. 2018 Nov; 7(6):e324. doi: 10.1002/wdev.324. Reproduced with permission. Andrea Yung and Noah Druckenbrod provided diagrams and images for the figures.

The auditory system connects animals to their external environments in myriad ways: it allows them to locate and identify sounds, to communicate with other organisms, and to do all of this even amidst a jumble of background noises. To perform these complex tasks, animals rely on precisely wired and tuned auditory circuitry. As in other sensory systems, sound is detected by highly specialized receptor neurons in the peripheral nervous system (PNS) and then encoded in the activity of primary sensory neurons that project into the central nervous system (CNS). However, whereas visual signals are processed extensively in the retina before being transmitted to the thalamus, the bulk of early auditory processing occurs instead in the brainstem. Moreover, within the auditory brainstem is housed a small but crucial population of neurons that project back to the cochlea, establishing a route for efferent feedback that both protects sensory cells from damage and directly tunes afferent activity. The formation of these reciprocal connections between the CNS and the PNS presents some unusual developmental challenges, including specification and generation of diverse types of efferent neurons, navigation of efferent axons through and out of the brainstem, and alignment with the afferent connections forming in the cochlea. The function of these feedback projections offers a separate puzzle, as direct efferent modulation at the level of sensory receptors or primary sensory neurons is virtually unheard of in other sensory systems. Work over the past several decades has offered crucial insights into many of these problems, although research has long been hampered by a limited knowledge of differences between efferent cell types and a lack of genetic tools to label or manipulate these neuronal populations.

OVERVIEW OF AFFERENT AND EFFERENT ORGANIZATION

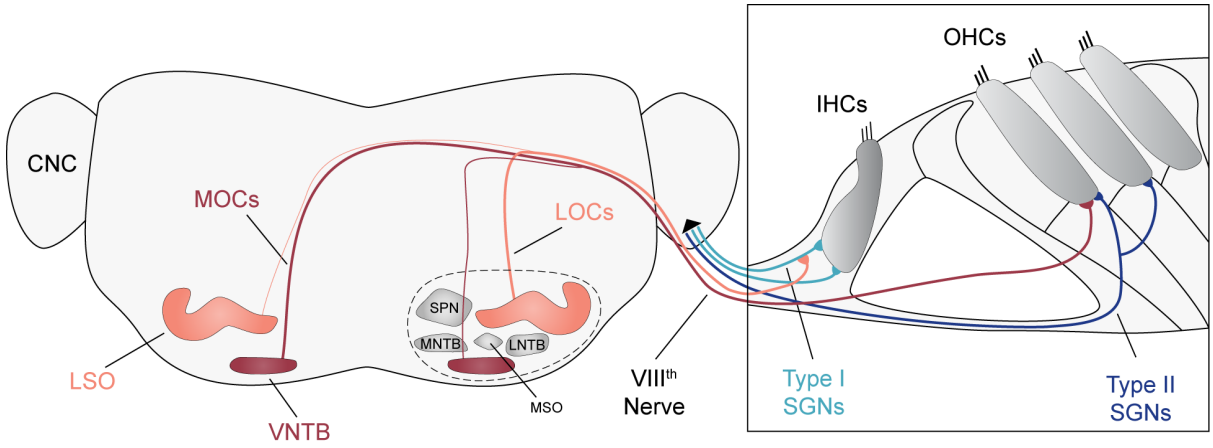

Figure 1.1. Organization of the mammalian olivocochlear efferent system. Auditory information transduced by inner (IHCs) and outer hair cells (OHCs) is conveyed to the auditory brainstem via Type I and Type II spiral ganglion neurons (SGNs), respectively. SGNs project into the brain via the VIIIth nerve and synapse onto neurons in the cochlear nuclear complex (CNC). The superior olivary complex (SOC, dashed circle) contains multiple nuclei involved in sound localization, including the medial superior olive (MSO), lateral superior olive (LSO), ventral nucleus of the trapezoid body (VNTB), lateral nucleus of the trapezoid body (LNTB), medial nucleus of the trapezoid body (MNTB), and the superior periolivary nucleus (SPN). Medial (MOCs) and lateral (LOCs) olivocochlear neurons reside primarily in VNTB and LSO, respectively, and project back to the sensory epithelium via the VIIIth nerve. Other types of neurons are also housed in VNTB and LSO, including neurons that mediate afferent responses, but only MOCs and LOCs are indicated for simplicity. Within the cochlea, LOCs form synapses with Type I SGNs, whereas MOCs terminate on OHCs.

In mammals, incoming sounds are transduced by hair cells in the cochlea and transmitted to the brainstem via spiral ganglion neurons (SGNs) (**Figure 1.1**). SGNs are divided into two primary groups: Type I SGNs, which receive synaptic signals from inner hair cells (IHCs), and Type II SGNs, which connect with outer hair cells (OHCs). The IHCs and Type I SGNs are almost

certainly the primary carriers of perceptual auditory information, while the OHCs control cochlear gain. Although their precise function remains unclear, Type II SGNs are proposed to convey information about damage and pain[1,2]. Hair cells and SGNs are organized tonotopically along the axis of the cochlea, from high characteristic frequencies in the base to low characteristic frequencies in the apex. All SGNs maintain this tonotopic organization as they extend their central axons into the VIIIth cranial nerve[3–5].

The central projections of auditory nerve fibers terminate within the cochlear nucleus complex (CNC), a collection of nuclei on the dorsal surface of the brainstem, tucked beneath the cerebellum (**Figure 1.1**). The CNC contains a number of distinct cell types that differ in their morphology, responses to sound, projections, and functions[6]. Globular bushy cells provide a major source of output from the CNC, crossing the midline and terminating within the contralateral medial nucleus of the trapezoid body (MNTB). Spherical bushy cells, on the other hand, innervate the lateral and medial superior olives (LSO, MSO), which contain principal neurons that integrate information from both ears, enabling sound localization in the horizontal plane[6–8]. These nuclei reside in the superior olivary complex (SOC), a large collection of nuclei devoted to auditory processing that sits just dorsal to the trapezoid body in the pons. Additionally, some neurons of the CNC project directly to the inferior colliculus (IC), where their information is integrated with ascending projections from the SOC[6]. At each level, nuclei are tonotopically organized[3].

In addition to this feedforward, afferent pathway, normal hearing also relies on feedback circuits present at every level of auditory processing. At the most peripheral level, a small population of efferent neurons project from the auditory brainstem back into the cochlea to modulate both hair cells and SGNs[9]. The cell bodies of these olivocochlear neurons (OCNs) reside in the SOC, amidst circuitry required for early auditory processing and sound localization[10,11]. Collectively, the OCNs help to protect the ear against acoustic trauma[12–16], separate speech sounds from background noise[17,18], and may balance inter-aural differences[19–23].

Like the hair cells and SGNs, mammalian OCNs are divided into two main subtypes, a medial and a lateral component, based on the positions of their somata in the SOC[24,25]. Medial olivocochlear neurons (MOCs) send both ipsilateral and contralateral projections to OHCs, while lateral olivocochlear neurons (LOCs) project predominantly ipsilaterally to innervate Type I SGN terminals near the base of IHCs[24]. This general architecture is widely preserved across the mammalian class, although the precise location of efferent somata, the overall number of efferents, and the ratio of MOC to LOC neurons vary across species[26,27]. In mice, MOC cell bodies reside mainly in the ventral nucleus of the trapezoid body (VNTB), whereas LOC neurons are found in and around the lateral superior olive (LSO). Both MOC and LOC neurons are intermingled with neurons that mediate afferent responses[27]. Like the other auditory brainstem nuclei, LOCs are tonotopically organized in the LSO, with high frequencies represented medially and low frequencies more laterally[28–31].

MOC neurons represent a relatively uniform population of neurons that act primarily to dampen cochlear activity via inhibitory, cholinergic synapses onto OHCs. OHCs receive this cholinergic input through nicotinic acetylcholine receptors (nAChRs) comprised of α9 and α10 subunits[32–34]. In mature hair cells, efferents terminate opposite a postsynaptic cistern containing calcium stores that is closely apposed by calcium-gated SK2 channels. The α9/α10 nAChR is permeable to divalent cations, and calcium entry through this channel is amplified by calcium-induced calcium release from the nearby postsynaptic cistern. In turn, localized release of calcium triggers potassium efflux through local SK2 channels, thus resulting in OHC hyperpolarization in response to acetylcholine released from MOC fibers[22,34]. In some OHCs, BK channels are also present at this synapse and appear to contribute to hair cell hyperpolarization[35,36]. Like other cholinergic neurons, at least some MOCs also express GABA and CGRP, although a definitive role for those neurotransmitters at the OHC synapse has yet to be established[37,38]. It has been proposed that Type II SGNs provide input to the MOC circuit, but strong evidence for this hypothesis is lacking[39,40].

In contrast to the relatively uniform MOC population, LOC neurons exhibit a puzzling array of differences in their morphological and signaling properties. These neurons express a diverse range of neurotransmitters and neuropeptides, including acetylcholine, CGRP, GABA, urocortin, and dopamine, and there is mixed evidence indicating the presence of additional signaling molecules[41,42]. Immunohistochemical studies suggest that many of these signaling molecules are found only transiently during development or in a subset of LOC neurons, in some cases along a tonotopic gradient[43–45]. Like several other neuronal populations, LOCs can also dynamically regulate their expression of dopamine[46–48]. In LOCs, this neurotransmitter switching can be provoked by acoustic trauma; it remains unknown whether signaling molecules other than TH can be modulated by sound exposure and whether other stimuli can evoke changes in neurotransmitter expression. LOC neurons also show obvious differences in the morphology and extent of their cochlear projections, but it is unknown how these anatomical differences correlate with variability in neurotransmitter expression or other aspects of LOC function[49]. Several researchers have noted, however, that LOC shell neurons found adjacent to the LSO vary from LOC neurons housed within the LSO itself with respect to their morphologies, projection patterns, and neurotransmitter expression[27,44,49,50]. At a functional level, stimulation studies indicate that LOC neurons can provide both excitatory and inhibitory signals to auditory nerve fibers[51]. Thus, although all LOC neurons appear to target auditory nerve fibers, the structure of LOC-SGN synapses remains mysterious, and there is poorly understood heterogeneity at the level of both anatomy and function that could influence exactly how LOC activity alters the encoding of sound information in the cochlea.

In addition to the cochlear efferent pathway, similar efferent projections target hair cells of the vestibular and lateral line systems. Indeed, efferent neurons have been identified in virtually every species with a hair cell sensory system—including cephalopods[26]. In non-mammalian species, efferent neurons to the vestibular, auditory, and lateral line (if present) systems all reside in the same brainstem nucleus[26]. Even in mammals, where the vestibular and auditory efferents

reside in distinct brain regions, the two efferent populations develop together[52,53]. Although birds and mammals are separated by 300 million years in evolution, efferent innervation of the sensory epithelium in birds (the basilar papilla) is analogous to what is observed in mammals, with differential innervation of tall (IHC-like) and short (OHC-like) hair cells[54,55]. Likewise, the developing inner ear efferents share a common developmental history in chickens and mice, with some differences[53,56,57]. The ubiquity of these feedback systems across widely divergent species, along with their common developmental origins, suggest that the efferent neurons of these various sensory modalities may share a common evolutionary origin, and may even have co-evolved with hair cells themselves[58].

Across species, these inner-ear efferents (IEEs) also share many properties of branchial cranial motor neurons, both functionally and developmentally. Like the pre-ganglionic motor neurons of the autonomic nervous system, IEEs represent a subset of motor neurons, despite the fact that they do not form connections with muscles. IEEs originate in a motor neuron progenitor zone, express many markers of motor neuron identity—including *Chat*, *Tbx20*, and *Isl1*—and develop alongside the facial branchial motor neurons (FBMNs)[58,59]. FBMNs provide the motor division of the VIIth nerve, which innervates the face and is closely affiliated with the VIIIth nerve as they project together in the internal auditory meatus. Indeed, in all vertebrates, IEE and FBMN axons project together for at least some distance[26,58]. Given the many similarities between these two neuronal populations, it is hypothesized that IEEs are evolutionarily derived from FBMNs[58].

Origin, specification, and migration of OCNs within the brainstem

During development, OCNs are progressively specified, starting with the induction of generic IEE precursors and ending with the formation of functionally distinct populations of LOC and MOC neurons that form anatomically distinct connections with SGNs and OHCs, respectively. As in other regions of the nervous system, this gradual diversification of cell fates depends on

combinatorially acting transcription factors, including factors that coordinate the migration of each efferent subtype to its proper location in the SOC.

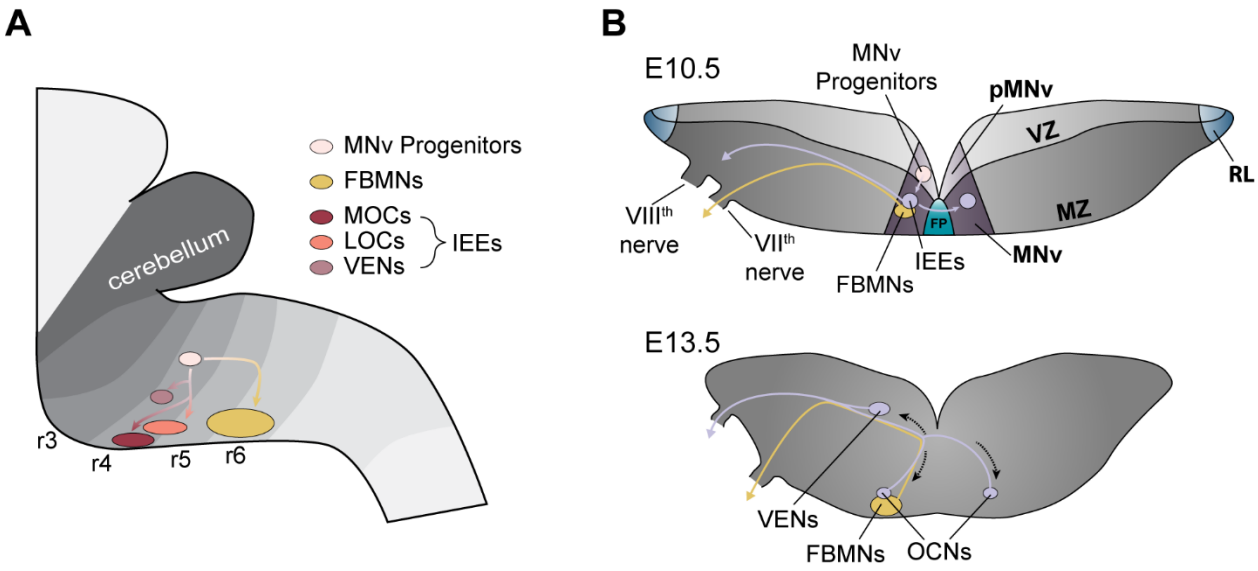

Figure 1.2. Cell body movements of inner ear efferents (IEEs) and facial branchial motor neurons (FBMNs) during mouse embryogenesis. (A) As shown in a sagittal view, FBMNs and IEEs both derive from a common pool of visceral motor neuron (MNv) progenitors in rhombomere 4 (r4). During embryogenesis, FBMNs move caudally. IEEs gradually separate into distinct subtypes and migrate to their final positions in r4 and r5. Rostral is left and dorsal is up. LOC, lateral olivocochlear neuron; MOC, medial olivocochlear neuron; VEN, vestibular efferent neuron. **(B)** Starting around E9, IEEs and FBMNs begin to differentiate from a shared pool of cells in the progenitor domain of visceral motor neurons (pMNv), directly adjacent to the floor plate (FP), illustrated in a transverse view of r4. As they develop, immature neurons exit the cell cycle and migrate from the ventricular zone (VZ) to the mantle zone (MZ). By E10.5, IEEs and FBMNs have begun to separate: FBMN cell bodies migrate caudally (see A), while IEEs begin to send projections (or translocate) across the floor plate. Both FBMNs and IEEs also begin extending projections to the periphery via the VIIth and VIIIth nerves. By E13.5, FBMNs and IEEs have fully

Figure 1.2 (Continued)

separated, and olivocochlear neurons (OCNs) have separated from VENs. OCNs migrate towards the pial surface whereas VENs migrate dorsally.

The earliest stages of IEE specification depend on the overall patterning of the axes of the hindbrain, with IEEs developing from neural progenitors with a specific rostral-caudal and dorsal-ventral address (**Figure 1.2**) (reviewed in ref. 59). During development, the brainstem is divided into discrete segments along the rostral-caudal axis called rhombomeres[60–65]. Each rhombomere is defined by combinations of transcriptional regulators that control the patterning of neuronal populations developing within that segment, with homeobox (Hox) transcription factors playing a leading role[66]. Distinct neural progenitor domains also exist along the dorsal-ventral axis of each rhombomere. In the ventral neural tube, the formation of these domains is guided by a gradient of the morphogen Sonic hedgehog (SHH) and by suites of homeodomain proteins induced by varying levels of SHH[64,67,68]. Thus, the identity of developing hindbrain neurons, including the IEEs, is determined by a combination of their extracellular milieu and the particular slate of transcription factors expressed within individual cells.

Within the brainstem, OCNs develop in parallel with many other related neurons essential for auditory processing. Indeed, the majority of the auditory brainstem is derived from rhombomeres 2-5[59,69], with most neurons exiting the cell cycle between E9 and E14 in mouse[69–71]. Within this region, some neurons, including the OCNs, develop from progenitors in the ventricular zone, whereas others arise from the rhombic lip, a highly migratory pool of progenitors lining the roof of the fourth ventricle (**Figure 1.2**). Moreover, many nuclei are comprised of neurons from multiple sources. For instance, neurons of the cochlear nucleus complex (CNC) arise in r2-5, primarily from *Wnt1*-expressing cells in the rhombic lip, but also from *Wnt1*-negative precursors ventral to the rhombic lip, which instead are marked by expression of Ptf1a and go on to produce

GABAergic neurons in the CNC[59,69,72,73]. Distinct CNC cell types originate in different rhombomeres and in different progenitor domains along the dorsal-ventral axis[59,73].

More ventrally, the various nuclei of the SOC, where OCNs eventually reside, develop primarily in r5[59,74–77]. Like the CNC, the neurons that will eventually populate the SOC derive from multiple sources, including *Atoh1*- and *Wnt1*-positive precursors in the rhombic lip and *En1*-expressing precursors of the ventricular zone[59,77–79]. For instance, the LSO contains glycinergic neurons derived from the ventricular zone and glutamatergic neurons derived from the rhombic lip[59]. All IEEs, however, originate from a distinct pool of progenitors in the ventricular zone of r4[52,53,57,76]. Notably, the CNC interneurons that innervate MOCs are also r4-derived, suggesting that the rhombomeric origins of auditory brainstem neurons may inform their later circuit connectivity and functions[76].

The various nodes for auditory processing in the brainstem become interconnected early in embryogenesis. Beginning around E9.5 in mouse, SGNs start to delaminate from the otic placode, which forms from epithelium adjacent to r5-6[80–82]. Around E11.5, SGNs begin sending projections into the region where the CNC will develop, while both types of neurons are still being born[82–85]. By E15, those early projections have begun to form functional synaptic contacts with target neurons in the ventral cochlear nucleus, and by E17, electrical stimulations in the nascent cochlea can elicit responses from neurons in the SOC, indicating the formation of functional contacts both between SGNs and CNC neurons, and between CNC neurons and their targets in the SOC[86]. Thus, neurons throughout the auditory brainstem—including OCNs and their precursors—navigate through a complex and changing environment that is physically connected to the cochlea from very early stages.

Olivocochlear efferents develop together with typical motor neurons

The earliest stages of IEE development are intertwined with those of FBMNs. In all vertebrate species examined thus far—including mice, chickens, and zebrafish—IEEs and FBMNs originate

together in the progenitor domain of visceral motor neurons (pMNv) in the ventricular zone, just medial to the floor plate of r4[52,53,56,57,76,87]. This NKX2-2+ domain, analogous to p3 in the spinal cord, produces branchial and visceral motor neurons, while somatic motor neurons are generated from a more dorsal PAX6+ progenitor domain[88,89]. The overall identity of r4 is determined by the homeobox transcription factor HOXB1,whose expression is restricted to r4 by E8.5 in mice[62,64,66,90–93]. Loss of *Hoxb1* has major consequences for r4, including loss of both IEEs and the facial motor nucleus, where FBMN cell bodies reside[94–96]. However, ISL1-positive motor neurons are still present, suggesting that *Hoxb1* is not necessary for motor neuron development *per se*, but instead directs a subset of motor neuron precursors to assume "r4" identities[76,94].

IEEs, like FBMNs and other branchial motor neurons, also express a collection of transcription factors that together assign a motor neuron identity. These genes include *Isl1*[97,98], *Phox2a* and *Phox2b*[99–101], *Nkx* genes (most critically *Nkx2-2*, *Nkx2-9*, *Nkx6-1*, and *Nkx6-2*)[64,67,102–105], and *Tbx20*[106–108]. Expression of these transcription factors is restricted to motor neuron progenitors as part of the broader SHH signaling network, with pMNv forming just ventral to the somatic pMN domain[68,88].

Motor neuron progenitors are subsequently diversified to produce subtypes of motor neurons by integrating patterning information from the anterior-posterior and dorsal-ventral axes. For IEEs and FBMNs, this means assuming a branchiovisceral fate within r4. The branchiovisceral fate is controlled by the combined action of NKX2-2 and NKX2-9 in progenitors within the pMNv domain[105]. A key effector is the homeodomain protein PHOX2B, which promotes expression of *Ascl1* (formerly referred to as *Mash1*) and production of branchial and visceral motor neurons while inhibiting an alternative serotonergic fate[100,101,109–112]. Thus, *Phox2b* knock-out animals lack all branchial and visceral cranial motor nuclei[109]. In these animals, NKX2-2+ progenitors are specified normally but progress atypically to the next stage of development[109]. This general PHOX2B-driven MNv program is customized in r4 through the combined action of HOXB1 and NKX family members. HOXB1 is required for *Phox2b* expression[95] and can directly

bind to regulatory sequences in the *Phox2b* locus that are necessary and sufficient for expression in ventral r4, where the IEEs and FBMNs develop[113]. Moreover, NKX2-2 synergizes with HOXB1 and other co-factors, such that expression of *Phox2b* is a direct readout of the intersection between the A/P (i.e. HOXB1) and D/V (i.e. NKX2) patterning systems. NKX6 proteins reinforce this system by maintaining expression of *Hoxb1* in r4[100]. Hence, in the absence of NKX6 protein activity, *Hoxb1* expression decreases prematurely and very few IEEs are produced[100]. As a result of this complex spatiotemporal network, MNv progenitors in r4 produce only branchial and visceral MNs, including both IEEs and FBMNs.

IEEs also depend on unique genetic programs to differentiate them from the FBMNs developing simultaneously in pMNv. In chicks and mammals—but not zebrafish[114,115]—IEEs are distinguished from FBMNs early on by the expression of zinc-finger transcription factors GATA2 and GATA3[116–119]. Although both GATA2 and GATA3 are expressed in the pMNv progenitor domain, analysis of *Gata3* mutants indicates that GATA3 is not expressed by postmitotic FBMNs[101,116,117]. In mice lacking either GATA2 or GATA3, efferent neurons project aberrantly and fail to cross the floorplate, with axons instead joining the VIIth nerve[116,117,119]. In r4, *Gata3* expression is downstream of *Gata2*[116,119]. Thus, a GATA2/3 network may drive a binary IEE versus FBMN fate decision, similar to the role of GATA factors in the immune system[120]. This network, in turn, is downstream of both *Hoxb1* and *Phox2b*. Thus, misexpression of *Hoxb1* in r2 induces ectopic expression of both *Gata2* and *Gata3*, as well as aberrant midline crossings, suggesting an induction of IEEs[91,116]. PHOX2B may serve as an intermediary for this effect, as HOXB1 can induce *Phox2b*[113], and PHOX2B in turn drives expression of *Gata3* in the ventral region of r4[101]. Indeed, IEEs in *Phox2b* knock-out mice fail to differentiate normally, exhibit reduced levels of GATA3, and occasionally mis-specify as serotonin progenitors[101]. *Phox2a*, on the other hand, is not required for IEE development[101]. Thus, IEE differentiation depends on a general HOXB1/PHOX2B network, with further specificity arising through the action of GATA factors.

The segregation of IEEs and FBMNs is reflected in their migration to distinct nuclei

Shortly after undergoing their final mitotic division, both FBMN and IEE cell bodies begin to migrate away from their shared point of origin (**Figure 1.2**). In mice, these movements are initiated at about E10 and conclude around E15.5[53,94,121–124]. During this time, IEEs and FBMNs separate from each other, as FBMNs travel caudally into their final position in r5 and r6[125]. The IEEs populate r4-5, and are subsequently subdivided into the vestibular efferent neurons (VENs), which migrate dorsally, and the OCNs, which migrate ventrally and eventually give rise to MOCs (residing mainly in VNTB) and LOCs (located in and around LSO)[53,101]. Importantly, FBMNs and IEEs extend axons together from their common origin and into the periphery as early as E10.5, so the trajectory of axons within and out of the brainstem reflects their migratory history[52].

Whereas FBMNs project ipsilaterally to innervate muscles on the same side of the body, many IEEs project to the contralateral cochlea. In particular, MOCs tend to project contralaterally and LOCs tend to project ipsilaterally, although the proportions of ipsilateral and contralateral projections vary across species[27]. In the mouse, about 66% of MOCs (but only 1% of LOCs), project contralaterally, with some neurons even projecting to both ears[27,126,127]. The contralateral projections, which form the olivocochlear bundle (OCB), appear as early as E10[116,117], and the OCB is fully formed by E13.5[53], thereby overlapping substantially with the period of IEE migration. Indeed, in chickens, contralateral projections are achieved by a translocation of IEE cell bodies across the floor plate, thereby leaving a crossed projection in their wake[56,57]. In mice, the means of midline crossing are less clear, as extensive cell body translocations have not been detected[52,53,128]. However, neurons positive for the IEE marker GATA3 have been observed in the midline of E10.5 mice, suggesting that at least some IEE soma may move from one side to the other[101,117]. In mammals, the formation of a contralateral projection may involve the axon guidance receptor EPHB2. In mice, EPHB2 is expressed by IEEs, FBMNs, and the floor plate[129]. In the absence of *EphB2*, IEE axons meander aberrantly across the midline before achieving anatomically normal projections, albeit several days later than wild-type controls[129].

The mechanisms that entice IEEs across the midline —and prevent FBMNs from following— may also involve the Slit-Robo pathway. In *Slit1*, *Slit2* double knock-out mice, the total number of fibers crossing the midline in r4 is decreased by about half compared to wild-type controls, with some axons turning and running longitudinally along the floor-plate rather than crossing directly[130]. In contrast, *Robo2* knock-out animals show a marked increase in the number of projections crossing the floor plate, as well as aberrant migration of ISL1-positive cell bodies onto the floor plate[130,131]. These findings suggest that ROBO2 may ordinarily provide a repulsive cue that keeps FBMNs away from the midline. One can speculate that a similar mechanism might be at play in guiding the ipsilateral projections of IEEs.

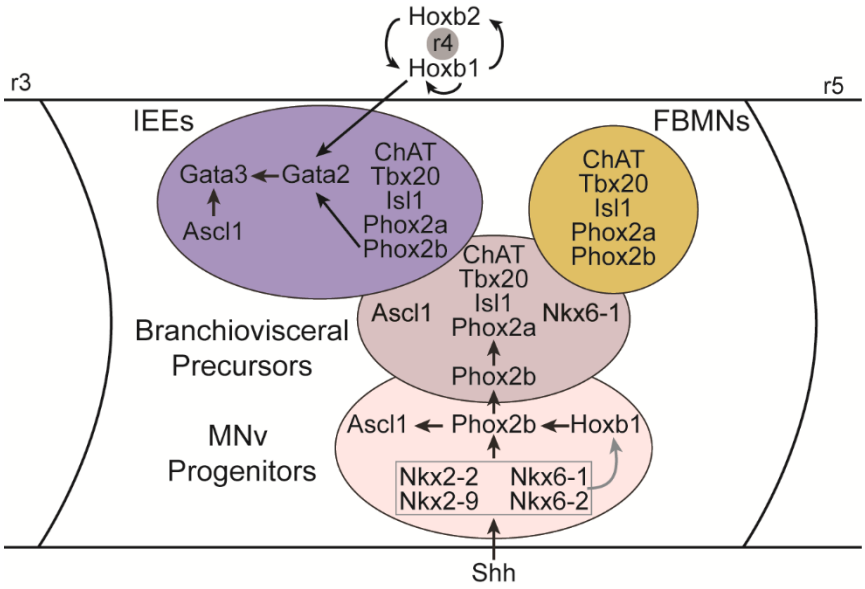

Figure 1.3. Transcription factors driving the production of FBMNs and IEEs. FBMNs and IEEs arise in the fourth rhombomere (r4), which is specified by an autoregulatory Hoxb1/b2 network. Within the pMNv domain of r4, SHH induces expression of a suite of transcription factors (grey box), including Nkx2-2, Nkx2-9, Nkx6-1, and Nkx6-2, that direct a branchiovisceral MN fate. The presence of Hoxb1 and Nkx factors collectively induce Phox2b, which is subsequently maintained in branchiovisceral precursors, including those that become IEEs or FBMNs. Within r4, Nkx6 factors are required for the maintenance (but not the onset) of Hoxb1 expression (grey

Figure 1.3 (Continued)

arrow). In branchiovisceral precursors, Phox2b drives expression of early markers of visceral and branchial MN identity, including Phox2a, Isl1, and Chat. In addition, Nkx6-1 and Ascl1 expression persists after the MNv progenitors exit the cell cycle and become branchiovisceral precursors. Within this pool of precursors, those that will become IEEs likely deviate from an FBMN fate due to the expression of Gata2/3. Together, Phox2b and Hoxb1 drive expression of Gata2, which in turn drives expression of Gata3. Ascl1 remains active in postimitotic IEEs (but not FBMNs) until about E12.5 and influences the level of Gata3 expression. Many of these transcription factors impinge on each other and on common cassettes of gene expression, with some acting at multiple stages and in multiple ways. For simplicity, only the key transcriptional interactions that drive the specification and differentiation of IEEs are shown. See **Table 1.1** for additional details regarding the specific contributions of each factor.

Some IEE migratory decisions appear to depend on transcriptional networks active in all motor neurons (**Figure 1.3**). For instance, both IEEs and FMBNs require the pan-motor neuron marker ISL1 for proper differentiation. For FBMNs, ISL1 is crucial for their caudal migration, as reflected by an accumulation of FBMNs in r4-5 rather than r6 in mice with reduced ISL1 levels[132]. Although no major IEE migratory phenotypes were described, the IEEs developed truncated and disorganized projections out of the brainstem, with the few remaining axons barely reaching the ear by E11.5. Both types of defects may be due to altered expression of *Slit2*, as *Slit2* levels are decreased in *Isl1*-deficient motor neurons[132].

Like ISL1, TBX20 is expressed by both IEEs and FBMNs, but has distinct effects on the migration of each population[106]. Caudal migration of FBMNs is controlled by the planar cell polarity (PCP) pathway[115,133–145], and *Tbx20* mutant mice exhibit defects in caudal FBMN migration as well

as a downregulation of PCP genes in FBMN somata[106]. *Tbx20* expression is also required for midline crossing of IEEs, but it is unclear whether this phenotype is also due to changes in PCP gene expression[106]. Nevertheless, IEEs exhibit aberrant midline crossing in mice lacking the PCP component PRICKLE1, with reduced contralateral projections and some axons turning to wander along the floorplate longitudinally[137]. In zebrafish, the caudal migration of octavolateralis efferents is also stalled in animals lacking the PCP proteins Scrib or Celsr2[134,145]. More work is needed to understand what role—if any—the PCP pathway plays in the migration of mammalian IEEs. Thus, despite a common reliance on TBX20 and possibly PCP genes, there appear to be significant differences in how these genes act in IEEs and FBMNs.

Shortly before the IEEs and FBMNs have fully separated, IEEs begin to further diversify and separate from each other, with VENs migrating dorsally, MOC neurons moving ventrally, and LOC neurons settling in a more ventrolateral position[53]. In mice, this migration happens between E12.5 and E14.5, with VENs and OCNs separating first, followed by a separation of MOC and LOC neurons[53]. This process requires the transcription factor ASCL1, as the VEN nucleus does not form in *Ascl1* mutants[101]. ASCL1 is also expressed in OCNs and FBMNs[101,109,146]. However, although *Ascl1* deletion delays the caudal migration of FBMNs, it has no effect on the movement of OCNs[101,146]. Unfortunately, the identity of additional cell-type specific transcription factors that might direct subsets of OCNs to their final destinations remains unclear.

The final separation of VENs from OCNs relies in part on a ventral migration of OCNs, with both OCNs and FBMNs undergoing similar migrations away from the ventricular zone to arrive close to the ventral pial surface of the hindbrain[122,124] (**Figure 1.2**). This process of radial migration depends on the *Reln* gene in both OCNs and FBMNs, although LOC neurons only appeared to be partially affected in *Reln* mutant mice, suggesting that additional mechanisms may be at work[122]. In FBMNs, *Reln* interacts with Dab1 and Cdk5. It is unknown whether similar mechanisms mediate its effects in OCNs[122,147] (see **Table 1.1** for a summary of genes involved in OCN specification, migration, and guidance).

Table 1.1. Genetic factors influencing IEE identity and migration.

Gene	Protein type	Effect on IEE Development	References
Hoxb1	Homeodomain transcription factor	Critical for establishing an r4 identity. No IEEs or FBMNs in *Hoxb1* mutant mice; branchiovisceral MNs are mis-specified. Mutants fail to maintain *Phox2b* expression in progenitors and exhibit no *Gata3* expression in r4. Ectopic expression outside of r4 induces aberrant midline crossings and *Gata3* expression.	76,91,94–96,100,116
Nkx2-2, *Nkx2-9*	Homeodomain transcription factors	Both genes are key for interpreting graded SHH signals and assigning a dorsal-ventral identity. In *Nkx2-2*, *Nkx2-9* double knock-out mice, hindbrain branchiovisceral MNs lose *Phox2b* expression and mis-specify as somatic MNs. In the presence of *Hoxb1*, ectopic expression of *Nkx2-2* induces *Phox2b* expression and a branchiovisceral MN identity.	67,89,100,102,105,113
Nkx6-1, *Nkx6-2*	Homeodomain transcription factors	Both genes are key for establishing dorsal-ventral patterning and hence motor neuron development. Somatic MN identity is mis-specified in *Nkx6-1* mouse mutants. FBMN migration—but not initial specification—is also altered, likely through altered expression of cell surface receptors like RET and UNC5C. Effects on IEE migration are unknown. In *Nkx6-1*, *Nkx6-2* double knock-outs, some visceral MNs differentiate as serotonin neurons. After E10.5 in double knockouts, *Hoxb1* expression decreases in ventral r4.	67,100,103,104

Table 1.1 (Continued)

Phox2b	Homeodomain transcription factor	Key regulator of branchiovisceral MN specification. *Phox2b* mutants lack all branchial cranial motor neuron nuclei, with no IEEs and no FBMNs. Visceral motor neurons are mis-specified. Sufficient to induce itself, *Isl1*, *Phox2a*, and *Chat* in branchiovisceral MN precursors. Can cooperate with *Nkx2-2* to induce *Ascl1* and generic neuronal differentiation. Upstream of *Gata2/3* in IEEs.	101,109–112
Ascl1	bHLH transcription factor	Promotes motor neuron development widely with specific effects branchiovisceral MN development. Can induce *Gata3* expression in chicks, and mouse mutants exhibit a reduced number of GATA3-positive progenitors in ventral r4. FBMN migration is delayed and the vestibular efferent nucleus fails to form.	101,146,148
Isl1	Homeodomain transcription factor	Promotes motor neuron development widely with specific effects on FBMN and IEE differentiation. In mouse mutants, spinal motor neurons fail to develop. In hypomorphs, IEE axons are disorganized and short, barely reaching the periphery. FBMN migration stalls in r5.	132,149
Tbx20	T-box transcription factor	Important for FBMN and IEE differentiation. In nervous-system-wide conditional knock-out mice, FBMNs do not migrate caudally and IEEs do not form contralateral projections. *Gata2* expression is diminished. In FBMNs, *Tbx20* recruits PCP machinery.	106

Table 1.1 (Continued)

Gata2	Zinc-finger transcription factor	Important for IEE differentiation. *Gata2* mutants show no expression of *Gata3*. Mutants also show fewer fibers crossing the floor plate, with fewer cells in r4 and fewer FBMNs.	116,119
Gata3	Zinc-finger transcription factor	Important for IEE differentiation. IEE migration and targeting is aberrant in *Gata3* mutants: embryos have no contralateral IEE projections and IEE axons exit with the facial nerve instead of the VIIIth, failing to reach the inner ear. SGN wiring is also disrupted. Autonomous function of *Gata3* in IEEs remains to be defined.	116,117,150–152
Reln	Extracellular matrix protein	Influences FBMN and IEE migration. Both FBMNs and OCNs fail to reach the pial surface of the hindbrain in *Reln* mouse mutants. VENs develop in a normal location.	122
Prickle1	Planar cell polarity protein	Influences FBMN and IEE migration. In *Prickle1* mutant mice, some IEE projections fail to cross the midline and appear to run the length of the floor plate instead of crossing it. Aberrant caudal and radial migration of FBMNs.	137
celsr2	Cadherin	Influences branchiovisceral MN migration. In mutant zebrafish, octavolateralis efferents do not migrate caudally with FBMNs.	145
scrib	Planar cell polarity protein	Influences branchiovisceral MN migration. In mutant zebrafish, octavolateralis efferents do not migrate caudally with FBMNs.	134
EphB2	Eph receptor	Mouse mutants exhibit aberrant, delayed targeting of IEE axons.	129

Table 1.1 (Continued)

Robo2	Transmembrane receptor	*Robo2* mouse mutants show increased and aberrant projections across the floor plate in r4, potentially from FBMN axons. Aberrant migration of ISL1+ cell bodies onto the midline.	130,131
Slit1, Slit2	Glycoprotein	*Slit1*, *Slit*2 double knock-out mice have reduced midline crossing in r4.	130

AFFERENT-EFFERENT INTERACTIONS IN THE COCHLEA

Efferents grow along existing nerves to find their synaptic targets

As they are migrating and settling into their final locations, OCNs begin to extend axons out of the brainstem and into the cochlea, ultimately terminating with post-synaptic targets in the organ of Corti (**Figure 1.4**). These initial guidance events occur after the VIIIth nerve has begun to form, with SGN axons reaching the brainstem by E11.5[84], days before the IEEs have scattered to their distinct locations across the brainstem. The formation of efferent projections coincides with the formation of connections within the auditory brainstem, with bushy cell neurons in the CNC beginning to extend axons towards the midline around E13 and reaching the contralateral SOC by E17[153].

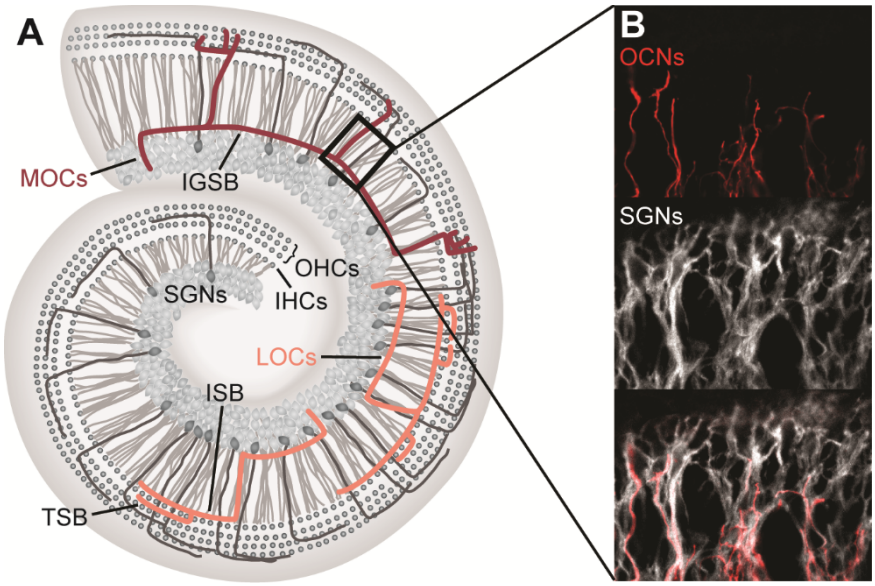

Figure 1.4. Organization and growth of OCN and SGN projections in the cochlea. (A) Organization of the mature cochlea. MOC axons project along the intraganglionic spiral bundle (IGSB) before turning to branch among the OHC layers. LOCs also travel within the IGSB before turning to the IHC layer. LOCs either turn unilaterally or branch to spiral on either side of IHCs in the inner spiral bundle (ISB) and tunnel spiral bundle (TSB). MOC and LOC neuron traces inspired by Brown 2011 (ref. 27). (**B)** E17.5 mouse cochlea showing OCNs (red) and SGNs (white). OCNs appear to grow along SGN axons, as indicated by the close association between OCNs and SGNs and the way incoming OCN projections lag behind extending SGN peripheral axons. Image provided by N. Druckenbrod.

Consistent with the close relationship with the FBMNs, OCN axons initially follow along the facial genu in the brainstem but bypass the VIIth nerve and instead exit to join the nascent VIIIth nerve[53]. Almost nothing is known about the mechanisms that direct OCN axons to grow into the VIIIth nerve, rather than continuing to follow the VIIth. One possibility is that the inner ear provides an attractive signal that could attract any motor neuron axons, but that OCN axons are in the best location to

respond to the signal, an idea that has been supported by the behavior of motor neuron axons presented with an ectopic otic vesicle[154,155]. However, the inner ear is not necessary for growth into the periphery, as OCN axons mis-route into the VIIth nerve if the VIIIth nerve is absent[156]. IEEs also join the VIIth nerve inappropriately in *Gata3* mutant mice, but more work is needed to understand whether this effect reflects a role for GATA3 in IEEs specifically, since GATA3 is also expressed in the developing cochlea and SGNs[117,150].

Upon reaching the VIIIth nerve exit point, OCN axons are thought to grow along a scaffold of SGN processes into the sensory epithelium of the inner ear[157,158]. In support of this hypothesis, a wide array of mutations affecting SGN development and targeting also affect efferent innervation of the cochlea, with the phenotype of efferent neurons often matching the aberrant projections of SGNs[150,151,156,159–161]. Lateral line efferents in zebrafish appear to rely on a similar mechanism to reach their targets[162]. However, no molecular cues mediating fasciculation between afferents and efferents have been identified to date. In other peripheral nerves with both afferent and efferent components, this process depends on axon-axon interactions mediated by Eph signaling[163,164], but analogous roles for Eph receptors in the auditory system have not yet been described[165]. Even more mysterious is the subsequent targeting of OHCs by MOC axons and of SGN terminals by LOC axons. However, it is thought that MOC outgrowth toward the OHCs may not rely on SGN scaffolding, as MOCs and Type II SGNs follow different trajectories between the IHC and OHC regions (schematized in **Figure 1.1**), and MOCs still reach the OHCs in *BDNF* mutant mice that lack afferent innervation of OHCs[166,167].

Efferents reach the mammalian sensory epithelium during a period of circuit refinement

Efferents sit in a key node for auditory processing, both receiving sound information through the afferent pathway in the brainstem and transmitting signals back to the afferents through synaptic contacts in the cochlea. It is therefore not surprising that this final pattern of connectivity depends on activity-dependent mechanisms that operate after the basic axon tracts have formed and

synaptogenesis has begun, which occurs right around birth in mice[168]. Indeed, the first two weeks of postnatal development in mice are a transformative epoch for the inner ear. Both SGNs and auditory brainstem neurons undergo extensive remodeling during this period to adopt distinct functional properties and converge on their final targets[3,169]. As in other developing neural circuits, spontaneous activity plays a major role in the maturation and refinement of auditory circuitry[170]. Before the onset of hearing (~P10 in mice[171]), IHCs produce spontaneous calcium spikes, which propagate throughout the auditory system[172–180]. In parallel, neurons in the auditory brainstem segregate into ever-more refined tonotopic arrangements, a process that is thought to depend on spontaneous activity from the inner ear[181].

During development, MOC axons are poised to influence the pattern of activity emanating from the cochlea, though the precise functions of this early cholinergic signaling remain unclear. In mice, tracing studies reveal that MOC neurons are the first to arrive in the sensory epithelium, appearing in the IHC region as early as E16.5 and in the OHC region around E18.5[53]. Experiments in rats, hamsters, and gerbils identified a similar pattern, with dye-labeled MOCs first appearing near IHCs by P0, and extending to OHCs between P2 and P5, depending on the species[182–185]. This time course also aligns with the appearance of choline acetyltransferase (ChAT) and acetylcholinesterase (AChE)-positive terminals in the cochlea. Both enzymes, which regulate acetylcholine synthesis and degradation, have been identified in the inner ear at birth or shortly thereafter in mice, rats, and hamsters[186–188]. Consistent with dye-labeling studies, ChAT staining is first visible in the region of IHCs and can be seen around OHCs several days later[188]. Like other aspects of cochlear development, OCNs arrive first in the base, and development progresses toward the apex[182].

Collectively, these findings suggest the existence of a “developmental waiting period,” in which MOC neurons transiently innervate the IHC region before synapsing onto their final targets, the OHCs[157,184]. During this waiting period, OCNs also send projections to Kölliker’s organ[53,183], a transient structure believed to induce spontaneous activity in IHCs before the onset of hearing[172].

It is not known whether OCNs form synapses with cells in this structure; however, subunits of acetylcholine receptors are expressed in Kölliker's organ, raising the possibility of functional contacts[189,190]. While the purpose of these temporary connections is unknown, transient innervations do influence the maturation of other developing circuits, such as thalamocortical neurons, which form short-lived connections in the subplate that prepare them for subsequent formation of synapses in layer four of the cortex[191–193].

MOC neurons affect prehearing synaptic activity

During this early postnatal waiting period, MOC terminals form synaptic contacts with IHCs, which transiently express SK2 channels and AChR subunits that mediate post-synaptic responses (**Figure 1.5**)[194,195]. Although little is known about how the MOC-to-IHC synapse forms, this transient connection does appear to be functional. Electrophysiological recordings from IHCs of rats during this time identified the presence of iPSCs that disappeared with the application of the AChR antagonists strychnine and alpha-bungarotoxin, indicating that MOC neurons (the only cholinergic cells presynaptic to IHCs) inhibit IHCs[194,195]. Similarly, both efferent stimulation and exogenous application of acetylcholine in cochlear explants reduce IHC firing rates, whereas blockade of cholinergic signaling with strychnine increases IHC firing rates[195–198]. In rodents, MOCs innervate virtually all IHCs within the first few postnatal days, and this MOC-to-IHC synapse is gradually strengthened over the first postnatal week before disappearing shortly after the onset of hearing[199–202]. In rats, IHCs cease to respond to acetylcholine sometime between P13 and P21[199,200]. IHCs in mice remain responsive to acetylcholine slightly longer than those in rats, but the proportion of IHCs responding OCN stimulation decreases dramatically by P16[201]. Across species, IHCs of adult animals respond to neither acetylcholine nor OCN stimulation[201,203].

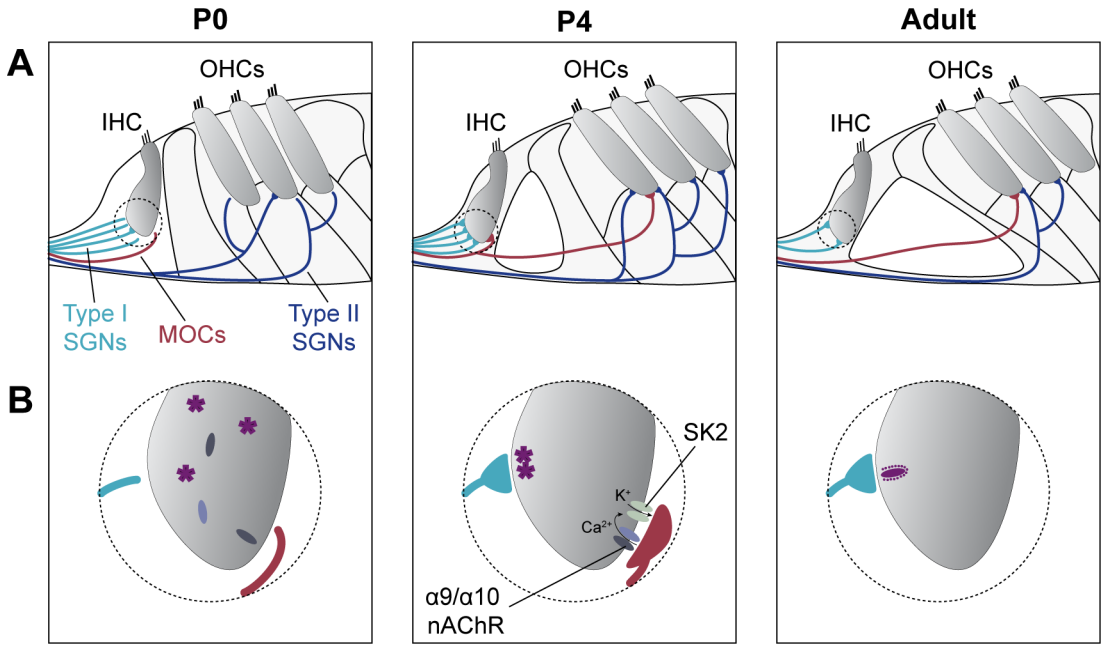

Figure 1.5. Development and refinement of cochlear wiring in the mouse. (A) By P0, MOCs have arrived in the vicinity of IHCs. Both Type I and Type II SGNs have projected to IHCs and OHCs, respectively. Between P0 and P4, both MOC neurons and Type I SGNs form synapses with IHCs, while Type II SGNs form connections with OHCs. The MOC axons then grow on towards the OHC region. At least some of these axons appear to be branches from MOC axons in the IHC region. Over the next two weeks, both SGNs and MOCs prune excess synapses. By adulthood, MOCs project exclusively to OHCs. **(B)** Development of IHC synapses. At P0, both Type I SGN and MOC projections are present at the IHC surface. Although synaptic machinery is present in IHCs, many components are not yet localized to the cell membrane. Synaptogenesis proceeds over the next several days, and by P4, all IHCs respond to MOC stimulation. The arrival of MOC terminals coincides with the expression of SK2 calcium-gated potassium channels and α9/α10 nicotinic acetylcholine receptors in IHCs. Ribbon synapses (purple) presynaptic to Type I SGNs also mature over this time period. By adulthood, both MOC terminals and their postsynaptic receptors in IHCs have been eliminated. LOCs also innervate the cochlea during this period (not shown).

Given the evidence that spontaneous activity originating in the cochlea ultimately propagates along the entire developing auditory neuraxis, it is tantalizing to suppose that efferent inhibition of IHCs during early postnatal stages might also shape auditory circuits in the CNS. Several studies have attempted to address this question by investigating auditory development in mice lacking the nAChR subunits α9 or α10, which are required for OCNs to form functional cholinergic synapses on hair cells[204,205]. Indeed, tonotopic refinement of brainstem circuitry is disrupted in *nAChRα9* knockout mice, and these knockout mice exhibit behavioral deficits in frequency discrimiation[181,206]. Knock-in mice expressing the enhanced α9 receptor allele *Chrna9L9'T* also have altered tonotopic profiles in the brainstem, indicating that MOC input onto cochlear circuitry needs to be tailored precisely to generate fully functional frequency maps[207,208]. IHCs of *α9* knockout mice also appear to have defects in vesicle fusion at ribbon synapses, indicating a possible role for early efferent signaling on hair cell maturation[209], although other properties of IHCs seem to be normal in mice lacking cholinergic OCN innervation[209,210].

Following this period of temporary MOC-IHC contacts, MOC axons gradually transition into the OHC region, concomitant with the arrival of LOC neurons in the sensory epithelium during the first postnatal week, although distinguishing LOCs from MOCs by morphology at this stage remains a challenge. In rats, OHCs begin responding to acetylcholine at P6, shortly after the onset of SK2 expression[211,212]. In the cat and rat, MOCs first form transient, axo-dendritic synapses on Type II SGNs before synapsing directly onto OHCs[168,213,214]. At least some of the early contacts onto OHCs appear to be branched projections from MOCs innervating the IHC region[185,215] (**Figure 1.5**). The transition from IHCs to OHCs may involve BDNF, as MOC innervation of the OHC region is delayed in *BDNF* mutant mice[167]. However, the factors that ultimately guide MOCs toward the OHC region have yet to be identified.

The arrival of MOC neurons in the OHC region also coincides with a loss of Type II afferent synapses in several species and the onset of OHC electromotility (the physical contraction of OHCs in response to sound)[214,216,217]. These findings led early researchers to speculate that the

arrival of MOC neurons influences the final maturation of OHCs, including the formation of synapses with Type II SGNs[218,219]. In support of this idea, in *Hoxb1* mutant mice, MOC neurons fail to develop and their absence is accompanied by a gradual degeneration of OHCs, and hence progressive hearing loss[76]. However, other essential auditory nuclei are also disrupted in these mutants, and the loss of OHCs is limited to the apical turn, leaving the specific contributions of MOCs unclear. Additionally, OHCs still become electromotile in the absence of functional MOC inputs[220,221]. Other research suggests that MOCs are not required for normal synaptic connectivity between Type II SGNs and OHCs: in cats that have had all efferent connections to the cochlea severed neonatally—before MOC neurons typically reach the OHCs—SGN synapses are still pruned to a number similar to that seen in wild-type animals[222]. Whether the removal of MOC contacts with IHCs makes room for the newly arrived LOC axons remains unknown.

Does the arrival of LOC neurons affect SGN subtype determination?

During this period of efferent rearrangement, SGNs acquire their own unique traits, raising the possibility that these two aspects of circuit maturation are causally linked. Type I SGNs are generally classified into three subtypes, based on their spontaneous firing rates and thresholds[223]. In rats, diversification of firing rates occurs primarily between the second and third postnatal weeks, around the time OCNs are finalizing their own connections[224]. Moreover, LOCs preferentially innervate the subclass of SGNs with the lowest spontaneous firing rate and highest firing threshold, raising the possibility that SGN subtype differentiation may involve cues from LOC neurons[225,226].

This hypothesis was tested directly in kittens by severing the OCB shortly after birth and measuring the firing rates of single auditory nerve fibers. Although firing rates overall were decreased in these animals, all three SGN subtypes remained present, as assessed by recording from fibers in the VIIIth nerve[227]. LOC neurons do, however, seem to play a role in both establishing and maintaining morphological properties of the SGN-IHC synapse[228,229]. Detailed anatomical

studies suggest that low spontaneous firing rate (low-SR) SGNs form synapses on the modiolar side of the IHC (i.e., closer to the ganglion) whereas high spontaneous firing rate (high-SR) SGNs synapse instead on the opposite side (i.e., the pillar side). SGN axon segregation is accompanied by differences in synaptic morphology: low-SR SGNs receive signals through small post-synaptic boutons apposed to large pre-synaptic ribbons, whereas high-SR SGNs develop larger boutons opposite small ribbons[230]. This distribution of synapses emerges gradually over the first month of life, with the mature pattern apparent right around the time that OCN axons exhibit fully mature electrophysiological properties. When the OCB was severed in adult mice, the gradient of synaptic morphology was disrupted[228], raising the possibility that LOC axons influence SGN firing rates and hence synaptic morphology. Unfortunately, since no genetic tools are available to manipulate LOC or MOC neurons prior to birth, the full extent of OCN influence on auditory maturation remains unclear.

Implications for human health

As in other species, human OCNs influence auditory function. Human OCNs appear to be especially important for protecting the cochlea against acoustic trauma and in separating speech sounds from background noise[17,23,231]. Furthermore, studies in rodents suggest that animals raised in loud environments occasionally fail to develop normal temporal acuity, an effect that is exacerbated in animals lacking functional efferent synapses[232,233]. OCNs may play a similar protective role in human development.

The OC efferent system has also been implicated in a number of human neurological disorders that involve altered auditory processing, including autism spectrum disorder (ASD), schizophrenia, and tinnitus. For patients with ASD, abnormalities in auditory processing are associated with a diminished SOC[234,235] and diminished or asymmetrical MOC activity[236,237], suggesting that OCNs may play a role in the altered processing of auditory stimuli. Altered MOC symmetry has also been identified in patients with schizophrenia[238,239]. However, differences

between patients and normal-hearing controls tend to be small, and seem to vary both across patients and with experimental methods[240,241]. More work is also needed to determine whether effects seen in these various disorders are specific to efferents, or reflect broader changes in brain structure and connectivity[242].

Efferent synapses are also altered in aging animals, and thus may contribute to age-related defects in auditory processing shown in human studies. In particular, older mice lose MOC synapses onto OHCs[243]. OCNs also begin to re-form synapses onto IHCs later in life[244,245]. The effects of this re-emergent IHC contact are not understood, nor are the mechanisms that cause these alterations in OCN projections. This change may, however, contribute to defects in auditory processing, especially in discriminating speech sounds. Animal models also suggest that the presence of OCNs can delay age-related hearing loss, as acutely de-efferented animals exhibit an accelerated decline in auditory thresholds with age[246]. Ultimately, developing successful therapies to treat any of these conditions will likely hinge on a robust understanding of both the development and function of OCN circuitry.

Despite their important position at the intersection of the central and peripheral auditory systems, efferent neurons remain poorly understood at many levels. Unresolved issues include the range of diversity among OCNs in general and among LOC neurons especially, as well as the nature of cues that direct each subtype to its proper location in the developing brainstem. A related question is how each of these populations navigates to distinct synaptic targets in the cochlea, as well as subsequent effects of LOCs on the number, size, and positions of contacts between IHCs and SGNs. The role LOCs play in both sound detection and cochlear protection also remain mysterious. Controversy persists around even basic questions about LOC function, such as which neurotransmitters they use to communicate with SGNs.

Efforts to tackle these questions have been hindered by the lack of markers for subtypes of OCNs, as well as the lack of genetic tools to selectively access OCNs or OCN subtypes. My thesis overcomes several of these bottlenecks by profiling the transcriptional identity of OCN

subtypes across post-natal development using single-cell RNA sequencing (**Chapter 2**). This sequencing data identifies genetic patterns that distinguish OCNs from FBMNs and transcriptionally defines subtypes of OCNs, including a novel population of peptidergic LOCs. In order to gain a deeper understanding of LOC anatomy and function, I leveraged our understanding of OCN genetics to generate and characterized two novel transgenic mouse lines that intersectionally target LOC neurons (**Chapter 3**). Collectively, this work provides a window into key differences between OCN subsets, offering clues about their function and development as well as new tools for investigating their role in the development and function of the auditory system.

CHAPTER TWO

Molecular evaluation of olivocochlear neuron subtypes

Michelle M. Frank and Lisa V. Goodrich designed all experiments. Austen A. Sitko and MMF generated the single-cell sequencing data. MMF analyzed the data and performed all subsequent experiments.

INTRODUCTION

For decades, researchers have classified olivocochlear neurons based on the location of their cell bodies and their targets in the cochlea: LOCs reside in and around the LSO and project to type I SGNs, whereas MOCs reside in the VNTB and project to OHCs. Although these anatomical distinctions have proven fruitful for unraveling the biology of these cells, many fundamental questions remain about how these cell types differ from one another. In particular, we still lack markers to distinguish these cell types reliably, which has proved particularly limiting in circumstances when OCNs aren't making contacts with their usual synaptic partners, as during development or aging[244,245]. We also know very little about the developmental cues that cause MOCs and LOCs to segregate from one another and from the neighboring FBMNs. Previous work suggests that *Gata3* is likely a key factor in driving an IEE fate, but additional differences between OCNs and FBMNs remain a mystery, as do developmental cues that govern the separation of OCN subtype[58,116,117].

Many aspects of OCN function also remain ambiguous. Although LOCs are heterogeneous with respect to both their morphology[49] and their neurotransmitter profiles[43,44], the functional consequences of these differences are unclear. Work is also needed to clarify whether subsets of LOCs vary in their inputs or downstream effects in the cochlea. Developing a better understanding of the sources of variation across OCNs—and how OCN subtypes associate with both upstream and downstream neurons—could go a long way in resolving longstanding questions about olivocochlear circuitry. To address these crucial gaps in our knowledge, we performed single-nucleus sequencing of neonatal and mature brainstem neurons. Our analysis identified numerous factors that distinguish each of these cell types, suggesting differences in the developmental trajectories and functional consequences of each group of neurons.

RESULTS AND DISCUSSION

In order to capture sufficient OCNs to generate reliable single-cell libraries of MOC and LOC neurons, we adopted a single-nucleus sequencing strategy. The SOC and surrounding area are heavily myelinated; dissociating whole cells from this brain region therefore generates large amounts of debris that can interfere with single-cell suspensions. Sequencing single nuclei has become an increasingly popular approach in recent years because isolated nuclei are more robust to perturbations like fluorescence-activated cell sorting (FACS) and can be filtered out from cellular debris to generate purer samples of a cell population of interest[247]. In addition, because OCNs represent a relatively rare population of cells—in mice, there are about 1,000 OCNs per brain[27]—we used a genetic label to enrich for our cells of interest. Because essentially all OCNs are cholinergic[42], we crossed Chat-Cre mice to animals with the nuclear-localized GFP allele Sun1-GFP[248]. After dissecting out a region of the brainstem including both the SOC and the FBMNs, we isolated cholinergic brainstem neurons by FAC sorting dissociated nuclei from *Chat*^{Cre}*; Rosa26*$^{Sun1\text{-}GFP}$ animals. We then encapsulated the nuclei and generated barcoded single-cell libraries using the 10x Genomics platform (**Figure 2.1A**). We performed these experiments at P1 (n = 13 animals), P5 (n = 16 animals), and P26-P28 (n = 32 animals) in order to examine how OCNs mature during postnatal development and to identify functionally relevant differences and candidate markers in mature animals.

After filtering out low-quality cells and infrequently expressed genes, our final dataset includes 45,828 nuclei: 16,753 cells from P1 animals; 15,542 from P5 animals; and 13,533 cells from P26-P28 animals. Unsupervised, graph-based clustering analysis identified 56 clusters (**Figure 2.1B**). These clusters primarily consist of neurons, as indicated by the expression of neuronal markers like *Snap25* (**Figure 2.1E**). This dataset also includes a cluster of oligodendrocytes, identified by expression of myelin oligodendrocyte glycoprotein, *Mog* (**Figure 2.1F**), and populations of astrocytes and oligodendrocyte precursors. Each of the neuronal clusters includes cells from all three time points (**Figure 2.1C**). Non-neuronal cells primarily

originate from the adult dataset, likely because there is less myelination in the neonatal mouse brain. Although cell types vary somewhat in the number of genes and UMI detected—oligodendrocytes, in particular, tend to express fewer genes than neurons—the structure of our data is not primarily driven by these technical variables (**Figure 2.1D, S1**).

Several motor neuron clusters are identifiable based on their co-expression of known motor neuron markers like *Isl1*, *Tbx20*, and *Phox2b* (**Figure 2.1G**). Two of these motor neuron clusters also express the transcription factor *Gata3*, which is expressed in OCNs but not in other motor neuron populations (**Figure 2.1H**)[117]. In addition, we identified a cluster of FBMNs based on co-expression of known markers including *Etv1* and *Epha7* (**Figure 2.1I, J**)[249]. Because there are several known sub-populations of FBMNs[249], it is possible that additional clusters in our dataset may also include FBMNs. Given the dearth of published markers for mature subtypes of cranial motor neurons, however, we were unable to conclusively identify any of the other motor neuron clusters in our dataset. We expect that large-scale differences between OCNs and FBMNs will be identifiable regardless of which subset of FBMNs is being examined, and therefore chose to focus our analysis on comparisons with the single cluster FBMN cluster that we were able to identify with confidence.

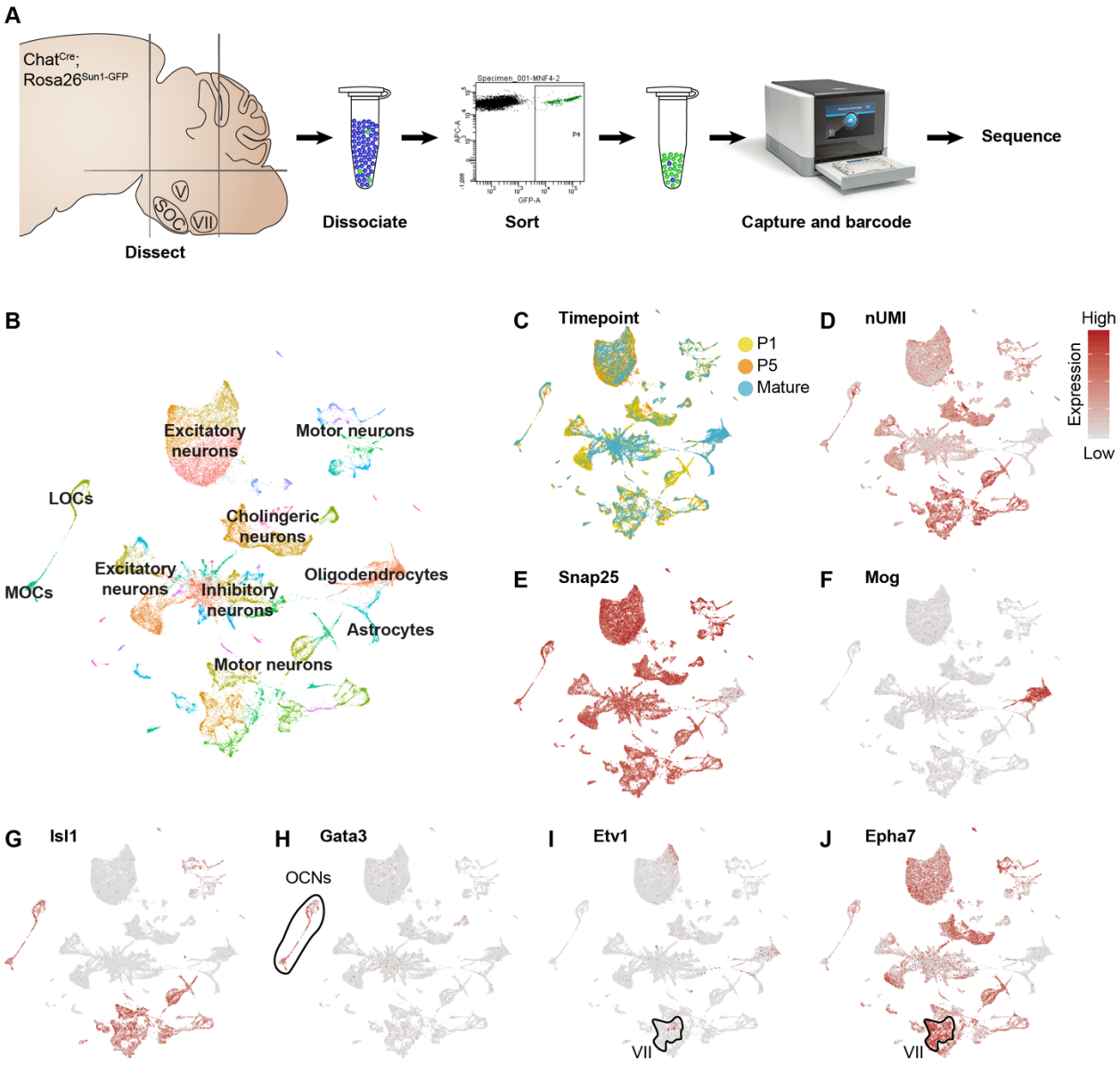

Figure 2.1. Single-nucleus sequencing of brainstem neurons reveals two subtypes of OCNs. (A) Schematic of single-nucleus collection protocol. The ventral brainstem of P1, P5, or P26-P28 *Chat*^{Cre}*; Rosa26*$^{Sun1\text{-}GFP}$ mice was dissected out, including the entire superior olivary complex (SOC) and the facial motor nucleus (VII). Several other cholinergic populations were also included in our dissection boundaries, including the trigeminal motor nucleus (V). Individual nuclei were dissociated and FAC-sorted to isolate GFP+ cholinergic nuclei. We then used the 10x Genomics platform to encapsulate individual nuclei and generate barcoded single-cell libraries.

Figure 2.1 (Continued)

(B) UMAP plot summarizing sequencing data of 45,828 single nuclei from 61 animals across all three timepoints. The data includes 56 clusters, including clusters of MOCs, LOCs, and several different motor neuron types, as well as a few non-neuronal populations. **(C)** UMAP plot showing contributions from each timepoint. Each neuronal cluster includes cells from all three timepoints, indicating that the clusters are not being driven by variability across timepoints or batches. **(D-J)** Feature plots denoting the normalized expression levels of various genetic markers. For visualization purposes, high expression on the color scale is capped at the 95th percentile of gene expression. **(D)** Feature plot detailing the number of genes detected in each cell. Although some cell types vary in their gene expression levels, the architecture of the data overall is not driven primarily by differences in gene expression or read depth. **(E)** The main non-neuronal population in our dataset is labeled by *Mog*, an oligodendrocyte marker. **(F)** *Snap25* expression labels neuronal clusters, which constitute the majority of the dataset. **(G)** *Isl1* is a key regulatory gene for motor neuron fate; its expression identifies motor neuron clusters. **(H)** Among brainstem motor neurons, the transcription factor *Gata3* is confined to the OCNs. **(I)** *Etv1* is a transcription factor selectively expressed in a subset of FBMNs. It is primarily expressed in only one motor neuron cluster. **(J)** *Epha7* was previously identified as a marker for a subset of FBMNs. Among the motor neurons in our dataset, it is expressed at high levels in the same cluster as Etv1, implying that cells in that cluster correspond to FBMNs.

Genetic differences between OCNs and FBMNs

OCNs develop in close proximity to the FBMNs and share many similarities with this group of motor neurons. Indeed, in *Gata3* mutant animals, OCNs deviate from their usual trajectory, following the VIIth nerve out of the brain with FBMN axons rather than joining the VIIIth nerve to

target the ear[117]. This close relationship between OCNs and FBMNs has led to the hypothesis that OCNs are evolutionarily derived from FBMNs[58]. Much remains to be discovered about which genetic factors cause OCNs to deviate from a typical motor neuron fate to play such an unorthodox role in peripheral sensory modulation.

Our sequencing dataset revealed many transcriptional differences between OCNs and FBMNs (**Figure 2.2A**). One prominent OCN-specific marker was the calcium-dependent secretion activator *Cadps2* (**Figure 2.2B**). We verified the differential expression of this gene with fluorescent *in situ* hybridization in P27-P28 mice and found that *Cadps2* is expressed broadly in both MOCs and LOCs but is not detectable in FBMNs (**Figure 2.2C, D**; n = 3 animals).

Differential expression of adhesion molecules and cell-surface receptors define patterns of neuronal migration, targeting, and synaptic specificity. As expected given their divergent anatomy and function, FBMNs and OCNs express varying combinations of adhesion molecules. These differences are particularly prominent at P1 and P5, while OCN axons are still arriving in their final targets in the inner ear and before many developmentally salient molecules become downregulated (**Figures 2.2E, S2**). Several of these differentially expressed genes, including *Cdh8* and *Cdh20* have previously been reported play an important role in the formation of the facial motor nucleus[121,250]. Far fewer genes for guidance and adhesion molecules were significantly enriched in OCNs compared to the cohort of genetic factors enriched in FBMNs. This may be because OCNs have already diverged into multiple subtypes by P1; the heterogeneity of gene expression across OCN subtypes may play a larger role in driving expression of adhesion or guidance molecules than differences between FBMNs and OCNs as a whole.

Divergent expression of transcription factors is also crucial for the diversification of cell types. In addition to *Gata2* and *Gata3*, several transcription factors are uniquely expressed in either FBMNs or OCNs (**Figures 2.2F, S3**). In particular, *Pbx3* is expressed only in FBMNs and *Sall3* is expressed only in OCNs. Pbx homeoproteins serve as cofactors with Hox genes to regulate the diversification of motor neuron subtypes[64,251–253]. In zebrafish, *pbx4* is required for

proper migration of FBMNs; in mammals, *Pbx3* may play an equivalent role. While its interactors are less clear, *Sall3* is also expressed in several populations of cranial motor neurons, and is required for proper development of the glossopharyngeal nerve[254]. Although our sequencing data suggests that *Sall3* is absent from FBMNs, it is expressed in the embryonic cochlea[254]. This observation raises the intriguing possibility that *Sall3*, like *Gata3*, may act across cell types in the auditory system to regulate expression of shared genetic pathways. Future work might examine whether *Sall3* expression is absent in *Gata3* mutants or Chat-Cre conditional knock-outs and whether OCN projections into the ear are mis-targeted in *Sall3* mutant animals; if, for example, *Sall3* indeed coordinates shared expression of adhesion molecules across auditory neurons, *Sall3*-mutant OCNs may recapitulate the *Gata3* knock-out phenotype, aberrantly leaving the brain with the facial nerve rather than the vestibulocochlear nerve.

Ultimately, OCNs and FBMNs are integrated into distinct functional circuits and contribute different signals to their downstream targets. In keeping with these varying functional roles, our sequencing data indicates that these cell types differ in the expression of molecules relevant to mature circuit function (**Figures 2.2G-l, S4**). In particular, although both MOCs and LOCs express *Gad2*, FBMNs express neither *Gad1* nor *Gad2* (**Figures 2.2G-l**). This finding suggests that OCNs—but not FBMNs—may use GABA to signal to their downstream targets. FBMNs also express high levels of the *Htr2c* serotonin receptor, suggesting that FBMNs may be uniquely positioned to respond to serotonin (**Figure 2.2G**). We did, however, detect some expression of the serotonin receptors *Htra1*, *Htr1d*, *Htr1f*, and *Htr2c* in a subset of mature MOCs and LOCs (6.1%-26.8% of cells in either population), in keeping with previous data which suggests that OCNs can be modulated by serotoninergic inputs[255,256]. The low expression of these receptors may indicate that only subsets of OCNs are positioned to respond to serotonin.

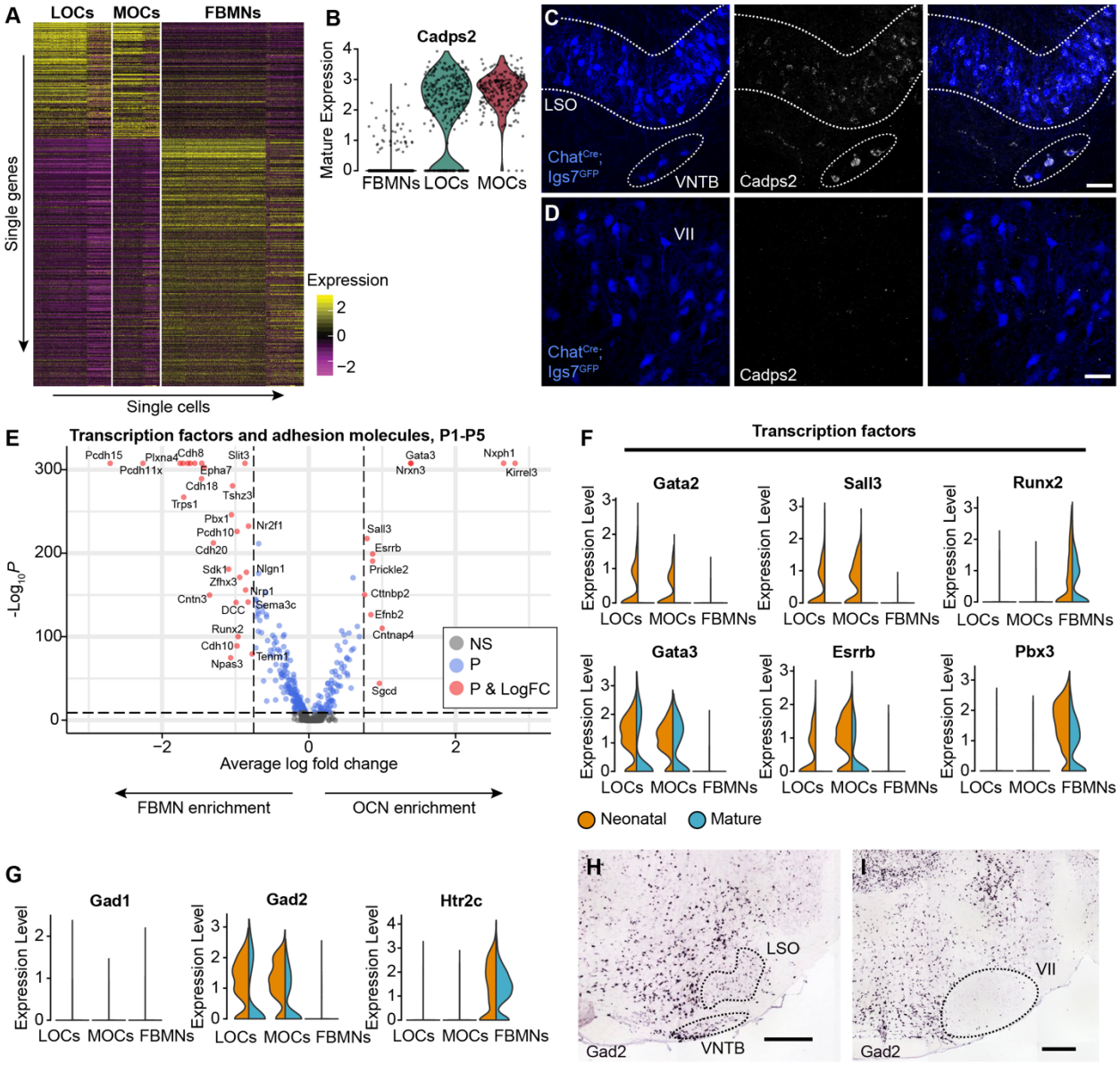

Figure 2.2. OCNs and FBMNs are transcriptionally distinct and vary in their expression of transcription factors, adhesion, and signaling molecules. (A) Heatmap denoting the expression of 434 genes with significant differences in expression level between OCNs and FBMNs at both neonatal and mature timepoints ($p < 0.05$, Wilcoxon rank sum test, Bonferroni post-hoc correction). Plot includes all genes expressed in at least 10% of either OCNs or FBMNs with an average log fold change greater than 0.25. For visualization, scaled expression levels were capped at -2.5 and 2.5. **(B-D)** *Cadps2* is expressed in both MOCs and LOCs but not FBMNs.

Figure 2.2 (Continued)

(B) Violin plot displaying expression levels of *Cadps2* in P26-P28 nuclei in our single-nucleus sequencing dataset. **(C)** HCR in-situ hybridiziation of *Cadps2* in the SOC of P28 $Chat^{Cre}$; $Igs7^{GFP}$ mice. *Cadps2* is expressed in both LOC and MOC neurons in the lateral superior olive (LSO) and the ventral nucleus of the trapezoid body (VNTB), respectively (n = 3 mice). Scale bar, 50 μm. **(D)** HCR in-situ hybridiziation of *Cadps2* in the facial motor nucleus (VII). No *Cadps2* expression was detected in facial motor neurons (n = 3 mice). Scale bar, 50 μm. **(E)** Volcano plot denoting differential expression of transcription factors, guidance, and adhesion molecules between OCNs and FBMNs at P1-P5. Red, genes with an average log fold change >0.75 and $p < 10^{-10}$ (Wilcoxon rank sum test, Bonferroni post-hoc correction). Blue, genes with *an average log fold change* < *0.75 and* $p < 10^{-10}$. **(F)** Selected differentially expressed transcription factors between OCNs and FBMNs. **(G)** OCNs and FBMNs differ in the expression of functionally relevant genes, including genes required for synthesizing GABA and the serotonin receptor *Htr2c*. **(H, I)** *In situ* hybridization on a coronal section of a P56 mouse brain verifies that *Gad2* is expressed in the LSO and VNTB **(H)** but not the facial motor nucleus **(I)**. Both images are from the Allen Mouse Brain Atlas[257]. Scale bars, 420 μm.

Olivocochlear neuron subtypes are transcriptionally distinct

Although OCNs share several properties that broadly distinguish them from FBMNs, OCNs are themselves heterogeneous, with different subtypes playing distinct roles in auditory circuitry. As such, MOCs and LOCs comprise transcriptionally distinct cell types, with differential expression of genes in several key families, including transcription factors, adhesion molecules, and neurotransmitter receptors (**Figures 2.3, S6-10**). Our sequencing data includes two main clusters of OCNs, which we identified as MOCs and LOCs based on expression of known markers for

each subtype (**Figure 2.3B-E**). The Na,K-ATPase ATP1A3 was previously reported to be selectively expressed in MOCs in mature rats[258]. We found that *Atp1a3* is expressed in both MOCs and LOCs developmentally, but becomes enriched in MOCs in adulthood (**Figure 2.3B, C**). Conversely, Ucn is a peptide known to be expressed in only LOCs[43,259]. At the transcriptional level, *Ucn* expression is restricted to LOCs throughout postnatal development (**Figure 2.3D, E**). However, *Ucn* is only expressed in a subset of LOCs, and is largely absent at neonatal timepoints. These findings highlight the importance of identifying novel markers for OCN subtypes that selectively label the entirety of each population across developmental stages.

To that end, we identified several genes that were enriched in either the MOC or LOC cluster across all three timepoints and verified their expression in mature animals using *in situ* hybridization (**Figures 2.3F-M, S5**). *Bmp3* and *Col4a4* are expressed in virtually all LOCs in P26-P28 animals, whereas *Zfp804a* and *Kcnip4* are expressed in virtually all MOCs, as well as many FBMNs (**Figure S5**). These findings serve as further validation of the identity of MOC and LOC clusters in our sequencing data, as well as offering potential markers that may be useful for anatomically distinguishing MOC and LOC neurons.

In mature animals, OCN subtypes are integrated into distinct circuits, varying in both their inputs and downstream targets[27]. Retrograde tracing experiments using pseudorabies virus indicate that OCNs receive projections from numerous brain regions, including auditory cortex, the pontine dorsal raphe, and inferior colliculus, as well as inputs from within the auditory brainstem[255,260]. MOC neurons have also been shown to respond to numerous neurotransmitters and modulatory substances, including enkephalin, serotonin, glutamate, GABA, and glycine[256,261]. Less is known about the inputs that may drive or modulate LOC activity.

Figure 2.3. MOCs and LOCs exhibit distinct gene-expression profiles. (A) Heatmap summarizing expression of 368 genes that are differentially expressed between MOCs and LOCs both neonatally and in adults ($p < 0.05$, Wilcoxon rank sum test, Bonferroni post-hoc correction). Plot includes all genes expressed in at least 10% of either OCNs or FBMNs with an average log fold change greater than 0.25. For visualization purposes, scaled expression levels were capped at -2.5 and 2.5. **(B)** Feature plot denoting normalized expression of the published MOC marker *Atp1a3*. Across timepoints, *Atp1a3* is expressed quite broadly, including in LOCs. For visualization purposes, normalized expression levels were capped at the 95th percentile. **(C)** Violin plot summarizing expression of *Atp1a3* in MOCs and LOCs neonatally and in mature animals. *Atp1a3* expression becomes enriched in MOCs only after the first postnatal week. **(D, E)** The LOC-specific gene *Ucn* was detected in a subset of LOC neurons and is not expressed in MOCs. **(D)** Feature plot denoting the expression of *Ucn* in the combined dataset. **(E)** Violin plot showing the expression of *Ucn* in MOCs and LOCs at neonatal and adult stages. *Ucn* expression in LOCs is minimal at both P1 and P5 and is upregulated by P26-P28. **(F-I)** HCR in-situ hybridization on P27 *Chat^{Cre}; Igs7^{GFP}* animals validates novel OCN markers. In keeping with the expression patterns detected in our mature OCN sequencing data, LOC-enriched genes *Bmp3* **(F)** and *Col4a4* **(G)** are largely restricted to the LSO, whereas MOC markers *Zfp804a* **(H)** and *Kcnip4* **(I)** are expressed in cholinergic cells of the VNTB but not the LSO. Arrowheads, co-localization of Chat-Cre-driven GFP expression and HCR puncta in the LSO. Hollow arrowheads, co-localization in the VNTB. Scale bars, 50 μm.

Figure 2.3 (Continued)

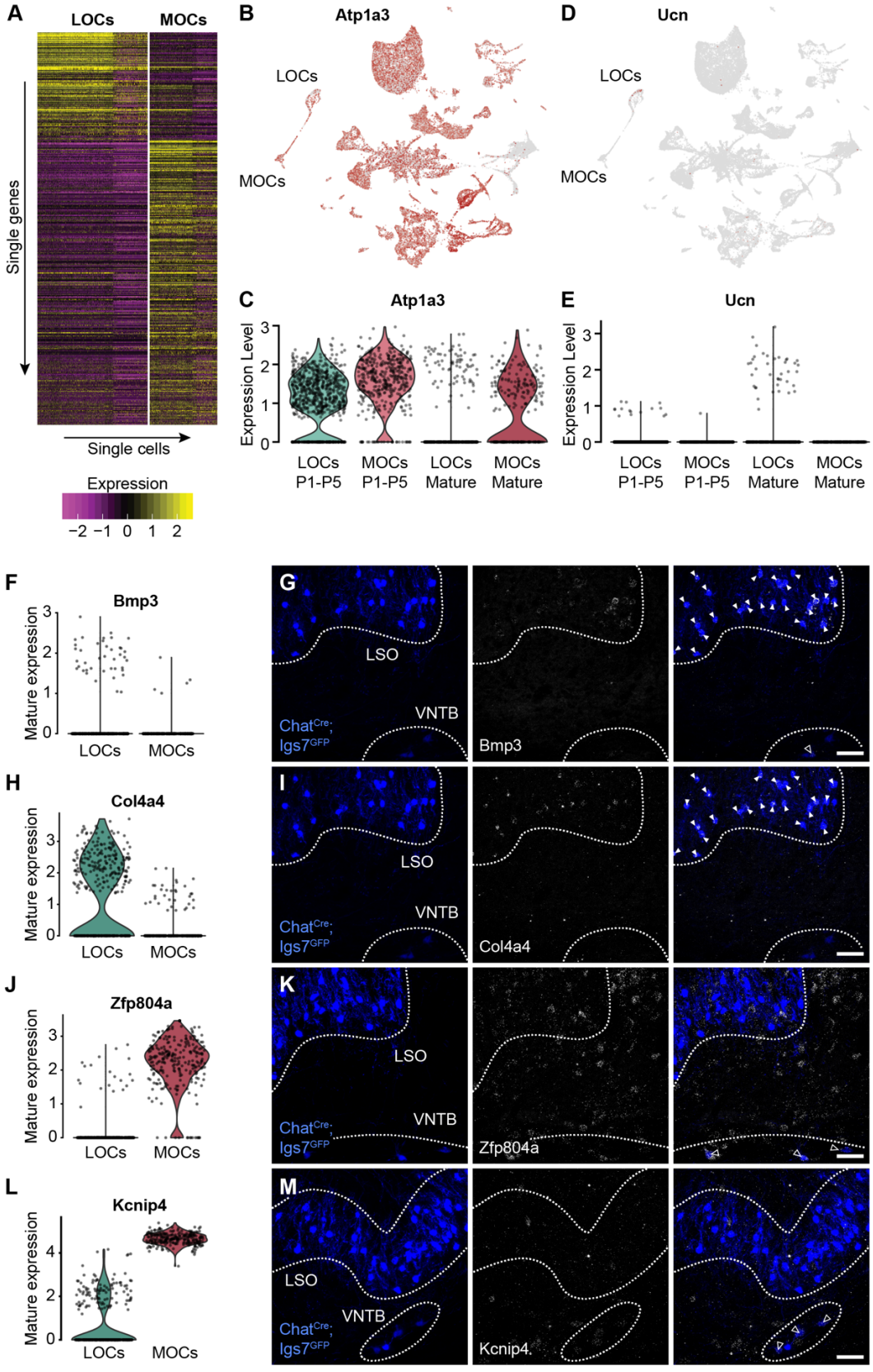

Our sequencing data indicates that MOC and LOC neurons are both positioned to respond to an array of neurotransmitters, including GABA, glycine, acetylcholine, and glutamate (**Figures 2.4A-D, S6**). Although many genes for receptors and receptor subunits are shared between MOCs and LOCs, other genes are differentially expressed between OCN subtypes, indicating that OCNs may respond differently to similar kinds of inputs (**Figures 2.4B-D, S7**). For example, although both MOCs and LOCs express the $G_{i/o}$-coupled muscarinic acetylcholine receptor *Chrm2*, MOCs also express the G_q-coupled receptor *Chrm3* (**Figure 2.4C**). This indicates that cholinergic inputs may affect OCNs differently, causing inhibition in LOCs and more variable effects in MOCs. Similarly, although both MOCs and LOCs express several different glutamate receptors, NMDA receptors are enriched in MOCs (**Figure 2.4D**). This divergent expression implies that MOCs and LOCs may exhibit differences in synaptic plasticity. Because both types of neurons can be driven by auditory inputs, variations in synaptic plasticity may affect how each of these neuronal types responds to extended sounds.

In other cases, differences in receptor expression between OCN subtypes suggests that MOCs and LOCs may receive distinct types of inputs entirely. In mature animals, MOCs preferentially express the opioid receptor *Oprm1*, which reflects previous work showing that MOCs can be modulated by enkephalins (**Figure 2.4E**)[256]. Conversely, only LOCs express the orexin receptor *Hcrtr2* (**Figure 2.4F**). It is possible that these divergent inputs mirror differences in the function of OCN cell types. For example, LOCs can exert long-lasting, modulatory effects on SGNs. Perhaps orexin, which also acts on long timescales to promote arousal, plays a role in these slow-acting LOC effects. Future work should verify whether LOCs indeed respond to the application of *Hcrtr2* receptor agonist[262] or to the stimulation of orexinergic fibers[263] *in vitro.*

Questions also persist about how OCNs affect their downstream circuitry. Previous work has postulated that LOCs, in particular, express a cornucopia of signaling molecules, including enkephalins, dynorphins, dopamine, serotonin, and various neuropeptides[41,42]. We detected expression of *Gad2* and *Chat* in both MOC and LOC clusters (**Figures 2.2G, 2.4G**), consistent

with previous reports indicating that most OCNs are both cholinergic and GABAergic[264]. However, we did not detect notable expression of *Th*, *Penk*, or *Pdyn*, genes involved in the production of dopamine, enkephalines, and dynorphins, respectively (**Figure 2.4G**). Because single-nucleus sequencing experiments can fail to detect transcripts, especially for genes expressed at relatively low levels, we also performed *in situ* hybridization for *Th*, *Penk*, and *Pdyn* (**Figure 2.4H, I**). Although we detected all three of these transcripts nearby the LSO, we did not detect expression of *Penk* or *Pdyn* in the LSO and observed *Th* expression in cholinergic LOC neurons in only a small handful of cases (n = 3 animals). Previous work has shown that *Th* expression in LOCs is upregulated after sound exposure[48]. In that light, the absence of *Th* expression in unexposed animals is unsurprising. Dopaminergic cells may also comprise a distinct and rare set of non-cholinergic LOCs[44]. If that is indeed the case, our sequencing data would exclude this cohort of OCNs, since we only collected cells expressing Chat-Cre. Future studies could address this question directly by injecting dye into the ear and collecting labeled OCNs via patch-seq[265] or laser capture microdissection.

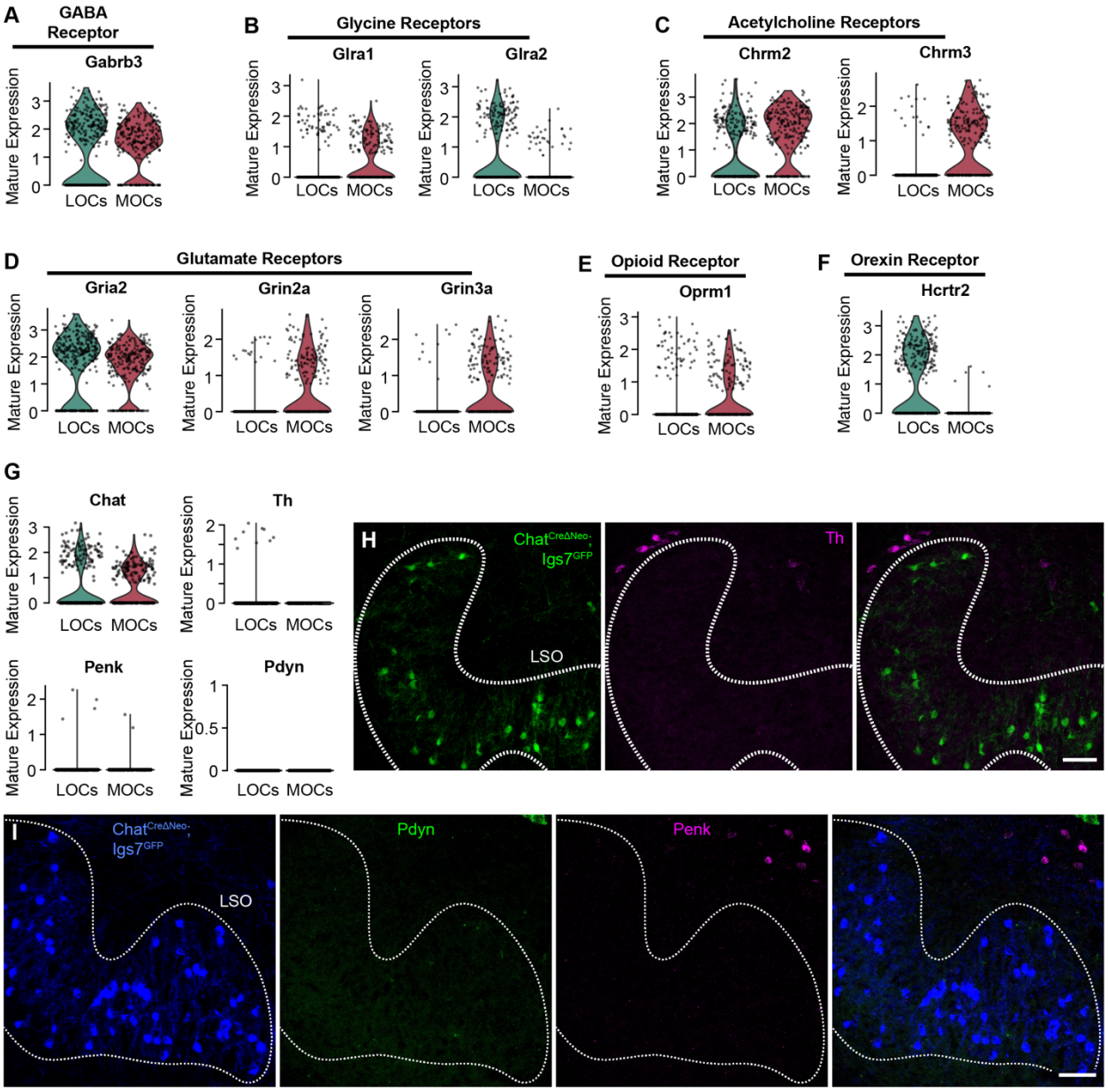

Figure 2.4. Functionally relevant differences in OCN subtypes. (A-F) Violin plots denoting normalized expression levels of genes for neurotransmitter receptor subunits. Both MOCs and LOCs have the ability to respond to numerous neurotransmitters, including GABA **(A)**, Glycine **(B)**, acetylcholine **(C)**, and glutamate **(D)**. In several cases, however, MOCs and LOCs express different receptor subunits or different classes of receptors (B-D). MOCs and LOCs also differ in their expression of more specialized receptors, including the mu opioid receptor *Oprm1* **(E)** and

Figure 2.4 (Continued)

the orexin receptor *Hcrtr2* **(F)**. **(G)** Both MOCs and LOCs express *Chat*, but our scRNAseq database did not detect expression of genes that would indicate expression of dopamine (*Th*) or opoid peptides (*Penk*, *Pdyn*), both of which have been suggested as neurotransmitters in LOCs. **(H-I)** HCR *in situ* hybridization for neurotransmitter-related genes in coronal sections of P28 $Chat^{Cre\Delta Neo}$; $Igs7^{GFP}$ animals. Scale bars, 50 µm. **(H)** Although *Th* (magenta) was detected in the vicinity of the LSO, it was not widely co-expressed in LOCs (green; n = 3 mice). **(I)** Neurons expressing *Pdyn* (green) and *Penk* (magenta) can be found dorsal to the LSO. No expression of *Pdyn* or *Penk* was detected in LOCs (blue; n = 3 mice).

Subsets of lateral olivocochlear neurons vary in neurotransmitter expression

Several previous studies have suggested that LOCs may themselves be divided into multiple subtypes. Anatomical studies have identified LOC fibers with distinct morphologies in the cochlea, with some fibers forming synapses over a relatively narrow domain while others stretch through long stretches of the cochlea[49,50]. These morphological differences were largely traced back to distinctions between LOCs with cell bodies inside or outside the LSO, but other work indicates that heterogeneity might also exist within LSO-intrinsic LOCs. In particular, the peptide Ucn was shown to localize to LOCs in only the lateral region of the LSO in gerbils[43]. Functional work has also suggested that LOCs may exert various effects on SGNs: indirectly stimulating LOC fibers by injecting current into the inferior colliculus can cause either excitation or inhibition of auditory nerve fibers[51]. Together with previous work suggesting that Ucn and TH are confined to only subsets of LOCs[43,44], it is reasonable to suspect that LOCs might contain multiple functional subtypes.

To address this question, we sub-clustered our OCN data, focusing on differences among LOCs. Because OCN properties emerge over postnatal development (**Figure 2.6**), we looked specifically at differences in mature OCNs. We extracted the OCNs from our adult dataset and re-clustered them to identify any subtypes of MOC and LOC neurons. The resulting data includes five clusters (**Figure 2.5**). Based on expression of our previously validated MOC and LOC markers, we identified a large cluster of MOCs (230 cells) and two main clusters of LOCs (242 cells, 75 cells). We also identified two smaller groups containing only 21 cells each. One localizes close to LOC neurons on the UMAP but does not express LOC markers *Col4a4* or *Bmp3*. The other localizes closer to MOCs and expresses several MOC markers. However, only 65 genes were differentially expressed between this small offshoot cluster and the main cluster of MOCs; none of these genes could conclusively specify the identity of these cells. This smaller cluster may represent a unique, sparser subtype of MOCs. Alternatively, they may contain a different cell type, like vestibular efferent neurons, or a series of doublets that include MOC neurons.

Among the two clusters of LOC neurons, we found that one population includes an upregulation of genes for the neuropeptides CGRP, CGRP-II, NPY, and Ucn (**Figure 2.5**). The fraction of mitochondrial genes detected does not vary between OCN subtypes, nor does the number of genes or UMI detected (**Figure 2.5H-J**). This suggests that these cell types correspond to genuine differences between LOC neurons and not mere technical artifacts. The transcription factor *Meis1* is also differentially expressed across OCN cell types, with high expression in MOCs and peptidergic LOCs, but low expression in other LOCs (**Figure 2.5O**). *Meis1* is a Hox cofactor that interacts with other genes in the Hox regulatory network to direct aspects of spinal motor neuron identity[253]. Its variable expression across OCN subtypes may indicate that similar gene regulatory networks are in play to establish properties of different OCN populations.

LOC subtypes also differ in their expression of several guidance and adhesion molecules, suggesting that peptidergic and non-peptidergic LOCs may have distinct targets in the cochlea. *Tenm3*, *Unc5c*, and *Epha6* are all enriched in the main LOC cluster, whereas *Tenm2* is expressed

at higher levels in peptide-enriched LOCs (**Figure 2.5P-S**). Differential expression of these cell-surface receptors and adhesion molecules may guide subsets of LOCs to synapse onto different SGN subtypes or to preferentially innervate different regions of the cochlea. Indeed, previous work found Ucn signal in the base and middle turns of the cochlea, but not in the apical turn[43]. More generally, LOC neurons are organized along a tonotopic gradient, with cells in the lateral wing of the LSO preferentially targeting low-frequency regions of the cochlea and cells in the medial wing targeting high-frequency regions[29,31]. Peptidergic LOCs are confined to the medial segment of the LSO (**Figure 2.5T, U**), suggesting that they likely do have tonotopic bias in their innervation of the cochlea. Disentangling the signals that guide this defined subset of LOCs to their appropriate targets in the ear is therefore likely to shed light on the broader question of how OCNs coordinate their positions along the tonotopic axis in both the cochlea and the brainstem.

Figure 2.5. LOC neurons include a peptide-enriched subset. (A-F) UMAP summarizing sub-clustering results of 590 OCNs from 32 *Chat*^{Cre}*; Rosa26*$^{Sun1\text{-}GFP}$ animals (P26-P28). **(A)** OCNs sub-cluster into five different groups. **(B)** Each detected OCN cluster includes data from all four independent collection rounds (Dataset 1-4), indicating that these clusters do not only reflect technical variability between batches. **(C-F)** Feature plots denoting normalized expression levels of various genes. For visualization, the upper level of expression was capped at the 95th percentile. **(C, D)** Clusters can be divided into major subtypes of OCNs based on their expression of the MOC marker *Zfp804a* **(C)** and the LOC marker *Col4a4* **(D)**. **(E, F)** The two LOC clusters differ in their expression of the neuropeptide genes *Calca* **(E)** and *Ucn* **(F)**, suggesting functional differences. **(G)** Volcano plot summarizing differences in gene expression between peptidergic and non-peptideric LOCs. Red, genes with $p < 10^{-10}$ and average log fold change > 0.5 (Wilcoxon rank sum test, Bonferroni post-hoc correction). Blue, genes with $p < 10^{-10}$ and average log fold change < 0.5. Green, genes with average log fold change > 0.5 and $p > 10^{-10}$. **(H-S)** Violin plots showing expression of various genes between MOCs, LOCs, and peptidergic LOCs. Only the main MOC cluster is included for comparison. **(H-J)** Peptidergic and non-peptidergic LOCs do not have major differences in the percent of mitochondrial genes **(H)**, number of UMI **(I)**, or number of genes detected **(J)**, indicating that differences between LOC clusters are not reducible to technical variability. **(K-N)** Expression of several neuropeptides is enriched in the peptidergic sub-cluster of LOCs, including *Calca* **(K)**, *Calcb* **(L)**, *Npy* **(M)**, and *Ucn* **(N)**. **(O-S)** LOC subtypes also vary in their expression of the transcription factor *Meis1* **(O)** and the guidance and adhesion molecules *Tenm2* **(P)**, *Tenm3* **(Q)**, *Unc5c* **(R)**, and *Epha6* **(S)**, suggesting that they may have distinct downstream targets. **(T)** In-situ hybridization for *Ucn* in a P32, *Chat*^{Cre}*; Rosa26*^{tdTomato} animal. Ucn expression is localized to the medial wing of the LSO in adult animals. Scale bar, 100 μm. L, lateral; M, medial. **(U)** HCR in-situ hybridization for Calca in a P27 *Chat*^{CreΔNeo}*; Rosa26*^{tdTomato} animal. Although *Calca* is expressed in LOCs throughout the LSO—and in MOCs—its expression level is highest in cells in the medial LSO. Scale bar, 100 μm.

Figure 2.5 (Continued)

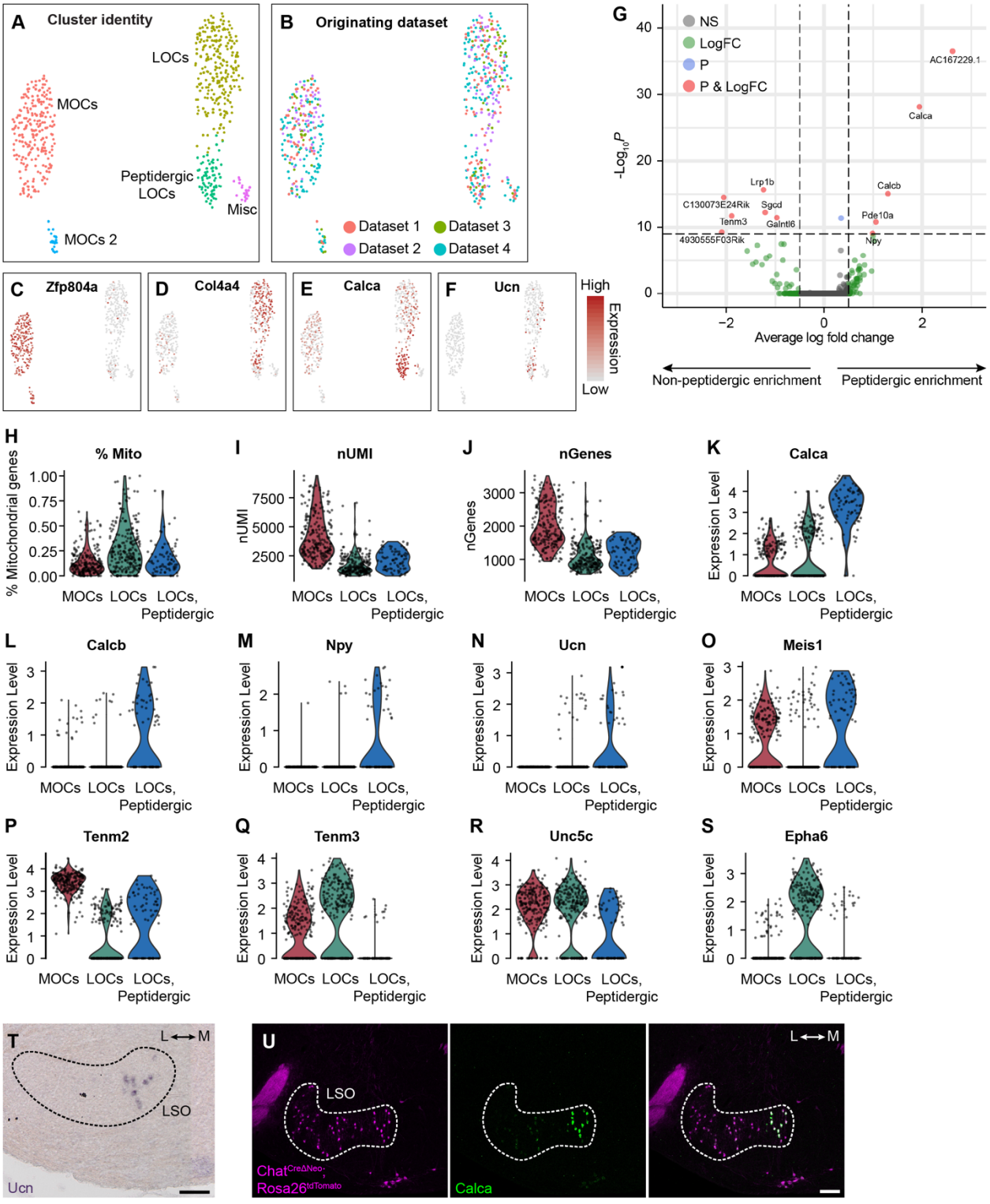

Mature OCN properties emerge over postnatal development

Auditory circuitry is gradually refined over the first four postnatal weeks: tonotopic fields are narrowed[3]; SGNs acquire their mature firing properties[224]; MOCs alter their projections, leaving their transient connection with IHCs and forming synapses with OHCs[266]; LOCs arrive at the sensory epithelium and synapse onto type I SGNs[266]. Commensurate with these many structural changes, OCNs alter their gene expression profiles during postnatal development, downregulating genes associated with neuronal development while also changing the expression of transcripts involved in neuronal signaling (**Figure 2.6**). For example, both MOCs and LOCs decrease the expression of cell-surface receptors and cell adhesion molecules like *Ncam2* and *Robo1* (**Figure 2.6C**). Both MOCs and LOCs also showed an increase in glial genes like *Plp1* and *Mbp* at the mature timepoint, likely reflecting increased contamination from the larger population of oligodendrocytes present by P26 (**Figure 2.6A, B**).

Changes in other gene categories may mirror developmental shifts in maturing auditory circuits. Alterations in expression of neurotransmitter receptors, for instance, may indicate changes in the types of inputs OCNs receive across developmental stages. Previous work has documented a decrease in expression of the GABA A receptor β2/3 subunit and an altered response to GABA in the LSO of gerbils between P4 and P14[267,268]. This observation may indicate that responses to GABAergic signals change throughout postnatal development, possibly because GABA is playing a role in the refinement of these circuits.

In keeping with these results, we detected lower expression of the GABA A receptor β2 subunit, *Gabrb2*, in LOCs at P26-P28 compared to P1-P5. Both MOCs and LOCs also downregulated several other receptors, including the GABA receptor subunits *Gabra1* and *Gabra2* and the glutamate receptors *Grid1* and *Grin2b*. Other changes are subtype-specific: LOCs transiently express genes for nicotinic acetylcholine receptor subunits *Chrna7* and *Chrna3*, downregulating both genes by P26-P28 (**Figure 2.6E**). Conversely, both populations of OCNs increase expression of the glycine receptor subunit *Glra1*, a finding consistent with previous work

showing an increase in responses to glycine and an elevated expression of gephyrin, a glycine receptor anchoring protein, during postnatal development of the LSO[267,268].

Both OCN subtypes also change their expression of various ion channels, indicating that aspects of neuronal excitability are likely altered during the first few postnatal weeks. For example, both MOCs and LOCs show a decrease in the expression of the voltage-gated potassium channels *Kcnq5* and *Kcnq3*, while MOCs upregulate expression of the inward-rectifying potassium channel *Kcnj3* (**Figure 2.6D**). A variety of chloride channels and transporters are also preferentially expressed developmentally, including *Clcn5* and *Slc12a5*. Changes in chloride channel and transporter expression correlate with known changes in the synaptic properties of LSO neurons in rats: during the first few postnatal days, GABA and glycine exert a depolarizing effect, which transitions to a hyperpolarizing effect more typical of adult neurons by the end of the first postnatal week[269–271]. This shift in GABA responsivity is mediated by a change in intracellular chloride concentration. Mature LSO neurons integrate excitatory inputs from the ipsilateral ear with inhibitory inputs from the contralateral ear to mediate sound localization. Early excitatory responses to GABA may therefore serve as inputs to a coincidence detector, allowing LSO neurons to generate a precise tonotopic map by matching frequency-specific inputs across ears.

Prior work has shown that LOCs are arranged tonotopically with respect to their projections into the cochlea[28,31]. However, almost nothing is known about the tonotopic specificity of LOC inputs, and even less is known about the tonotopic arrangement of MOC inputs and outputs. Our data reveals many similarities between postnatal development of olivocochlear neurons and the maturation of other neurons within the LSO, suggesting that MOC and LOC neurons may participate in a period of synaptic refinement similar to that of nearby afferent neurons in the auditory brainstem. Conversely, several of the changes we identified have not been previously reported in other cell types of the auditory brainstem and merit further investigation. For example, the function of the transiently expressed nicotinic acetylcholine receptor subunits *Chrna7* and *Chrna3* remain unclear. Changes in these subunits may reflect

developmental changes that are specific to LOC neurons, or they may be a part of a broader pattern of developmental change throughout the LSO that was previously unappreciated.

Throughout this period, OCNs also alter their neurotransmitter expression, turning on expression of the gene *Calca* (**Figure 2.6E**). Previous studies have also identified changes in expression of neurotransmitter-related molecules in the LSO of hamsters and gerbils, suggesting that the postnatal onset of various neurotransmitters is a conserved aspect of OCN maturation[43,272]. In gerbils, an earlier study identified a switch from *Gad2* (Gad65) in LOCs of neonatal animals to expression of *Gad1* (Gad67) in mature animals[272]. In contrast, we identified higher levels of *Gad2* than *Gad1* at both neonatal and adult timepoints, perhaps due to species-specific differences in OCN circuitry (**Figure 2.2G**).

Variations in gene expression across development are likely coordinated by shifting cohorts of transcription factors. We identified several transcription factors whose expression changes across postnatal development, many of which are shared between MOCs and LOCs (**Figure 2.6F**). Joint changes in transcription factor expression might indicate that some shared regulatory pathways govern the postnatal maturation of both subtypes of OCNs. Indeed, we identified no transcription factor genes that were significantly upregulated in only MOCs or LOCs with a log fold change greater than 0.5. This finding might indicate that transcription factors contributing to the specific identity of MOC or LOC neurons are already present by P1 and simply interact with new classes of transcription factors that turn on later in development to guide subtype-specific patterns of gene expression during postnatal maturation. Alternatively, expression of subtype-specific transcription factors may be restricted to subsets of MOCs or LOCs, and therefore cannot be detected when all MOCs or LOCs are analyzed as a group.

The time course of these changes in gene expression merits also further study; in the absence of intermediate timepoints between P5 and P26, it is unclear when exactly specific attributes are changing. One hypothesis is that gene expression profiles are largely stabilized around the onset of hearing. Changes in expression of GABA receptor subunits in gerbil happen

around P12-P13, roughly corresponding with the onset of hearing[267,268,273,274]. However, other changes—particularly in expression of chloride channels and exchangers—seem to happen earlier, during the first postnatal week[269–271]. Clarifying the timing of specific alterations in synaptic properties may also shed light on longstanding questions about the establishment and tonotopic refinement of auditory brainstem circuitry more generally.

Figure 2.6. MOC and LOC neurons alter their gene expression across postnatal development. (A, B) Volcano plots denoting changes in gene expression between P1-P5 and P26-P28 animals in LOCs **(A)** and MOCs **(B)**. All labeled genes have an average log fold-change >1 and $p < 10^{-10}$ (Wilcoxon rank sum test, Bonferroni post-hoc correction). Blue, genes passing threshold for log fold change but not significance. An increase in glial genes was also detected in both MOCs and LOCs, likely reflecting increased contamination from the myelination present in the mature brainstem (dark grey). **(C-F)** Both types of OCNs regulate the expression of many gene categories over development, including adhesion molecules **(C)**, ion channels **(D)**, neurotransmitters and neurotransmitter receptors **(E)**, and transcription factors **(F)**. Error bars, mean ± SEM.

Figure 2.6 (Continued)

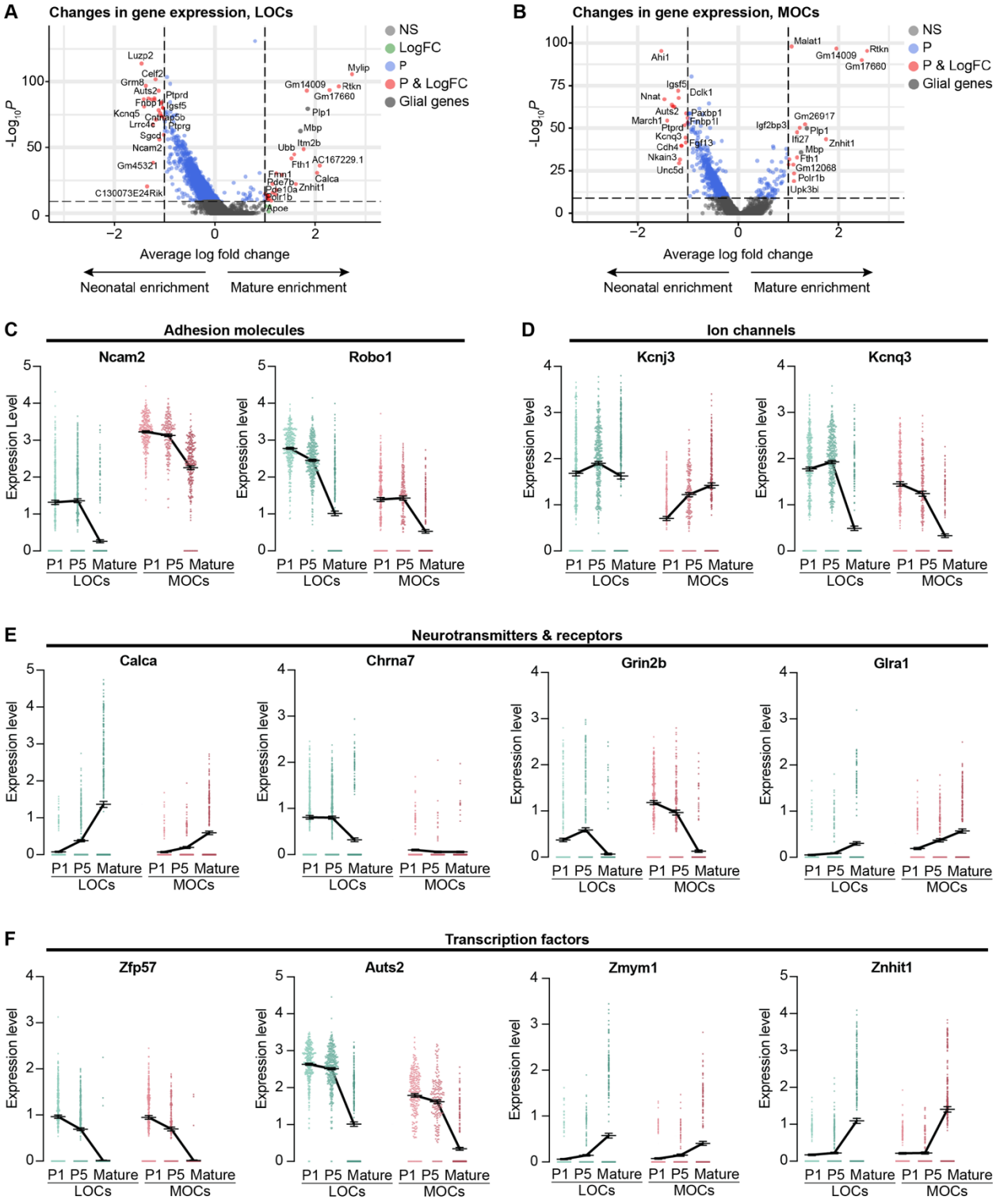

METHODS

Single-nucleus sequencing

For P26-P28 datasets, animals were *Chat*^{Cre}*; Rosa26*$^{Sun1\text{-}GFP}$. For P1 and P5 collections, animals were Chat^{CreΔneo}; *Rosa26*$^{Sun1\text{-}GFP}$. Each individual collection contained pooled tissue from 5-11 animals of both sexes. In total, collections included the following: P1, 8 males and 5 females; P5, 7 males and 9 females; P26-P28, 20 males and 12 females. All animals were on a mixed background of C57BL/J;129S6. First, we dissected out tissue from the ventral brainstem. In adults, we collected roughly the ventral half of the brainstem, in a fragment of the hindbrain that included the entire SOC as well as the FBMNs (**Fig. 2.1A**). In P1 and P5 animals, we used a brain matrix (Zivic Instruments BSMNS001-1) to align the brains, then removed a segment of approximately 2 mm along the rostral-caudal axis, beginning at the front of the brainstem and extending caudally to include the FBMNs. When it was possible to do so without damaging the tissue, we also removed the dorsal portion of the brain.

Tissue was dissected into an ice-cold buffer solution containing 0.25 M sucrose, 25 mM KCl, 5 mM $MgCl_2$, 1M Tricine-KOH, 1 μM tetrodotoxin (TTX), 50 μM APV, and 20 μM DNQX. After all tissue was dissected, brains were pooled together and placed into a dounce homogenizer containing 25 mM KCl, 5 mM $MgCl_2$, 1M Tricine-KOH, 1 mM DTT (Sigma D0632), 150 uM spermine tetrahydrochloride (Sigma S1141), 500 uM spermidine trihydrochloride (Sigma S2501), 80 u/mL RNAsin Plus RNase Inhibitor (Promega N2615), and one tablet of protease inhibitor cocktail (Roche 11836170001). Midway through homogenization, we added IGEPAL CA-630 (Sigma I8896) to a final concentration of 0.32%. Tissue was homogenized until no visible chunks of tissue remained, at which point we filtered the homogenate through a 40 μm cell strainer. Next, we added 5 mL of 50% iodixanol (OptiPrep Density Medium, Sigma D1556) with 7.5 mM KCl, 1.5 mM MgCl2, 6 mM Tricine-KOH, pH 7.8, and 80 u/mL RNAsin. Next, about 9 mL of homogenate was added to a density gradient of 30% and 40% iodixanol. The entire density gradient was spun down for 25 minutes at 10,000 g at 4°C. After removing the majority of the top layer, we extracted

400 µL of solution from the interface of the 30% and 40% iodixanol layers. Next, we added 600 µL 1% BSA in PBS and 10 µL of Draq7 to stain the dissociated nuclei. Finally, cells were filtered through a 40 um Flowmi cell strainer (Sigma BAH136800040).

To isolate Sun1-GFP-positive, cholinergic nuclei, cells were sorted on a BD FACSAria II (BD Biosciences). After FAC-sorting, nuclei were spun down at 4ºC for 5 min at 750 rpm and re-suspended in roughly 40 µL of 1% BSA in PBS. Cell concentration was then estimated by counting DAPI-labeled nuclei on a hemocytometer. Next, we loaded the cells into a single-cell 3' chip from 10x Genomics, following the manufacturer's directions. If the estimated cell concentration was greater than 300 nuclei/µL, we divided the sample in half and spread it across two lanes of the 10x Genomics microfluidics chip in order to reduce the proportion of multiplets. Otherwise, we loaded the maximum volume of our sample onto the chip. Mature datasets from P26-P28 animals were processed with the Chromium single-cell 3' library & gel bead kit v2 (10x Genomics, PN-120267); developmental datasets from P1 and P5 animals were processed with the Chromium single cell 3' GEM, library, & gel bead kit v3 (10x Genomics, PN-1000092). cDNA libraries were generated according to the manufacturer's directions. The final libraries were sequenced on an Illumina NextSeq 500 (75 cycle kit).

RNAseq Analysis

Alignment

Raw reads were converted to fastq files using the cellranger pipeline from 10x Genomics, v. 2.1.0-3.0.1. All datasets were aligned to a modified version of the mm10-3.0.0 reference transcriptome using cellranger v. 3.0.2. Because nuclei contain large amounts of unprocessed RNA, the standard mm10 reference transcriptome was altered so that reads were aligned to all annotated transcripts, rather than aligning exclusively to exons.

Filtering and exclusion criteria

Following alignment, data imported into R (v. 3.5.3) and analyzed with the Seurat package (v. 3.1.4)[275]. Initially, each individual library from independent 10x lanes was processed separately to remove low-quality cells and genes that were detected infrequently. Each library was filtered to remove genes that were not detected in at least 3 cells and cells that contained fewer than 500 unique genes. Each library was further filtered to discard any cell in which more than 1% of detected genes were from mitochondria. We chose a relatively strict cutoff for mitochondrial genes because the average mitochondrial content of our libraries was quite low (<0.45% in each dataset); moreover, because we sequenced individual nuclei rather than single cells, the presence of notable amounts of mitochondrial genes likely indicates contamination of RNA from outside the nucleus.

Because libraries from our P1 and P5 collections were prepared with the v3 kit, they had far higher nUMI and nGenes than the mature datasets, which were collected with the 10x v2 kit (median nUMI for developmental datasets was 6,157-10,171; for adult datasets, 1,935-3,978; **Figure S1**). We therefore established different filtering criteria for the developmental and adult data: we kept developmental cells that had more than 1,000 detected UMI and more than 750 genes and adult cells that expressed more than 750 UMI and more than 500 genes. In addition, we excluded some potential multiplets by removing all cells for which the nUMI or nGenes detected was more than two standard deviations away from the mean. We chose a standard deviation-based cutoff rather than a specific upper limit for nUMI or nGenes because the distribution of detected genes and UMI varied between datasets based on variability in sequencing depth.

Normalization and batch correction

After filtering low-quality cells, all libraries generated from parallel collections were merged prior to normalization (that is, all libraries that were collected simultaneously but distributed over

multiple lanes of the 10x microfluidics chip). Data was normalized by fitting the gene counts to a regularized binomial regression function, implemented in the scTransform package for Seurat, as previously described[276]. Next, we accounted for batch effects and variability between developmental and adult data using a CCA-based integration methods implemented in Seurat v. 3, as previously described[275]. We used 3,000 variable genes and 30 dimensions in CCA space for the integration, consistent with previous applications of this method.

After integrating the data, we normalized the counts for each cell by dividing the counts for each gene by the total counts for each cell. These values were then multiplied by 10,000 and natural-log transformed. For visualizing counts on heatmaps, data for each gene was centered around its mean value and scaled by dividing by the gene's standard deviation.

Clustering

To cluster the data, we performed principal component analysis (PCA) on the integration vectors produced in the previous steps. We used the top 21 PCs as input to the clustering algorithm based on the relative amount of variance explained by each PC, as visualized on an elbow plot. Finally, we clustered the data using a graph-based clustering algorithm implemented with the FindNeighbors and FindClusters algorithms in Seurat[275,277], using a resolution of 0.8. The number and proportion of MOCs and LOCs was stable across a range of input parameters, varying by only +/- 2 cells from a resolution of 0.4-1.6 and input dimensions of 16-30 PCs.

Differential expression analysis

Differential expression analysis was performed using a non-parametric Wicoxon rank-sum test on log-normalized counts data, implemented with the FindMarkers function in Seurat. Post-hoc adjustments were performed with a Bonferonni correction based on all genes in the dataset.

Sub-clustering of adult OCNs

To analyze subsets of adult OCNs, data was filtered and normalized as described above. However, in order to focus specifically on subtypes found in mature OCNs, batch correction and integration was applied only to the datasets from P26-P28 animals. After clustering the adult cell types as described above, we identified OCN clusters based on their co-expression of *Gata3* and motor neuron markers like *Isl1* and *Tbx20*. We then subset the data to include only cells in those two OCN clusters and repeated the clustering analysis. The counts data was then log-normalized and scaled prior to differential expression analysis and visualization.

Geneset analysis

Geneset enrichment analysis to identify specific categories of genes expressed in various cell populations was based on previously curated gene lists[278,279] and annotations from the HUGO Gene Nomenclature Committee (HGNC, genenames.org). In total, these genesets included 280 guidance and adhesion molecules, 215 ion channels, 215 neurotransmitter receptors, 1,634 transcription factors, and 120 genes involved in neuronal signaling or neurotransmitter or neuropeptide synthesis.

In-situ hybridization

Colorimetric

Mice were perfused with ice-cold, RNAse-free 4% PFA in 1x Sorenson's buffer. Brains were post-fixed overnight in 4% PFA at 4°C and cryopreserved in sucrose prior to embedding in NEG-50 (Richard-Allen Scientific; ca. no. 6502). Brains were then cryosectioned at 25 µm. All animals were *Chat*^{Cre}*; Rosa26*^{tdTomato} on a mixed background of C57BL6;129S6;CD1. The *in-situ* hybridization protocol was performed as previously described; a detailed protocol is available at http://goodrich.med.harvard.edu/uploads/3/7/7/1/37718659/in_situ.pdf. The *Ucn* probe sequence

was derived from the Allen Brain Atlas (mouse.brain-map.org). Slides were imaged on a VS120 slide scanner (Olympus).

HCR fluorescent in-situ hybridization

As above, mice were perfused with ice-cold, RNAse-free 4% PFA in 1x Sorenson's buffer. All animals were P27-P28 and maintained on a C57BL6 background. Brains were post-fixed overnight in 4% PFA at 4°C and cryopreserved in sucrose prior to embedding in NEG-50. Prior to staining, slides were brought to room temperature and incubated at 50-55°C for 15 minutes. Next, sections were fixed in 4% PFA in PBS for 10 minutes on ice, then rinsed twice in PBS with 0.1% TritonX-100 (Sigma T9284; PBST). Slides were then treated with 1 µg/mL Proteinase K (Sigma P-6556) for 10 minutes at room temperature, rinsed twice with PBST, and fixed again in 4% PFA in PBS on ice. After rinsing twice with PBST, slides were run through an ethanol dehydration gradient of 50%, 70%, and 100% ethanol. After drying, the HCR *in-situ* protocol was followed as previous described[280]. The following probes were synthesized by Molecular Instruments, Inc. and were used in the indicated concentrations: *Bmp3*, 1 pM; *Cadps2*, 2 pM; *Calca*, 1 pM; *Col4a4*, 2 pM; *Kcnip4*, 2 pM; *Zfp804a*, 2 pM. Additional probes were synthesized by IDT and used in the following concentrations: *Penk*, 2 pM; *Pdyn*, 1 pM; *Th*, 1 pM. All stains were imaged on a Leica SP8 confocal microscope.

Animal Models

Rosa26^{tdTomato} (Ai14; Jax strain 007914)[281]; *Igs7*^{GFP} (Ai140D; Jax strain 030220)[282]; *Rosa26*$^{Sun1\text{-}GFP}$ (Jax strain 021039)[248]; *Chat*^{Cre} (Jax strain 006410 and 028861) and *Chat*^{CreΔneo} (Jax strain 031661)[283] are all previously described. *Rosa26*^{tdTomato}, *Igs7*^{GFP}, and *Chat*^{CreΔneo} animals were maintained on a C57BL/6 background. *Chat*^{Cre} and *Rosa26*$^{Sun1\text{-}GFP}$ used for single-cell sequencing experiments were maintained on a mixed background of C57BL/6;129S6. All animal work was

conducted in compliance with protocols approved by the Institutional Animal Care and Use Committee at Harvard Medical School.

CHAPTER THREE

Generation of transgenic models to characterize olivocochlear neuron function

Michelle M. Frank and Lisa V. Goodrich designed all experiments. MMF conducted all experiments with histology assistance from Sarah Yoder, Cheuk Wong, and Mackenzie Hunt.

INTRODUCTION

Researchers have made many advances in understanding the olivocochlear efferent system since it was first described in the 1940s[284]. By taking advantage of differences in the anatomy and function of MOCs and LOCs, it has been possible to isolate contributions that each cell type makes to the development and function of the auditory system. This approach has been particularly fruitful for understanding the MOC system: because nearly all of the contralateral OCN projections arise from the MOCs, it is possible to manipulate the majority of MOCs by stimulating or severing those crossed projections[27]. MOCs also signal to hair cells through an unusual synaptic complex involving the α9/ α10 acetylcholine receptor subunits, which are not expressed in SGNs or elsewhere in the brain[32,33,204,205,279]. The selective expression of this receptor complex has made the α9 and α10 subunits useful tools for examining MOC function, and previous work has made use of both gain- and loss-of-function mutations in these genes to investigate how MOCs influence auditory development and function[204,205,207].

LOCs, however, have proven much more difficult to study. Previous efforts have largely focused on ablating LOCs by lesioning the LSO or on stimulating or severing a combination of MOCs and LOCs and attempting to isolate which effects derive from which cell type after the fact. For example, any effects involving OHC function can safely be ascribed to MOCs[51]. Although these approaches have been valuable in triangulating LOC contributions to auditory function, many questions still remain about LOC development and function still remain. In the absence of reliable markers to distinguish MOC and LOC neurons, many questions also persist about the anatomy of these cell types and how their projections change over the course of development and aging[244].

A more robust understanding of the olivocochlear efferent system—and the LOCs, in particular—therefore hinges on developing genetic tools that offer more precise control over these cell types. In recent years, Chat-Cre[283] has proved to be a useful tool for understanding OCN function, especially as a means of labeling these cells for anatomy and physiology. However,

Chat-Cre is expressed in both MOCs and LOCs, as well as other motor neuron populations, thereby limiting its utility for manipulating OCNs. Instead, a more promising avenue into LOC targeting is the peptide Urocortin (Ucn), which has been shown to be expressed selectively in LOCs—but not MOCs—in both mice and gerbils[43,259]. In addition, an intersectional genetic strategy would allow us to target LOC neurons with even greater specificity, or to use Chat-Cre to manipulate all OCNs without perturbing other motor neurons. This intersectional approach is particularly crucial for studying functional consequences of OCNs in adult animals, as ablating or silencing all cholinergic neurons will result in widespread paralysis, or even death. To that end, *Gata3* is a promising candidate: it is expressed in the OCNs, but mutant analyses indicate that it is never expressed in mammalian FBMNs[101,116,117]. Thus, in order to target both MOCs and LOCs with greater specificity than was previously possible, we generated both Ucn-Cre and Gata3-FlpO mouse lines.

RESULTS AND DISCUSSION

In order to gain specific genetic access to LOC neurons, we used CRISPR/Cas9 to generate a knock-in *Ucn-Cre* allele, inserting sequences for both a T2A peptide and a nuclear-localized Cre recombinase immediately downstream of the *Ucn* coding domain (**Figure 3.1A**). I confirmed that the construct was inserted into the correct genetic locus by PCR-amplifying and sequencing the entire construct, including several hundred base pairs up- and down-stream of the insertion. The sequencing results verified that the *Ucn-Cre* construct was inserted into the correct locus. Sequencing also revealed one point mutation within the *Ucn* coding sequence and two point mutations in the Cre recombinase sequence, likely caused by errors in the ssDNA synthesis process used to generate the homology repair template. However, tdTomato fluorescence is still detectable in mice expressing the Ai14 tdTomato allele[281] under the control of Ucn-Cre, indicating that the Cre recombinase is still functional. Mice heterozygous for Ucn-Cre also have normal auditory brainstem response (ABR) thresholds (n=5; data not shown). Because homozygous *Ucn*

mutants have elevated ABR thresholds, this finding suggests that the point mutation within the *Ucn* coding sequence of the *Ucn-Cre* allele has few, if any, functional consequences, at least in heterozygous animals.

We also verified that *Ucn-Cre* expression in OCNs is restricted to LOC neurons by examining both the brains and cochleae of mice expressing tdTomato under the control of Ucn-Cre. In these $Ucn^{Cre/WT}$; $Rosa26^{tdTomato/WT}$ animals, tdTomato-expressing fibers within the cochlea project extensively beneath the IHCs and do not extend to the OHC region, consistent with an LOC identity (**Figure 3.1B, C**). We did not observe tdTomato expression in any other cell types in the cochlea. Within the SOC, Ucn-Cre activity is confined to the cholinergic cells of the LSO, with no expression among the cholinergic MOCs in the VNTB (**Figure 3.1D**, n = 1). Although *Ucn* mRNA expression in adult mice is restricted to the medial wing of the LSO (**Figure 2.5T**), we observed Ucn-Cre expression throughout the LSO, labeling upwards of 90% of cholinergic LOCs (**Figure 3.1D**, n = 1). The broad activity of Ucn-Cre across the LSO suggests that *Ucn* is expressed more widely across LOCs developmentally than it is in adulthood. This interpretation is consistent with previous work in gerbil, which found that Ucn immunolabeling could be transiently identified in LOCs throughout the extent of the LSO before becoming restricted to the medial wing in adulthood[43].

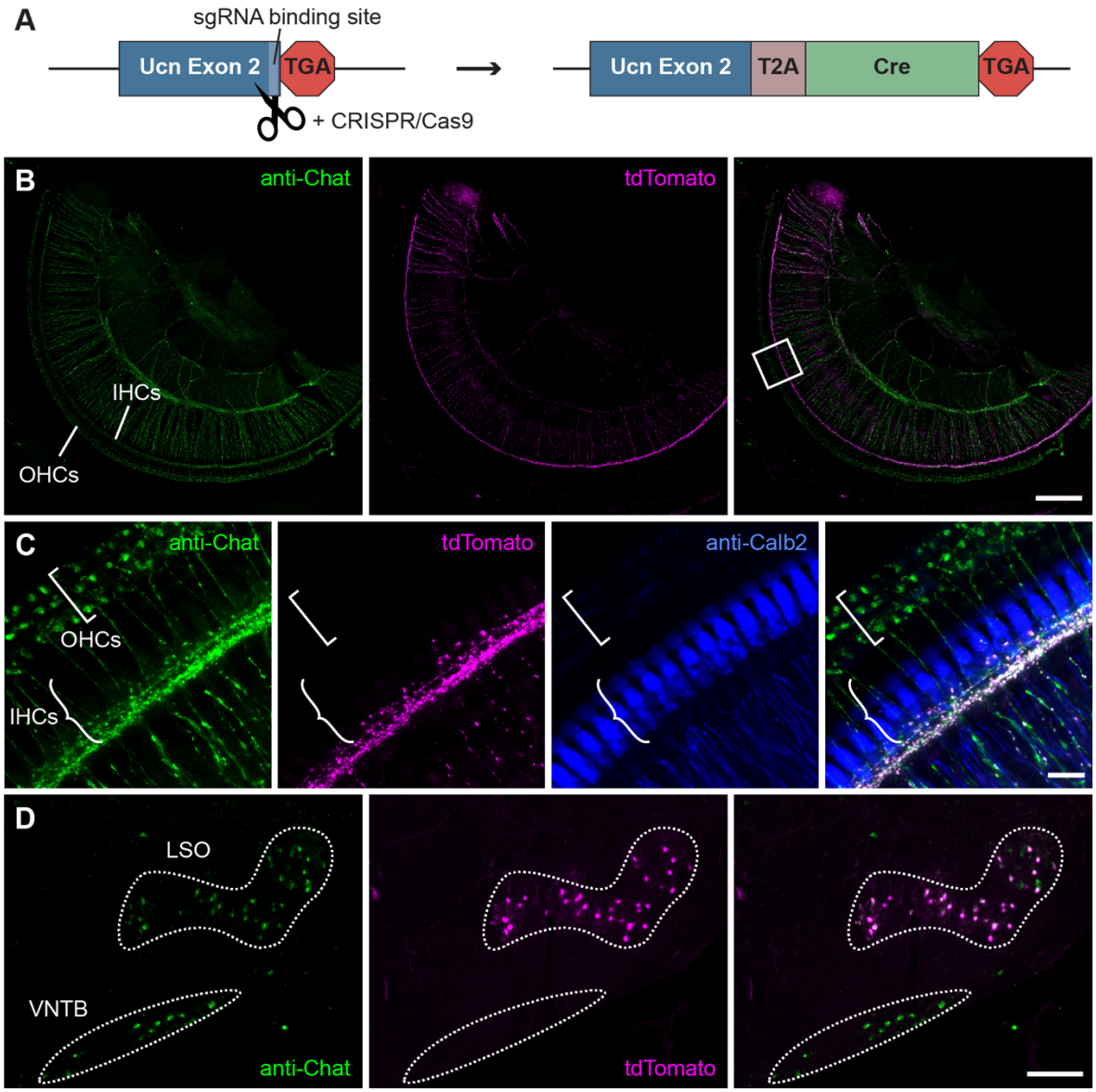

Figure 3.1. Ucn-Cre labels LOCs but not MOCs. **(A)** Schematic of *Ucn-Cre* allele. CRISPR/Cas9 was used to insert a T2A peptide and nuclear-localized Cre sequence immediately after the *Ucn* coding sequence, prior to the *Ucn* stop codon. **(B-D)** Fluorescent images from P27 $Ucn^{Cre/WT}$; $Rosa26^{tdTomato/WT}$ animals. Anti-Chat immunostain (green) labels both MOCs and LOCs. **(B, C)** Standard-deviation projections of confocal z-stacks showing Ucn-Cre-driven tdTomato expression in the middle turn of the cochlea. TdTomato fluorescence (magenta) is visible in the inner hair cell (IHC) region, but not the outer hair cell (OHC) region. **(B)** Scale bar, 150 µm.

Figure 3.1 (Continued)

(C) Ucn-Cre-expressing fibers course beneath the IHCs (labeled with Calb2, blue; curved brackets) and do not extend out to the OHC region (square brackets). Scale bar, 15 μm. TdTomato signal co-localizes with anti-Chat immunolabel, supporting the interpretation that fibers labeled by Ucn-Cre are LOCs. **(D)** Coronal section of the superior olivary complex (SOC). Within the SOC, Ucn-Cre-driven tdTomato expression (magenta) is restricted to the cholinergic cells of the LSO. Scale bar, 150 μm.

Although *Ucn* mRNA expression throughout the adult brain is extremely limited, Ucn-Cre activity is detectable in several other brain regions outside of the LSO, again suggesting that this peptide may be transiently expressed in several other nuclei throughout the brain (**Figure 3.2**). As expected, we identified Ucn-Cre-driven tdTomato fluorescence in the peptidergic Edinger-Westphal nucleus, which is known to express *Ucn*[259,285,286] (**Figure 3.2A, C**). TdTomato expression was also detectable in cortical neurons (**Figure 3.2A, D**), the small cell cap of the cochlear nucleus (**Figure 3.2B, E**), and both the trigeminal and facial branchial motor neurons (**Figure 3.3B, F and G**).

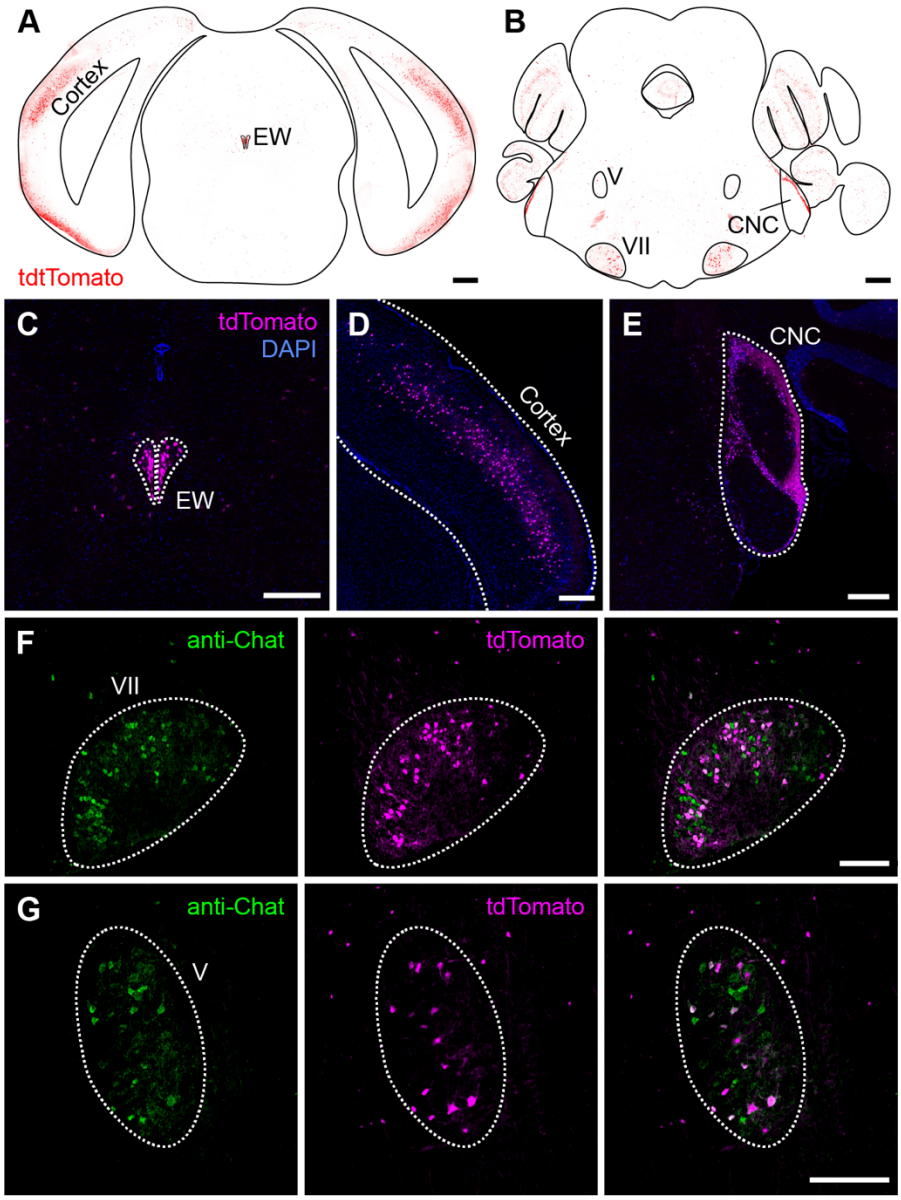

Figure 3.2. Ucn-Cre activity in the brain. (A-G) Coronal sections through a P27 $Ucn^{Cre/WT}$; $Rosa26^{tdTomato/WT}$ animal. **(A, B)** Overview of Ucn-Cre activity in the cortex and midbrain **(A)** or brainstem **(B)**. Scale bars, 500 μm. **(C)** Ucn-Cre-driven tdTomato expression (magenta) is visible in the peptidergic Edinger-Westphal nucleus (EW), a group of cells known to express Ucn. **(D)** Ucn-Cre activity is detectable in several regions of cortex. **(E)** Ucn-Cre labels cells in the cochlear nucleus (CNC). TdTomato expression appears to be confined to the small cell cap region.

Figure 3.2 (Continued)

(F) Ucn-Cre also labels a subset of facial branchial motor neurons (VII), as visualized with anti-Chat immunolabeling (green). **(G)** Ucn-Cre labeling is visible in motor neurons in the trigeminal nucleus (V), as identified with anti-Chat immunolabeling (green). **(C-G)** Scale bars, 250 μm.

The surprisingly broad expression of Ucn-Cre outside the LSO presents a confound for interpreting results of manipulation or ablation experiments driven by Ucn-Cre alone. The expression in the facial motor neurons represents a particular concern, as some facial motor neurons project to the middle ear muscle, triggering a reflex in response to loud sounds[287]. These projections present multiple challenges: any attempt to localize manipulations to LOCs by injecting a Cre-dependent virus into the ear is likely to drive expression in the FBMNs, as well. Moreover, any manipulation that influences both LOCs and FBMNs will be challenging to interpret, as both FBMNs and LOCs can influence hearing. Ablating or silencing a large population of facial motor neurons can also cause more general problems, including facial paralysis, which would preclude using those animals for any kind of behavioral experiment. Therefore, an intersectional strategy that further restricts the cell-type specificity of labeled neurons would be valuable for examining the function of LOC neurons.

To that end, we generated a Gata3-FlpO line. GATA3 is known to play a key role in the development of the auditory system and is expressed in many auditory cell types, including OCNs[117,152]. Moreover, mutant analysis indicates that *Gata3* is never expressed in the FBMNs, making this gene a useful candidate for intersectionally targeting OCNs[101,116,117]. As with Ucn-Cre, we used CRISPR/Cas9 to target the insertion of sequences for a T2A peptide and FlpO recombinase into the *Gata3* locus, immediately before the *Gata3* stop codon (**Figure 3.3A**). As with Ucn-Cre, we verified the insertion of the Gata3-FlpO construct by sequencing the entire

insertion construct, as well as several hundred base pairs up- and down-stream of the insertion. Our sequencing results identified two point mutations within the FlpO sequence, as well as an additional point mutation within the 3' UTR of *Gata3*. However, Gata3-FlpO successfully drives expression of effector alleles, including tdTomato (**Fig. 3.3**), indicating that the FlpO recombinase is still functional. Gata3-FlpO animals are also homozygous viable. Homozygous mutations for *Gata3* are embryonic lethal, indicating that the point mutations in the 3' UTR of Gata3-FlpO do not prevent the production of functional GATA3 proteins.

We investigated the expression pattern of this allele by crossing Gata3-FlpO mice to animals carrying the Ai65F Flp-dependent tdTomato allele[288]. As expected, Gata3-FlpO is active quite broadly throughout the auditory system, and we detected tdTomato fluorescence in many cell types of the cochlea, including SGNs, hair cells, and supporting cells (**Figure 3.3B, C**). In the brain, Gata3-FlpO is expressed throughout the superior olive and inferior colliculus, along with many different cells in the midbrain (**Figure 3.4D-F**). However, we identified very little expression in cortical structures, and no signal in the trigeminal or facial motor neurons (**Figure 3.4D-G**).

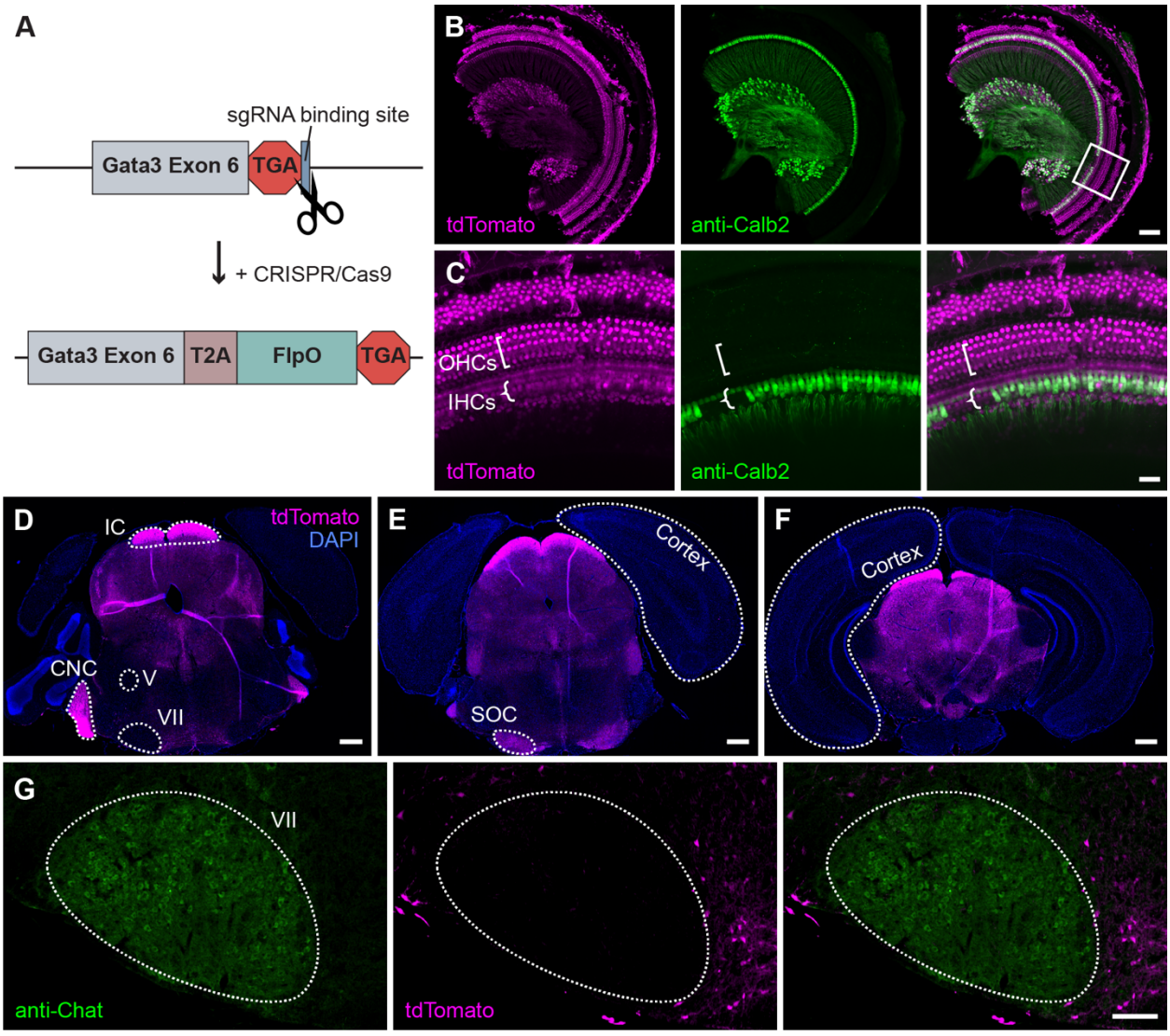

Figure 3.3. Expression pattern of Gata3-FlpO. (A) Schematic of *Gata3-FlpO* allele. CRISPR/Cas9 was used to insert a T2A peptide and nuclear-localized FlpO sequence immediately downstream of the final exon of *Gata3*. **(B, C)** Standard-deviation projections of confocal z-stacks from P28 *Gata3*$^{FlpO/WT}$*; Rosa26*$^{tdTomato/WT}$ cochlea. Gata3-FlpO-driven tdTomato expression (magenta) is detectable in numerous cell types of the cochlea, including Calb2-expressing spiral ganglion neurons and inner hair cells (green). **(B)** Scale bar, 100 μm. Box denotes region of higher magnification shown in (C). **(C)** Curved brackets denote inner hair cells (IHCs). Square brackets denote outer hair cell (OHC) region. Scale bar, 25 μm. **(D-F)** Coronal

Figure 3.3 (Continued)

sections through a P28 *Gata3*$^{FlpO/WT}$*; Rosa26*$^{tdTomato/WT}$ brain. Scale bar, 500 μm. **(D)** Gata3-FlpO is expressed in the cochlear nucleus (CNC) and inferior colliculus (IC), but not in the facial motor nucleus (VII) or trigeminal motor nucleus (V). **(E)** Gata3-FlpO-driven tdTomato expression is present throughout the superior olivary complex (SOC). **(F)** Gata3-FlpO activity is detected quite broadly throughout the midbrain, but not in the cortex. **(G)** No tdTomato fluorescence was detected in the cholinergic facial branchial motor neurons (green). Scale bar, 150 μm.

Together, Gata3-FlpO and Ucn-Cre should offer a way to selectively manipulate LOC neurons without affecting MOCs or many other cell types throughout the brain. We verified the specificity of this approach by examining the intersectional expression of Ucn-Cre and Gata3-FlpO in mice expressing the dual recombinase reporter RC::FLTG, in which only cells that express both Flp and Cre recombinases express GFP[289] (**Fig. 3.4**). As expected, these animals have high expression of GFP throughout the LSO (**Fig. 3.4C, D**). Although we did detect GFP expression sporadically in other brain structures, the total number of cells labeled is much lower than that of either Ucn-Cre or Gata3-FlpO alone. We identified no expression in either the facial motor neurons or the cochlear nucleus, and only limited expression in cortical structures (**Fig. 3.4A, B, E, F**; n = 3).

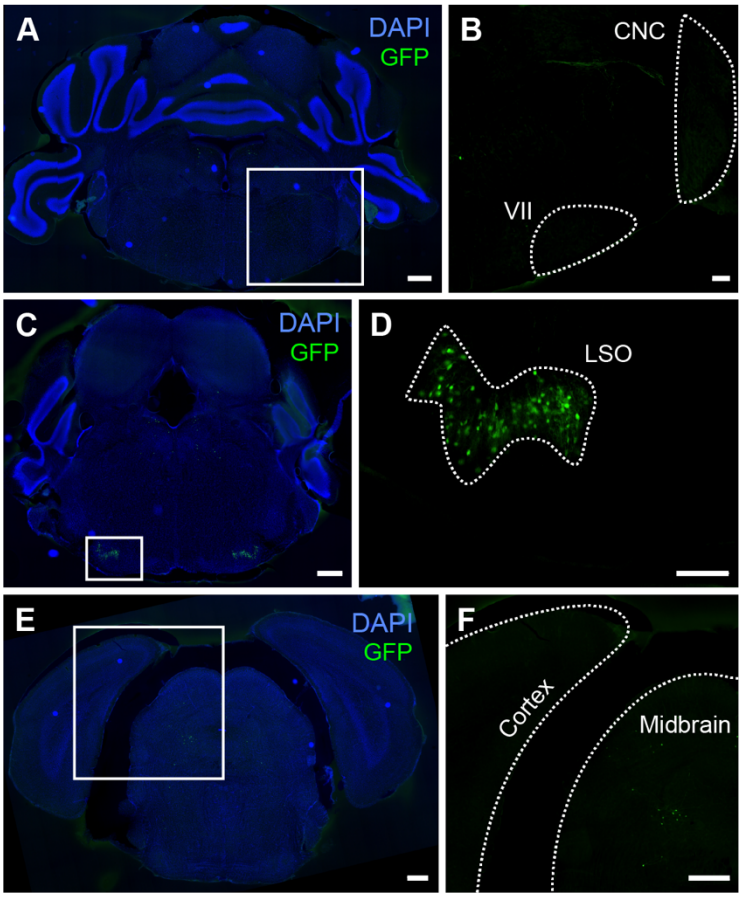

Figure 3.4. Intersectional expression of Gata3-FlpO and Ucn-Cre. (A-F) Coronal sections through the brains of eight-week-old *Gata3*$^{FlpO/WT}$*; Ucn*$^{Cre/WT}$*; Rosa26*$^{FLTG/WT}$ mice. Blue, DAPI. Green, intersectional expression of Gata3-FlpO and Ucn-Cre. **(A, B)** Gata3-FlpO, Ucn-Cre co-expression is extremely sparse throughout the brainstem, and no expression was detected in either the facial motor nucleus (VII) or the cochlear nucleus complex (CNC). **(A)** Scale bar, 500 μm. Boxed area denotes higher-magnification region shown in (B). **(B)** Scale bar, 150 μm. **(C, D)** Within the superior olivary complex, co-expression of Gata3-FlpO and Ucn-Cre was confined to the LSO. **(C)** Scale bar, 500 μm. Boxed area denotes higher-magnification region shown in (D). **(D)** Scale bar, 150 μm. **(E, F)** Sparse GFP expression was detected throughout the midbrain, but in very few cells in cortex. Scale bar, 500 μm. Boxed region in (E) denotes higher-magnification area shown in (F).

This combination of alleles therefore offers a powerful strategy for examining both the anatomy and function of LOCs. In the absence of specific genetic access or anatomical markers, many previous studies have struggled to ascribe LOC contributions to auditory function. Now, however, we have the ability to assign a conclusive LOC identity to any neurons expressing Ucn-Cre and to manipulate LOCs without also perturbing nearby motor neurons or auditory cell types. In the future, these tools should offer new insights into the way that top-down inputs can expand the processing repertoire of the sensory periphery.

METHODS

Generation of transgenic mouse lines

Both Gata3-FlpO and Ucn-Cre mouse lines were generated by homologous recombination via CRISPR/Cas9 targeting, using methods similar to those described previously[290,291]. *FlpO*[292] and *Cre*[293] sequences were directed to the endogenous locus of *Gata3* and *Ucn*, respectively, and inserted directly before the stop codon of each gene **(Fig. 3.1A, 3.3A)**. Single-stranded homology repair templates (Genewiz) included sequences for a T2A peptide[288] and SV40 nuclear localization sequence upstream of the FlpO or Cre recombinase sequence, as well as 400 bp homology arms on each side of the insertion construct. Each homology repair construct also induced a mutation at the targeted PAM site to prevent cutting of the repaired strand. In the *Ucn-Cre* construct, we made a synonymous change in the coding sequence that did not alter the amino acid sequence of the peptide. For *Gata3-FlpO*, we induced a C-to-G mutation within the gene's 3' UTR.

Potential guide RNA sequences were selected based on their proximity to the construct insertion site and their bioinformatically predicted off-target effects[294]. Guide RNAs were then screened *in vitro* to determine their efficacy at cutting a PCR-amplified fragment of target DNA. The final guides for targeting both *Ucn* (ccgcaucauauucgauucgg) and *Gata3*

(uuggagacuccucacgcaug) were synthesized as a combined CRISPR/tracr RNA molecule (Synthego). Finally, the guide RNA and homology repair templates were injected into zygotes of C57BL/6 mice along with Cas9 protein (IDT, Alt-R® S.p. Cas9 Nuclease V3; ca. 1081058) at Harvard's Genome Modification Facility.

Screening transgenic mouse lines

DNA was extracted from a tail clipping of each of the injected animals. We verified that each insertion was correctly targeted to the desired locus by PCR-amplifying specific fragments of the construct and surrounding DNA. Next, we amplified and sequenced the entire inserted construct along with several hundred base pairs on either side of the insertion to verify that the homology repair construct was integrated into the locus as expected. Although the full constructs were inserted correctly in both *Gata3-FlpO* and *Ucn-Cre* mouse lines, we identified a few unexpected point mutations, likely caused by errors in the ssDNA synthesis process. In *Ucn-Cre*, a G-to-T mutation transformed glutamine 104 of the *Ucn* coding sequence into a histidine; a G-to-T mutation in valine 126 of the Cre recombinase sequence turned that amino acid into a phenylalanine; and a synonymous G-to-T mutation in glycine 343 of the Cre sequence had no effect on its amino acid sequence. In *Gata3-FlpO*, a C-to-A mutation in the *FlpO* sequence transformed glutamine 12 into a lysine and a synonymous G-to-A mutation in valine 129 of the FlpO construct had no effect on the amino acid sequence. We also identified a G-to-T mutation in nucleotide 43 of the *Gata3* 3' UTR.

Upon verifying the insertion of *Gata3-FlpO*, we genotyped subsequent generations with the following primer sequences: GAAGGCATCCAGACCCGAAA; CACGTCACCGCATGTTAGAAGA; AACGCAAGTAGAAGGGGTCG. Wild-type animals display a band at 336 bp. Animals homozygous for the *Gata3-FlpO* allele yield a band at 291 bp. Heterozygous animals yield both the wild-type and mutant bands. We used the following primer sequences to genotype *Ucn-Cre* animals: GGATCCGAATCTGCGATGGA;

GCATCGACCGGTAATGCAGG; GGAGGCGAAATAGTCCCTCG. Animals homozygous for *Ucn-Cre* display a band at 393 bp, whereas wild-type animals yield a band at 686 bp; heterozygotes show both the wild-type and mutant bands.

Animal models

LSL-tdTomato (Ai14; Jax strain 007914)[281], FSF-tdTomato (Ai65F; Jax strain 032864)[288], and RC::FLTG (Jax strain 026932)[289] are all previously described. All animals were maintained on a C57BL/6 background. All animal work was conducted in compliance with protocols approved by the Institutional Animal Care and Use Committee at Harvard Medical School.

Immunohistochemistry: cochlear wholemounts

Animals were fixed via intracardial perfusion with ice-cold 4% PFA in PBS. Cochleae were removed and post-fixed overnight at 4°C. Cochleae were then decalcified in 120 mM EDTA for roughly 48 hours at 4°C. After dissecting out the three cochlear turns, tissue was permeabilized with protease for 30 min. at 37°C (ACD RNAscope Protease III; ca. no. 322340), then incubated in 30% sucrose in PBS for at least 20 min at room temperature and flash-frozen on dry ice. Tissue was then blocked for 1-2 hours at room temperature in 5% normal donkey serum (Jackson ImmunoResearch, 017-000-121) and 0.3% Triton-X (Sigma, T9284) in PBS. Primary and secondary antibodies were incubated overnight at 37°C in a solution of 1% normal donkey serum and 0.3% Triton-X in PBS. After mounting, cochleae were imaged in a Leica SP8 confocal microscope. Primary antibodies used were Goat anti-Chat (1:500; Millipore AB144P), Ms anti-Calb2 (1:1,000; Swant 6B3), and Rabbit anti-dsRed (1:1,000; Takara 632496). Secondary antibodies used were Donkey anti-Goat 488 (1:1,000; Jackson Immunoresearch 705-545-147), Donkey anti-Rabbit 568 (1:1,000; Abcam ab175470 or ThermoFisher A31573), and Donkey anti-mouse 647 (1:1,000; ThermoFisher A31571)

Immunohistochemistry: brain sections

Brain tissue was fixed via intracardial perfusion with ice-cold 4% PFA in PBS and post-fixed overnight at 4°C. Brains were either sectioned on a vibratome at 60 µm or cryoprotected in sucrose, embedded in NEG-50 (Richard-Allen Scientific, 6502), and cryosectioned at 20 µm. After sectioning, slices were blocked for 1-2 hours at room temperature with 5-10% normal donkey serum and 0.5% Triton-X in PBS. Primaries were incubated overnight at either room temperature or 4°C in 5% normal donkey serum and 0.5% Triton-X. Secondaries were incubated for 1.5-3 hours at room temperature in 5% normal donkey serum and 0.5% Triton-X, followed by a 10-minute incubation in DAPI. Primaries used were Goat anti-Chat (1:200; Millipore AB144P), Rabbit anti-dsRed (1:1,000-1:2,000; Takara 632496), and Chicken anti-GFP (1:2,000; Aves GFP-1020). Secondary antibodies were Donkey anti-Goat 488 (1:800; Jackson Immunoresearch 705-545-147), Donkey anti-Rabbit 568 (1:800-1:1,000; Abcam ab175470 or ThermoFisher A31573), and Donkey anti-Chicken 488 (1:800; Jackson ImmunoResearch 703-545-155). After mounting, all slides were imaged on a VS120 slide scanner (Olympus).

CHAPTER FOUR

Concluding Remarks

All sensory systems rely on interconnected feedforward and feedback networks to modulate sensory representations based on animals' prior experiences and current needs. The coordination of these networks constitutes a major developmental challenge, as parallel circuits must be aligned to one another with incredible specificity. Cells in the olivocochlear efferent system occupy a unique niche in the realm of sensory circuits, as they project into the farthest reaches of the sensory periphery. Although their positioning is unusual, the OCNs provide an intimate connection between the central and peripheral auditory systems in both developing and mature animals. Thus, these cells are poised to align the development of the central and peripheral auditory systems and to convey information about internal states like stress, attention, or arousal to the inner ear. I have identified many new molecules that may guide the development of these cells and direct their interactions with other cell types in the auditory system. Although many questions about OCNs remain unanswered, the tools presented here should open the doors for many more discoveries to come.

CLARIFYING THE FUNCTIONAL CONSEQUENCES OF OLIVOCOCHLEAR PROJECTIONS

Some variant of the olivocochlear efferent system exists for all hair cell sensory systems: groups of feedback cells project to auditory, vestibular, and lateral line neurons in all classes of vertebrates, and even some invertebrates[26]. The wide conservation of this circuitry across evolutionary time suggests that these cells play a crucial role in the function of these sensory systems. Even so, we still know relatively little about how different types of efferent neurons contribute to the function of various sensory systems. Many potential roles have been ascribed to the auditory efferent system: separating speech sounds from background noises[17,18]; balancing inter-aural differences[19,20,295]; protecting the ear from damage[15,16]; and promoting selective attention[296,297].

Top-down modulation can play an important role in determining which aspects of their surroundings animals attend to, especially in cases of competing sensory modalities[298]. Although

work in this area has primarily focused on modulation at the level of cortex or thalamus, evidence suggests that OCNs might also contribute to selective attention: chinchillas exhibit a decrease in cochlear sensitivity while performing a visual attention task, an effect presumably mediated by the olivocochlear system[296]. More direct evidence for OCN involvement in attentional modulation comes from work on *Chrna9* knock-out animals, which lack functional MOC inputs onto hair cells. Compared to controls, *Chrna9* knock-out mice perform worse on a selective visual attention task in the presence of an auditory distractor, suggesting that MOCs may play a role in filtering auditory stimuli[297]. Attempts to identify MOC effects on attention in humans, however, have generally led to mixed results[299]. Even so, MOC innervation appears to be sparser in humans than in other mammals[300], suggesting that attentional modulation may be an ethologically relevant component of MOC function in other species even if it is not in humans.

Essentially nothing is known about connections between LOCs and attentional modulation. Whereas MOCs act on fast timescales and project to a relatively narrow region of the cochlea, LOCs can have longer-lasting effects on auditory nerve fibers and typically project across a much wider range of frequencies[27,51]. The wide range of LOC axons—which sometimes project across more than 50% of the cochlea[49]—presents a particular puzzle: any feedback signal that simultaneously affects such a high proportion of afferents cannot be targeted to any specific stimulus features. Instead, LOCs are more likely to provide a broad, modulatory effect, perhaps altering the sensitivity of SGNs based on attributes of an animal's internal state.

We found that LOCs, but not MOCs, express the orexin receptor *Hcrtr2*, indicating that LOCs may respond to cues about arousal or attention (**Figure 2.4F**). Orexin-A and Orexin-B are wake-promoting peptides that have been implicated in various behavioral states, including sustained attention and feeding behaviors[301,302]. One hypothesis is that LOCs might convey signals about behavioral demands to the cochlea, perhaps increasing the sensitivity of SGNs in times of high arousal. Indeed, there is evidence that cues about arousal play this type of role in

the vestibular efferent system of fish, possibly to increase the sensitivity of vestibular afferent neurons prior to a rapid movement[303,304].

Research on the relationship between arousal signals and LOC function could begin by verifying whether and how orexins modulate LOC activity. Previous studies identified only sparse projections from orexinergic neurons in the vicinity of the LSO, indicating that more work is needed to determine whether orexin-expressing cells indeed target LOCs[305,306]. In addition, *Hcrtr2* can be coupled to either G_q or $G_{i/o}$ pathways, making it difficult to predict what kind of effect orexin signals might have on LOC activity[307]. Resolving these ambiguities will require careful physiology studies. Back-labeling studies tracing LOC inputs would also shed light on whether LOCs indeed receive innervation from orexinergic neurons.

Organization of LOC circuitry

Developing a thorough model of LOC function will require expanded knowledge about the architecture of LOC circuits, including a more robust understanding of the inputs that drive or modulate LOC activity and the downstream interactions between LOCs and SGNs. Longstanding questions exist about the expression and distribution of various neurotransmitters and neuromodulators within LOC neurons; although many signaling molecules have previously been reported in LOC neurons[41,42], it is unclear how many of those molecules actually contribute to LOC function. Single-cell sequencing studies of SGNs offer some hints to these questions[279,308,309], but further work is needed to verify which of the various receptor transcripts detected in SGNs mediate interactions with LOCs.

Previous work has also struggled to address how homogeneous LOCs are with respect to their signaling molecules. LOCs can have varying effects on SGNs, with efferent stimulation sometimes causing an excitation of auditory nerve fibers and other times causing inhibition[51]. These varied effects suggest that LOCs may contain discrete subsets of cells with different properties and different effects on SGNs. Although virtually all LOCs express Chat, GABA, and

CGRP, previous work has also suggested that discrete subsets of LOCs may express additional or alternative neurotransmitters, including Ucn[43] and dopamine[44]. However, nothing is known about how these potential subgroups correlate with variability in LOC effects on SGNs or with variability in LOC morphology.

We identified a distinct subgroup of LOCs with an enrichment for various neuropeptides, including *Ucn*, *Calca*, *Calcb*, and *Npy* (**Figure 2.5**). Although we identified many receptors whose expression varies between MOCs and LOCs (**Figures 2.4, S6, S7**), we detected almost no differences in receptor expression between peptide-enriched and peptide-low LOCs (**Figure 2.5**). However, peptide-enriched LOCs do show elevated levels of the phosphodiesterase gene *Pde10a*. This variation could influence the way these two types of LOCs respond to signals mediated by certain metabatropic receptors, as cells with greater expression of phosphodiesterases may clear intracellular cAMP more quickly.

Given that LOC subtypes appear to have fairly homogeneous inputs (at least in terms of their receptor expression), it's possible that various LOC subtypes integrate similar information, but pass those signals down to discrete subsets of SGNs. This hypothesis is supported by the variation in adhesion molecules between the two LOC cell types, which suggests that each population of LOC may have distinct targets within the cochlea (**Figure 2.5P-S**). Future studies should investigate the distribution of peptide-high and peptide-low LOC fibers within the cochlea as well as identifying any variation in the inputs between these two groups of LOCs. One useful tool for these investigations is Ucn-Cre: although many LOCs have a developmental history of Ucn-Cre activity (**Figure 3.1**), *Ucn* mRNA expression is confined to the medial wing of the LSO by the fourth postnatal week (**Figure 2.5T**). It should therefore be feasible to use this line to target the peptide-enriched subset of LOCs by injecting a Cre-dependent virus into either the LSO or the ear in adult animals.

Protective effects of LOC innervation

Various insults can cause damage to cells in the cochlea, including aging, sound exposure, and several types of drugs. Depending on the source and severity of the trauma, IHCs, OHCs, and SGN fibers are all susceptible to injury[310,311]. Several previous lines of research have suggested that the olivocochlear efferent system may play a role in mitigating the effects of various types of trauma. However, it has been pointed out that high-intensity sounds are rare in natural environments, suggesting that feedback systems may not have evolved to play a protective role[312]. Yet, exposure to even moderate sound levels can cause cochlear damage[14]. Support cells in the cochlea also express molecules known to be important for sensing and responding to various kinds of cellular stress, suggesting that cochlear circuits may have evolved sophisticated strategies for combatting sources of damage, even if that damage is not a result of high-decibel sound exposure[313].

Regardless of the evolutionary pressures that initially established the olivocochlear efferent system, there is ample evidence that both MOCs and LOCs can play a protective role in the cochlea[15]. In MOCs, this protective role is mediated by their interactions with OHCs[207,314]; it is less clear how LOCs are able to mitigate the effects of acoustic overexposure.

One possibility is that LOCs are able to prepare the cochlea for the possibility of injury by conveying signals about stress or prior sound exposure to the ear. Various kinds of stressors can have a protective effect on acoustic trauma, including a prior exposure to moderate sound, sham surgeries, and restraint[12,315]. Protective effects from these stressors appear to be mediated by the olivocochlear efferent system, as stress does not seem to play a protective role in de-efferented mice[12]. However, stress does still serve a protective function in animals lacking crossed MOC inputs to the cochlea; because crossed fibers constitute the majority of MOC inputs to the ear, this finding might indicate that LOCs are primarily responsible for mediating these protective effects. Alternatively, it may be the case that the remaining ipsilateral MOC fibers in these animals were sufficient to convey stress-induced protective effects to the cochlea.

Sound exposure also appears to have direct effects on LOCs. In particular, it is known that LOCs can turn on *Th* expression after sound exposure, likely altering their signals onto SGNs[46,48]. Future work could also examine whether other neurotransmitters are affected by sound exposure or whether other forms of stress—like restraint or sham surgeries—can also induce *Th* expression in LOCs. If so, that finding would suggest that the onset of dopamine expression in LOCs may be responsible for the protective effects of various kinds of stressors.

Future studies could also clarify the protective effects of LOC inputs by genetically manipulating LOC neurons before, during, or after sound exposure. The intersectional combination of Ucn-Cre and Gata3-FlpO will facilitate these experiments in ways that were previously unachievable. By crossing these animals to mice carrying Cre- and Flp- dependent alleles for a diphtheria toxin receptor or inhibitory DREADD, we can clarify how recovery from acoustic trauma is affected when LOCs are ablated or silenced. These experiments will be particularly useful in comparison to work with *Chrna9* knock-out mice, which lack functional MOC synapses in the cochlea.

Although prior work suggesting that LOCs may have functionally distinct subtypes, it is also unclear whether all LOCs contribute identical responses to acoustic overexposure. We identified a distinct subset of LOCs that is enriched for a variety of neuropeptides (**Figure 2.5**). In both mice and gerbils, this peptide-enriched subset is localized to the high-frequency region of the LSO (**Figure 2.5T, U**)[43]. The auditory system of mice and gerbils are specialized for very different frequency ranges, with mice tending to hear in higher frequencies and gerbils more specialized for lower frequencies. The observation that peptidergic LOCs are enriched in the high frequency region of both species therefore suggests that peptide-enriched LOCs may not be organized around frequency regions of particular behavioral relevance. Instead, peptidergic LOCs may be positioned to serve a special protected role, as high-frequency regions of the cochlea appear to be particularly vulnerable to damage across species[311].

The means by which these various peptides contribute to normal hearing or protection from injury remain mysterious. Expression of neuropeptide receptors in SGNs appears to be extremely sparse: a previous sequencing study did not identify any canonical receptors for CGRP or CGRP-II, and receptors for Ucn and NPY are only found in a small subset of high-frequency SGNs in the base of the cochlea[279]. Given that peptide-enriched LOCs seem to be localized to high-frequency regions of the LSO, it may be the case that these peptides exclusively modulate high-frequency SGNs. It is also possible that these peptides may signal to cells in the cochlea other than SGNs: CRHR1, which binds Ucn, is expressed in border cells nearby the LOC-SGN synapse[313]. It has been hypothesized that border cells—along with other support cells in the cochlea—may play a protective role by recognizing and responding to cellular damage. This response likely involves the CRF signaling system, which includes Ucn[313]. Ucn release from LOC terminals might contribute to this protective response, perhaps conveying signals from the brain or feedforward auditory pathways about stress or acoustic overexposure.

EMERGENCE OF OLIVOCOCHLEAR CIRCUITRY

Divergence of OCNs and FBMNs

Across vertebrates, olivocochlear efferent neurons develop alongside the facial branchial motor neurons. OCNs and FBMNs both originate in the progenitor domain of visceral motor neurons (pMNv) and their axons travel together in the brain before OCN fibers branch off to join the VIIIth nerve. Although the transcription factor *Gata3* appears to play a crucial role in distinguishing mammalian OCNs from FBMNs[116,117], we know little else about how these cell types diverge either developmentally or evolutionarily. Our sequencing data confirmed the selective expression of *Gata2* and *Gata3*, both of which are expressed only in OCNs and not in FBMNs (**Figure 2.2F**). Even more tellingly, we did not detect activity of *Gata3-FlpO* in FBMNs, indicating that FBMNs have no developmental history of *Gata3* expression (**Figure 3.3G**).

OCNs and FBMNs also differ in the expression of several transcription factors known to play a role in motor neuron diversification and cranial nerve development, pointing to additional mechanisms that might guide the bifurcation of these cell types. FBMNs, MOCs, and LOCs express varying levels of the Hox cofactor genes *Meis1*, *Meis2*, *Pbx1*, and *Pbx3* (**Figures 2.2F, S3, S9**). *Pbx3* expression is confined to the FBMNs; although LOCs and MOCs both express *Pbx1*, it is expressed at higher levels in FBMNs. *Meis1* and *Meis2* are expressed in MOCs, LOCs, and FBMNs, although expression of *Meis2* is highest in MOCs. Variations in expression of these genes are known to regulate motor neuron diversity[64,251–253]; a similar regulatory network is likely at play in promoting the diversification of FBMNs and OCNs.

In contrast, *Sall3* expression is upregulated in both MOCs and LOCs, with almost no expression in FBMNs (**Figure 2.2E, F**). *Sall3* is also known to be important for cranial nerve development and is expressed in the developing cochlea as well as subsets of cranial motor neurons[254]. The shared expression of this transcription factor across MOCs, LOCs, and regions of the auditory periphery suggests that it may play a role in the emergence of shared aspects of auditory circuitry. One longstanding question in OCN development concerns the cues that cause OCN fibers to transition from their association with the facial nerve to join the olivocochlear nerve and project out to the ear. This transition might be guided by shared expression of homophilic adhesion molecules in OCNs and other fibers in the vestibulocochlear nerve. Coordinated expression of homophilic adhesion molecules might be driven by shared transcription factors throughout the auditory system—factors like *Gata3* or *Sall3*. Future work could test this hypothesis directly by looking for changes in OCN innervation in *Sall3* knock-out mice.

Additional research is also needed to understand how OCNs and FBMNs coalesce into their final arrangements in the brainstem and which molecules guide the co-fasciculation of FBMN and OCN axons. The many cell-adhesion molecules we identified in each of these cell populations should serve as a fruitful starting point for future investigations (**Figures 2.2E, S2**). Focusing on

variations in cadherin expression might be of particular value, as cadherin proteins have been shown to play a role in the formation of distinct brainstem motor nuclei[121,250].

Segregation of OCN subtypes

The developmental bifurcation between MOCs and LOCs is perhaps even more mysterious than the divergence of OCNs and FBMNs: although *Gata3* has long been postulated as a key in driving the separation of OCNs and FBMNs, no similar transcription factors have been identified that might lead to the diversification of OCN subtypes. We identified several transcription factors that are differentially expressed between MOCs and LOCs—or between LOC subtypes—that may play a role in the establishment of distinct OCN identities (**Figures 2.5O, S9**).

Throughout much of their development, MOC and LOC axons follow a similar trajectory: they both travel with the facial nerve to exit the brain, and it is likely that they both follow a scaffold of SGN processes to reach the sensory epithelium[266]. Other decisions are unique to each population of OCN: MOC and LOC cell bodies migrate to distinct locations in the brainstem and their axons target different cells in the cochlea. OCNs likely rely on different sets of guidance and adhesion molecules to navigate each of these stages of development.

We detected expression of many different adhesion and guidance molecules in both MOCs and LOCs. Many of these genes are shared across OCN subtypes, suggesting that they may be involved in shared aspects of OCN development; others are enriched in only a subset. For example, the neuronal cell adhesion molecule *Nrcam* is expressed in MOCs, LOCs, and FBMNs, as well as cells in the cochlea[316]. This gene might therefore promote non-specific fasciculation between OCNs and their various substrates in both the brain and the cochlea. In contrast, differential expression of genes like *Epha6*, *Epha5*, and *Ephb1*—which are enriched in LOCs—and *Ntng1*, *Dcc*, and *Unc5d*—which are enriched in MOCs—point to mechanisms that selectively guide MOCs and LOCs along their distinct developmental trajectories (**Figure S8**). Although our dataset cannot pinpoint the subcellular localization of any of these proteins, it may

be possible to develop hypotheses about where each of these molecules is acting by querying previously published sequencing datasets. For example, the identification of ligand/receptor pairs between MOCs and hair cells or LOCs and SGNs might indicate that these molecules contribute to efferent target selection within the cochlea[279,308,309,317].

One intriguing candidate for mediating the selective adhesion of LOCs to SGNs is collagen IV. Throughout postnatal development, LOCs express high levels of the genes *Col4a3* and *Col4a4* (**Figure 2.3H, I**). Collagen IV is best known for its role in the structure of the basement membrane; in fact, it is commonly believed that collagen IV is exclusively produced by cells that comprise basement membranes[318]. Fundamentally, however, collagens are cell-adhesion proteins that mediate intercellular interactions, so it is possible that these proteins serve to promote cell adhesion between LOCs and other cell types, perhaps guiding their interactions with SGNs[319]. In other cell types, collagen IV can interact with combinations of integrins and the receptor tyrosine kinase *Ddr1*[318,319]. Both *Ddr1* and several integrin subunits are expressed in SGNs at high levels, indicating that SGNs possess the needed molecular components to interact with collagen chains on LOCs[279].

In basement membranes throughout the body—including the kidney, eyes, testes, lungs, and cochlea—cells expressing collagen IV undergo a developmental switch: *Col4a1* and *Col4a2* are expressed early in development, transitioning to expression of *Col4a3*, *Col4a4*, and *Col4a5*[318,320]. In keeping with this pattern, LOCs express *Col4a1* and *Col4a2* at P1 and P5, but downregulate these genes in mature cells, maintaining expression of only *Col4a3* and *Col4a4*. However, LOCs do not appear to express *Col4a5*: *Col4a5* was only detected in 2% of LOCs at P1 and P5, whereas *Col4a3* and *Col4a4* were each detected in 83% of LOCs. Although collagen IV typically forms heterotrimers of Col4a3, Col4a4, and Col4a5 in basement membranes[318,320], it is possible that Col4a3 and Col4a4 alone might also form a heteromer in the absence of Col4a5;

because collagen IV expression has not been previously described in neurons, it may be that neuronal collagen IV uses a different variant of this protein assembly.

If Col4a3 and Col4a4 are indeed playing a cell adhesion role in the LOCs, the absence of these genes may cause disruptions in LOC innervation. Given the role that LOCs seem to play in protecting the cochlea from sound damage, it is plausible that an alteration of LOC innervation might contribute to progressive hearing loss. Indeed, human patients with mutations in either *Col4a3* or *Col4a4* suffer from Alport's syndrome, a condition characterized largely by kidney disorder and progressive sensorineural hearing loss, particularly in high-frequency regions[320,321]. The mechanisms that lead to hearing loss in Alport's syndrome patients are not fully understood. *Col4a3* and *Col4a4* are expressed in the basilar membrane and the stria vascularis of the cochlea[322] and defects in the stria vascularis have been reported in patients with Alport's syndrome[323,324]. In severe cases, the entire Organ of Corti can become detached from the underlying basement membrane[324]. In other cases, damage is much milder. To date, no investigation has systematically examined efferent innervation in human patients with Alport's syndrome or in *Col4a3* or *Col4a4* knock-out mice. A promising first step would be to examine LOC innervation in ears that lack either *Col4a3* or *Col4a4*.

TALKING FORWARD WHILE TALKING BACK: EFFERENT EFFECTS ON AFFERENT CIRCUITRY

Building functional sensory circuits requires close alignment of ascending and descending networks, including contributions from both the CNS and PNS. Due to their projections into the sensory periphery, OCNs are uniquely positioned to coordinate the development of auditory circuitry across central and peripheral boundaries. Several previous studies have implicated OCNs in various aspects of auditory development, but much remains unknown about how OCNs influence the maturation of the auditory system or how inputs onto OCNs are themselves refined during postnatal development.

Postnatal refinement of auditory brainstem circuits

During postnatal development, neurons in the sound-localization circuits of the LSO undergo a transition from receiving GABAergic to glycinergic signals, downregulating GABA receptor subunits while increasing expression of the glycine receptor anchoring protein gephyrin[267,268]. This transition coincides with a shift in chloride transporters that leads to a change in the effects of GABAergic inputs, which are excitatory early in development and inhibitory in mature cells[269–271]. The alteration of this signaling pathway is thought to contribute to the tonotopic refinement of sound localization circuits[325].

We identified similar changes in OCNs over the course of postnatal development. Both MOCs and LOCs downregulate several GABA receptor subunits between P5 and P26-P28, while increasing expression of the glycine receptor subunit *Glra1* (**Figure 2.6E**). The expression of several chloride channels and transporters also changes during OCN development. The similarity of the changes in receptor expression across both efferent and afferent neurons in the LSO suggests that OCNs may undergo similar processes of tonotopic refinement as other cells in the auditory brainstem. In OCNs, these changes may be regulated by one or more of the transcription factors whose expression shifts between P1-P5 and P26-P28 (**Figure 2.6F**).

The excitatory nature of early GABAergic inputs onto LSO neurons may allow these cells to serve as coincidence detectors for closely timed inputs arriving from each ear. In mature animals, neurons in the LSO mediate sound localization by integrating excitatory inputs from the ipsilateral ear with inhibitory inputs from the contralateral ear[7]. The tonotopic specificity of these circuits is refined based on spontaneous activity from the cochlea, with some synapses being selectively weakened and pruned during the first one or two postnatal weeks[3,181]. It is possible that the maintenance of these synapses is driven by coordinated inputs from across both ears, with LSO neurons maintaining only bilateral inputs that correspond to similar frequencies.

Refinement of tonotopic circuits is also influenced by MOCs: in mouse models with enhanced or reduced MOC activity, the tonotopic architecture of auditory brainstem circuits fails to develop

normally[181,206,208]. The lack of tonotopic refinement in these models may be due to alterations in the precise timing of synaptic events within the auditory brainstem[181]. MOCs may affect this period of tonotopic refinement by coordinating the precise timing of synaptic activity across both ears: if brainstem neurons maintain connections because bilateral inputs arrived at similar times, perhaps MOCs direct this process by synchronizing the timing of spontaneous activity across the two hemispheres.

The processes that guide the innervation and refinement of non-auditory inputs onto OCNs remain even less clear. Although the changes in expression of GABA and glycine receptors correspond to previous work on developmental changes in other brainstem neurons, OCNs also alter their expression of several other receptors and channels that have not been previously studied in the context of the developing auditory brainstem. For example, LOCs downregulate expression of nicotinic acetylcholine receptors, glutamate receptors, and the opioid receptor *Oprk1* (**Figures 2.6E, S7**). It is unclear if these changes correlate with innervations that exist only transiently in development, or whether OCNs alter the way they respond to certain inputs over time. Careful back-labeling experiments from OCNs across postnatal development will be required to resolve these questions.

Effects of LOCs on developing SGNs

In addition to their effects on brainstem development, there is mixed evidence that OCNs may affect the maturation of cell types within the cochlea. In particular, it has long been speculated that LOCs may play a role in the establishment or refinement of type I SGN subtypes. Type I SGNs can be divided into three main subtypes based on their spontaneous firing rates, anatomy, and transcriptomes[223,279,308,309]. LOCs preferentially innervate the two SGN subtypes with the lowest spontaneous firing rates[225,226], which correspond to the molecularly defined type 1B and 1C SGNs[279,308].

Prior work from our lab has shown that the molecular roadmap for SGN identities is specified early in development: even before the onset of hearing or the diversification of SGN firing rates, SGNs express markers that correspond to mature SGN subtypes. However, the development of these subtypes is altered by the absence of hair cell-driven spontaneous activity[279]. This finding indicates that external factors—potentially including signals from LOCs—can play a role in establishing the final attributes of SGN subtypes, even if nascent SGNs are predisposed to adopt one identity over another.

The hypothesis that LOC innervation is required for the development of normal SGN firing properties was tested in cats by severing the entire olivocochlear bundle shortly after birth and recording spontaneous firing rates from single auditory nerve fibers[227]. In the absence of LOC inputs, SGNs still possessed a distribution of spontaneous firing rates, although the average firing rate was reduced for all SGN subtypes[227]. More recent work in mice found that severing LOC inputs to the cochlea in adults results in an alteration of synaptic morphology across SGN subtypes[228]. Together, these results suggest that LOCs have the ability to alter some aspects of baseline SGN function. However, neither of these studies was able to address other components of SGN identity, as no molecular markers had yet been characterized for SGN subtypes. It also remains unclear whether ablating LOCs earlier in development would have caused a more severe phenotype than those observed in these studies.

A first step in addressing these questions might come from uncovering the molecular pathways that guide target selection between LOCs and SGNs. Mature SGNs express genes for many adhesion molecules that may serve as post-synaptic partners to drive synaptogenesis between SGNs and LOCs. Several of these genes, such as *Tenm2*, are expressed predominantly in type 1B and 1C SGNs[279]. This observation suggests that selective expression of adhesion molecules is downstream of genetic networks that influence SGN identity. This does not, however, address the question of how LOC innervation influences SGN identity or maturation; even if adhesion molecules are selectively expressed in certain SGN subtypes, LOCs may still be poised

to modulate aspects of this nascent SGN identity, similar to the influence of spontaneous activity from IHCs.

Because Ucn-Cre activity gradually increases over the first two postnatal weeks, we still lack the tools to selectively ablate LOCs early in development. However, the finding that the morphology of SGN-IHC synapses is altered by lesioning OCN fibers in mature animals suggests that some aspects of SGN identity may still be malleable in adulthood. Future work might investigate whether other aspects of SGN identity, like expression of the subtype-specific markers *Calb2* and *Lypd1*, are altered after selectively ablating LOCs using *Gata3-FlpO; Ucn-Cre* animals. It may also be possible to alter LOC innervation of SGNs early in postnatal development by using AAVs to knock down expression of subtype-specific receptors like *Tenm2*, or to express them ectopically in the 1A subtype.

Understanding how OCNs affect SGN identity—and the cues that guide OCNs to their appropriate targets on SGN subtypes—may prove to be important for therapeutic applications that seek to prevent or repair hearing loss. Both aging and noise exposure can cause synaptopathic hearing loss, in which SGN fibers lose contact with IHCs[326–328]. Several interventions are now in development that may prevent synaptopathy or repair SGN-IHC synapses after damage. Application of neurotrophin 3 (NT-3) is particularly promising, as administration or overexpression of NT-3 can prevent synaptopathy and restore synaptic loss[329,330]. Although the restored synapses do mediate a functional recovery of auditory thresholds, more fine-grained aspects of synaptic circuitry—like properties of SGN firing rates or identity—remain unexplored. Moreover, almost nothing is known about how either SGN synapse loss or NT-3 administration affects OCN fibers. LOCs, in particular, express high levels of the NT-3 receptor *Ntrk3*, indicating that their innervation may be altered by neurotrophin administration. If LOC input does play a role in shaping or maintaining aspects of SGN identity, ensuring that LOC fibers are properly redirected to their targets on SGNs will be an important challenge when rebuilding these circuits.

OCNs may present an obstacle for therapeutic approaches for an additional reason: in aging animals, OCN fibers re-route their projections to form synapses on IHCs[244,245]. These OCN-IHC synapses are inhibitory, potentially exacerbating other causes of hearing loss by further dampening signals from IHCs onto SGNs. The presence of OCN fibers at the IHC membrane may also present a physical obstacle to the re-establishment of SGN-IHC synapses. At present, however, it remains completely unknown why OCNs re-innervate IHCs in aging animals. Indeed, it is unclear even whether the OCN fibers targeting IHCs stem from LOCs or MOCs. Repeating these experiments in *Ucn-Cre; tdTomato* animals would allow for a conclusive interpretation of the identity of re-routed OCN fibers, as all fluorescently labeled axons could be attributed to LOCs. A better understanding of the early developmental cues that govern OCN innervation of specific cochlear cell types will also clarify which factors may influence the aberrant projections of OCNs in pathological conditions like age-related hearing loss. Indeed, a more robust understanding of the olivocochlear efferent system and its role in protecting the ear from damage may itself offer new therapeutic strategies for preventing and repairing cochlear damage.

APPENDIX

Supplemental Figures

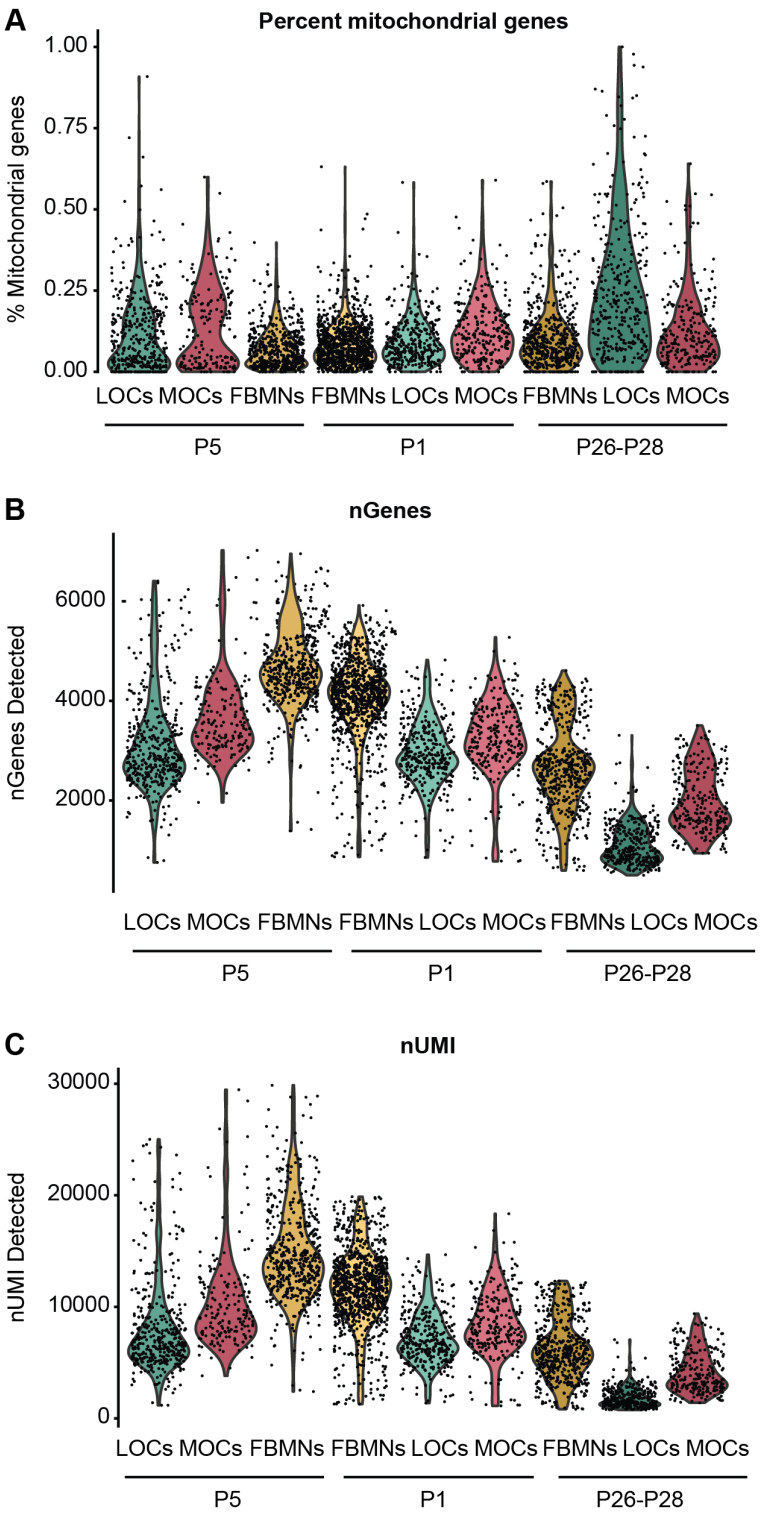

Figure S1. Quality-control metrics for FBMNs, LOCs, and MOCs at each collection timepoint. (A-C) Violin plots denoting detection of mitochondrial genes **(A),** number of unique genes **(B)**, and the total number of UMI **(C)** per cell for LOCs, MOCs, and FBMNs.

Figure S2. Differentially expressed adhesion molecules between OCNs and FBMNs. Violin plots denoting the normalized expression level of genes in neonatal and mature OCNs and FBMNs. Plots include all genes from a list of 280 guidance and adhesion molecules that are differentially expressed between FBMNs and OCNs at P1, P5, or P26-P28. Inclusion criteria: gene is expressed in at least 10% of either FBMNs or OCNs; the fraction of cells in each cluster expressing the gene differs by at least 20 percentage points; average log fold change > 0.75; $p < 0.001$ (Wilcoxon rank sum test, Bonferroni post-hoc correction).

Figure S2 (Continued)

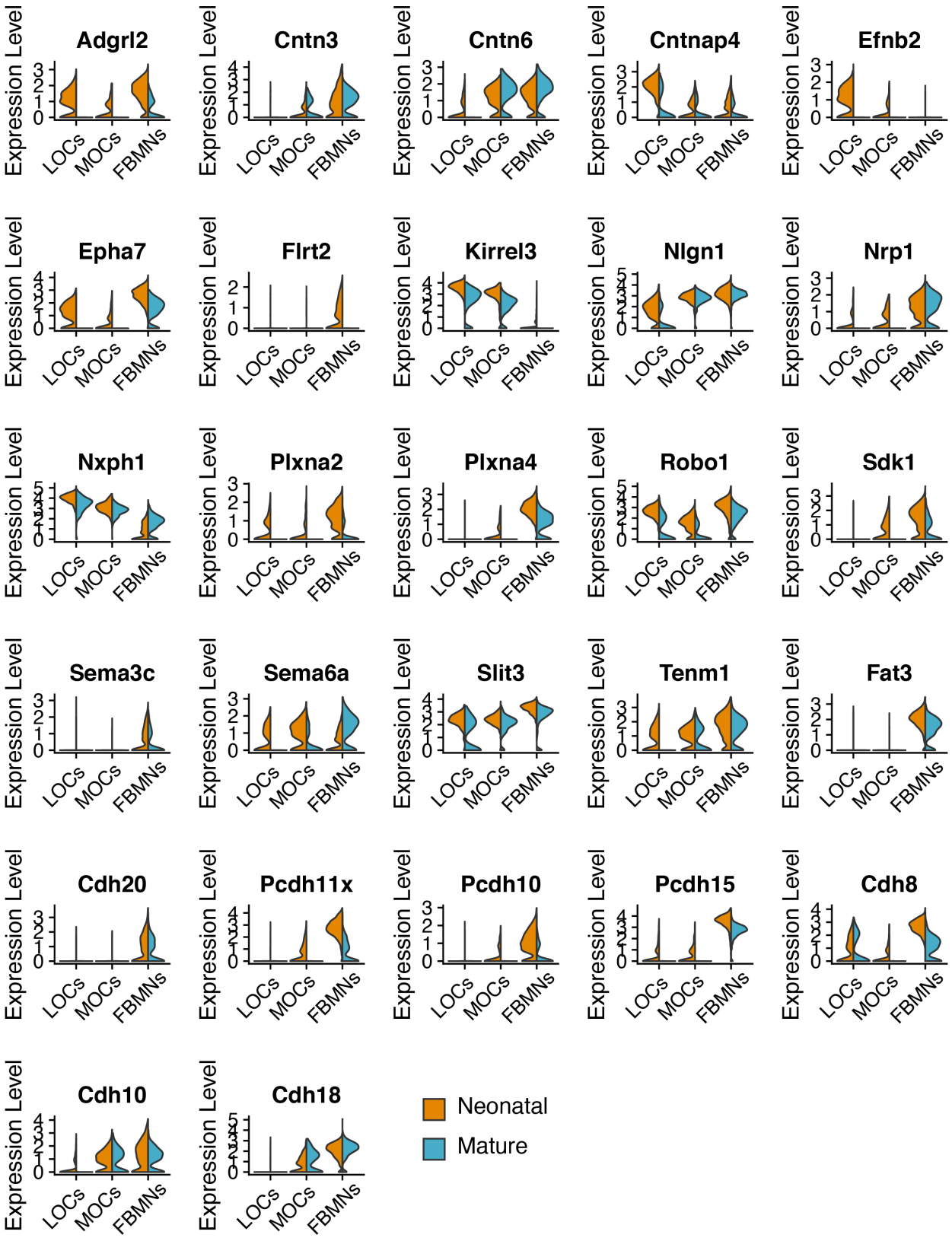

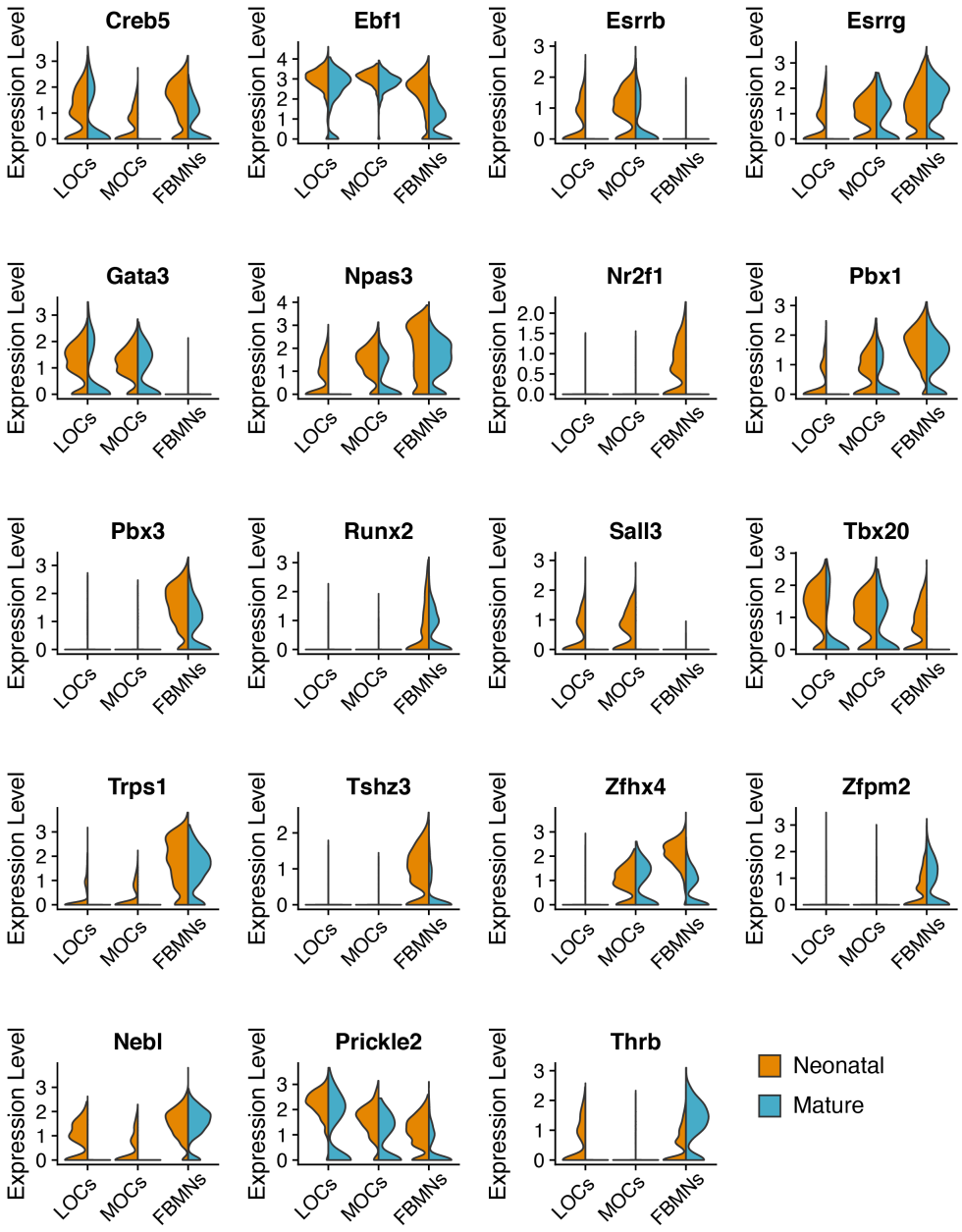

Figure S3. Differentially expressed transcription factors between OCNs and FBMNs. Violin plots denoting the normalized expression level of genes in neonatal and mature OCNs and FBMNs. Plots include all genes from a list of 1,634 transcription factors that are differentially expressed between FBMNs and OCNs at P1, P5, or P26-P28. Inclusion criteria: gene is expressed in at least 10% of either FBMNs or OCNs; the fraction of cells in each cluster expressing the gene differs by at least 20 percentage points; average log fold change > 0.75; $p < 0.001$ (Wilcoxon rank sum test, Bonferroni post-hoc correction).

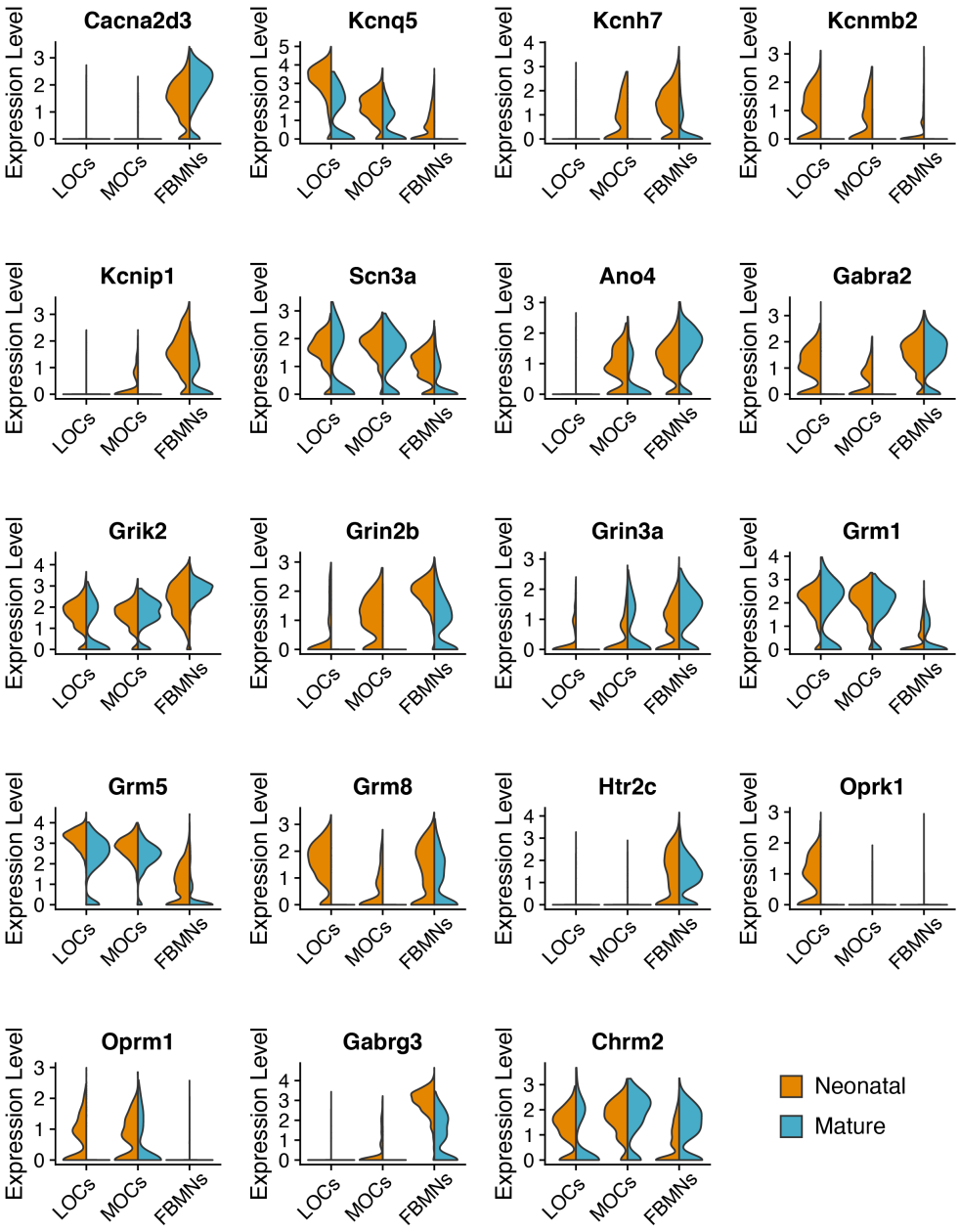

Figure S4. Differentially expressed ion channels and receptors between OCNs and FBMNs. Violin plots denoting the normalized expression level of genes in neonatal and mature OCNs and FBMNs. Plots include all genes from a list of 430 receptors and ion channels that are differentially expressed between FBMNs and OCNs at P1, P5, or P26-P28. Inclusion criteria: gene is expressed in at least 10% of either FBMNs or OCNs; the fraction of cells in each cluster expressing the gene differs by at least 20 percentage points; average log fold change > 0.75; $p < 0.001$ (Wilcoxon rank sum test, Bonferroni post-hoc correction).

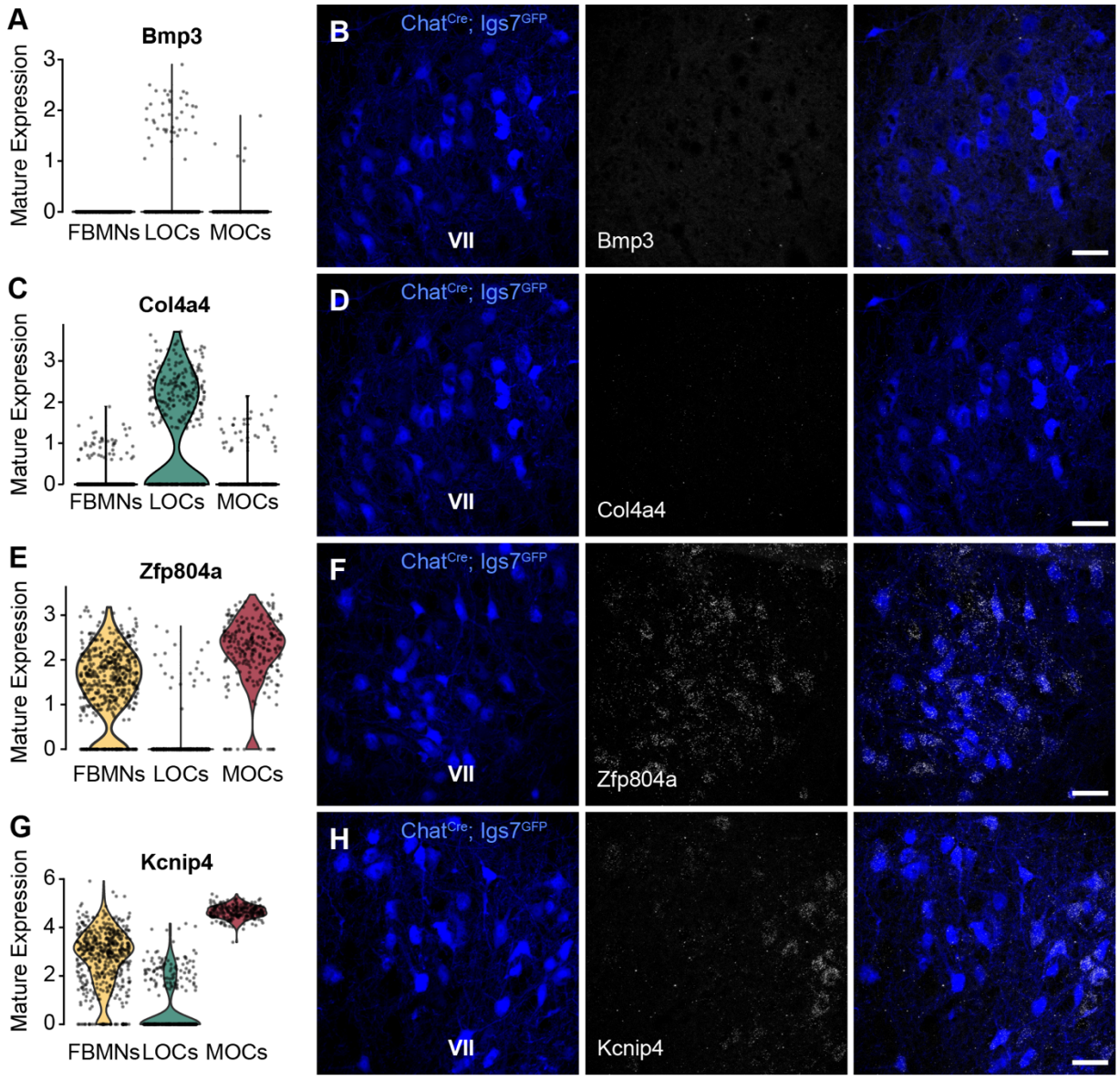

Figure S5. Expression of MOC and LOC markers in the facial motor nucleus. (A, C, E, G) Violin plots denoting normalized expression levels of MOC and LOC markers in mature FBMNs, LOCs, and MOCs. **(B, D, F, H)** HCR *in situ* hybridization in coronal sections through the facial motor nucleus (VII) of P27 *Chat*^{Cre}*; Igs7*^{GFP} mice. As expected from the single-nucleus sequencing data, expression of both *Zfp804a* **(E, F)** and *Kcnip4* **(F, H)** is detectable in cholinergic FBMNs (blue), whereas *Bmp3* **(A, B)** and *Col4a4* **(C, D)** are not expressed in FBMNs. Scale bars, 50 μm.

Figure S6. Neurotransmitter receptors expressed in mature OCNs. Violin plots denoting normalized expression levels of neurotransmitter or neuropeptide receptors and receptor subunits in mature MOCs and LOCs. Genes were extracted from a list of 215 genes related to neurotransmitters and neuropeptide receptors; plot includes all genes in this list expressed in at least 33% of either MOCs or LOCs.

Figure S6 (Continued)

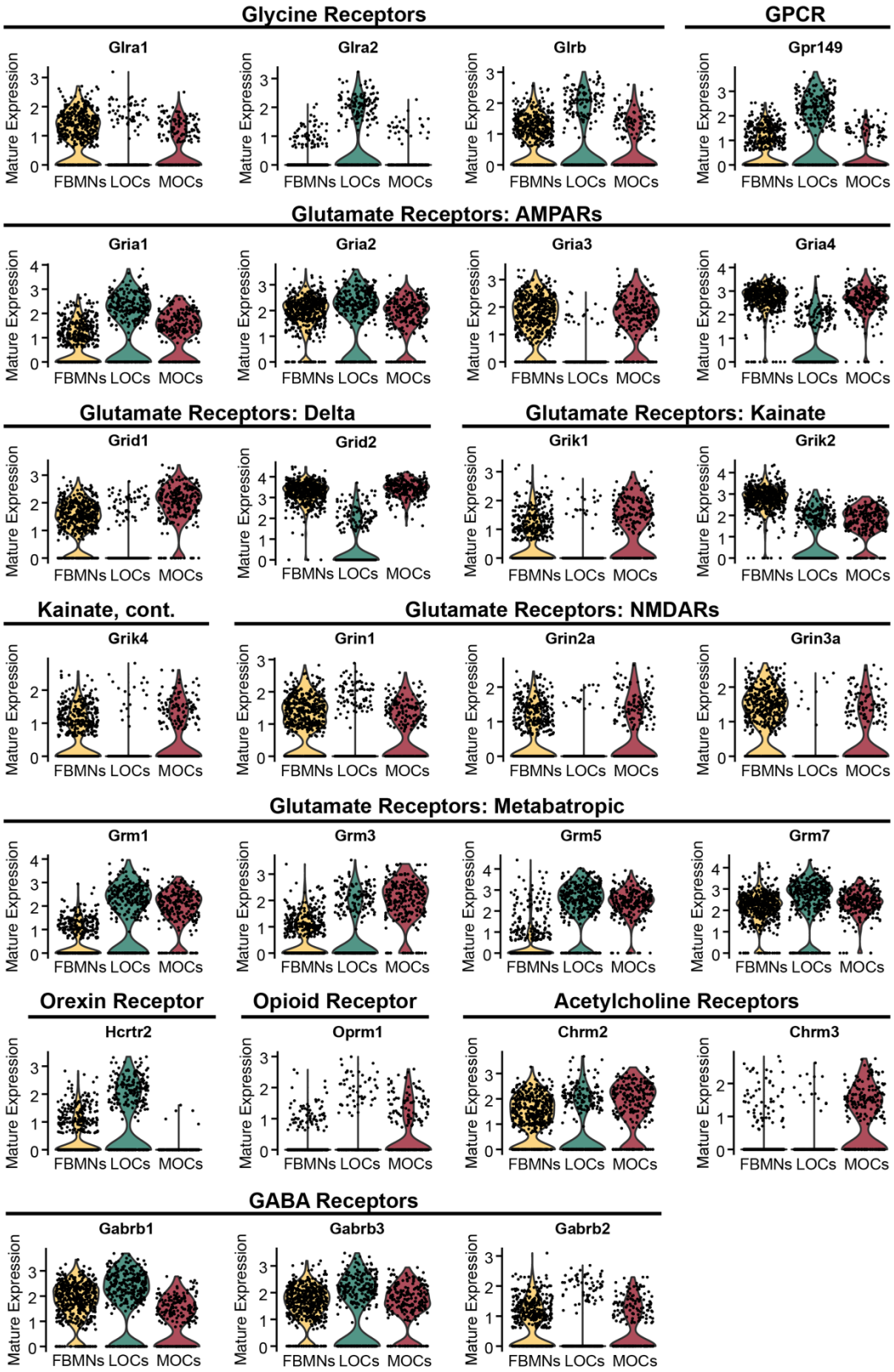

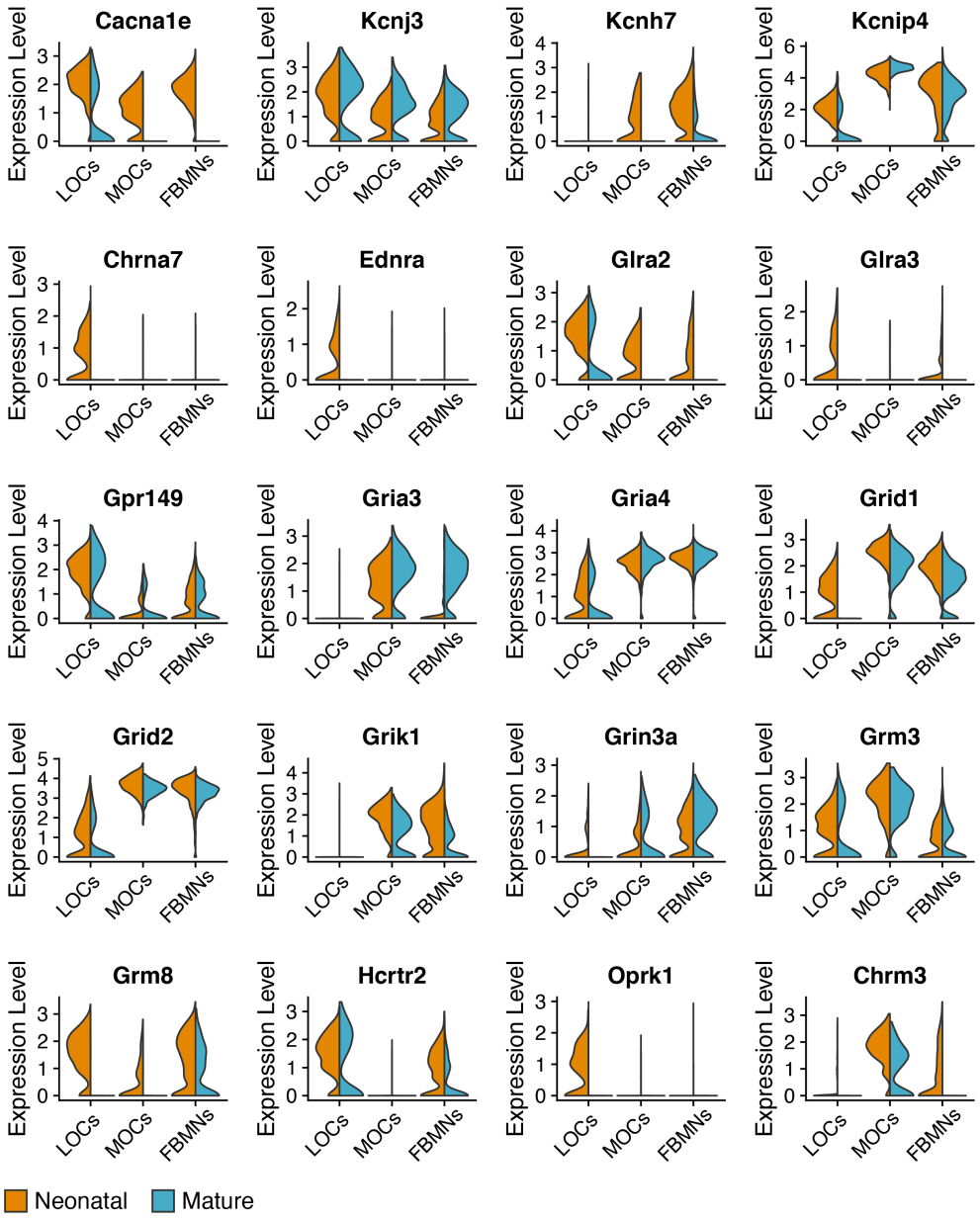

Figure S7. Differentially expressed ion channels and receptors between MOCs and LOCs. Violin plots denoting the normalized expression level of genes in neonatal and mature OCNs. Plots include all genes from a list of 430 receptors and ion channels that are differentially expressed between MOCs and LOCs at P1, P5, or P26-P28. Inclusion criteria: gene is expressed in at least 10% of either MOCs or LOCs; the fraction of cells in each cluster expressing the gene differs by at least 20 percentage points; average log fold change > 0.75; $p < 0.001$ (Wilcoxon rank sum test, Bonferroni post-hoc correction).

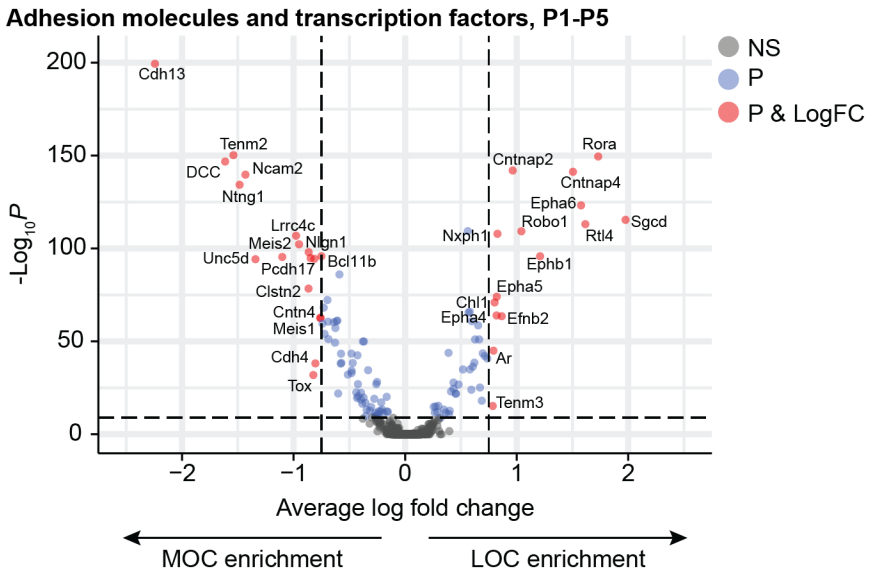

Figure S8. Differential expression of transcription factors and adhesion molecules in neonatal OCNs. Volcano plot displaying variations in expression of 1,916 genes with known DNA binding motifs or roles in guidance or intercellular adhesion. Red, genes with average log fold change > 0.75 and $p < 10^{-10}$. Blue, genes with average log fold change < 0.75 and $p < 10^{-10}$ (Wilcoxon rank sum test, Bonferroni post-hoc correction). Left, enrichment in MOCs. Right, enrichment in LOCs.

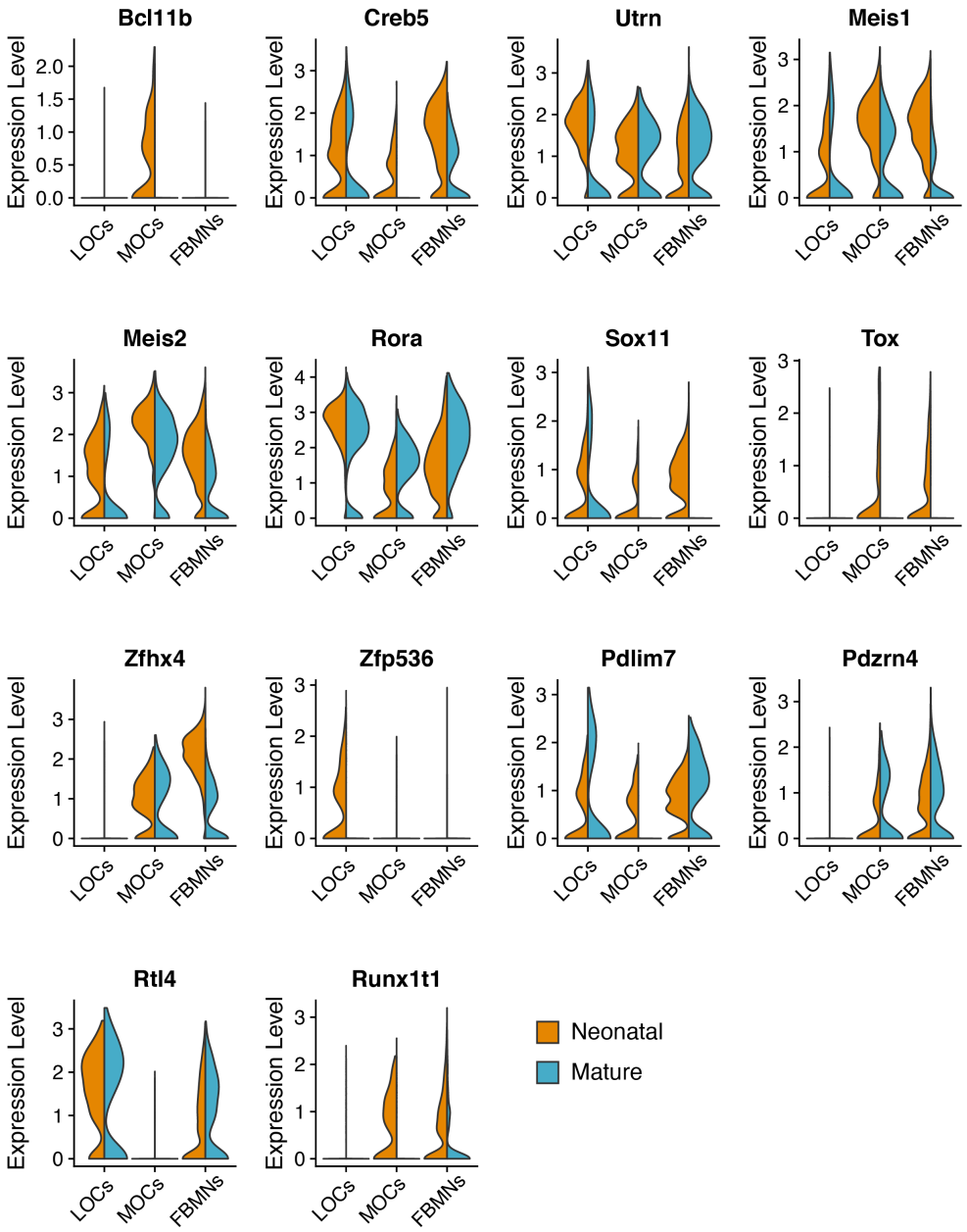

Figure S9. Differential expression of transcription factors between MOCs and LOCs. Violin plots denoting the normalized expression level of genes in neonatal and mature OCNs. Plots include all genes from a list of 1,634 transcription factors that are differentially expressed between MOCs and LOCs at P1, P5, or P26-P28. Inclusion criteria: gene is expressed in at least 10% of either MOCs or LOCs; the fraction of cells in each cluster expressing the gene differs by at least 20 percentage points; average log fold change > 0.75; $p < 0.001$ (Wilcoxon rank sum test, Bonferroni post-hoc correction).

Figure S10. Differentially expressed guidance and adhesion molecules between MOCs and LOCs. Violin plots denoting the normalized expression level of genes in neonatal and mature OCNs. Plots include all genes from a list of 280 guidance and adhesion mole that are differentially expressed between MOCs and LOCs at P1, P5, or P26-P28. Inclusion criteria: gene is expressed in at least 10% of either MOCs or LOCs; the fraction of cells in each cluster expressing the gene differs by at least 20 percentage points; average log fold change > 0.75; $p < 0.001$ (Wilcoxon rank sum test, Bonferroni post-hoc correction).

Figure S10 (Continued)

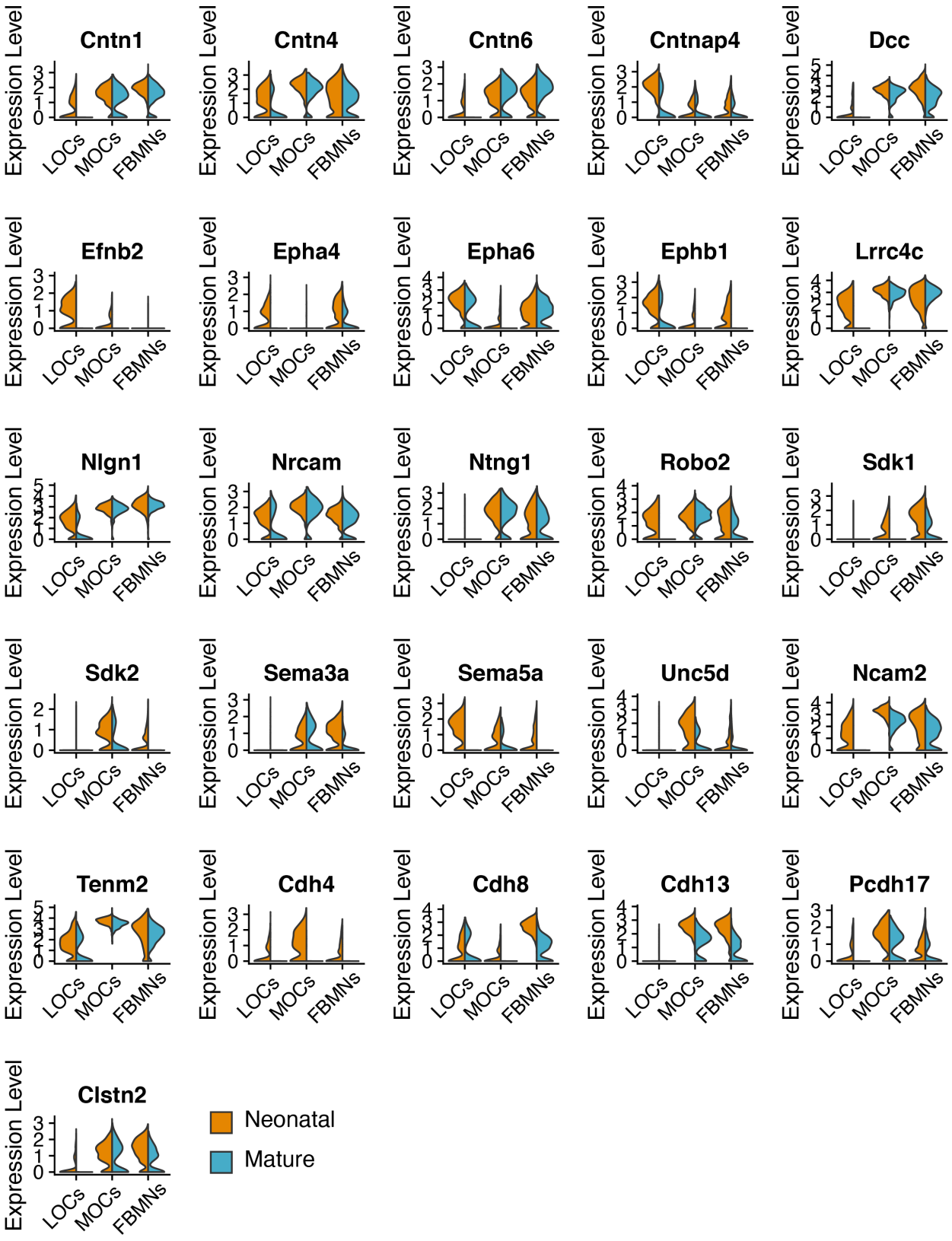

References

1. Liu, C., Glowatzki, E. & Fuchs, P. A. Unmyelinated type II afferent neurons report cochlear damage. *Proc. Natl. Acad. Sci.* **112**, 14723–14727 (2015).

2. Flores, E. N. *et al.* A Non-canonical Pathway from Cochlea to Brain Signals Tissue-Damaging Noise. *Curr. Biol.* **25**, 606–612 (2015).

3. Kandler, K., Clause, A. & Noh, J. Tonotopic reorganization of developing auditory brainstem circuits. *Nat. Neurosci.* **12**, 711–717 (2009).

4. Muniak, M. A. *et al.* 3D model of frequency representation in the cochlear nucleus of the CBA/J mouse. *J. Comp. Neurol.* **521**, 1510–1532 (2013).

5. Sando, I. The Anatomical Interrelationships of the Cochlear Nerve Fibers. *Acta Otolaryngol.* **59**, 417–436 (1965).

6. Malmierca, M. S. & Ryugo, D. K. Auditory System. in *The Mouse Nervous System* (eds. Watson, C., Paxinos, G. & Puelles, L.) 607–645 (Academic Press, 2012). doi:10.1016/B978-0-12-369497-3.10024-X

7. Grothe, B., Pecka, M. & McAlpine, D. Mechanisms of Sound Localization in Mammals. *Physiol. Rev.* **90**, 983–1012 (2010).

8. Nothwang, H. G. Evolution of mammalian sound localization circuits: A developmental perspective. *Prog. Neurobiol.* **141**, 1–24 (2016).

9. Guinan, J. J. Olivocochlear efferents: Their action, effects, measurement and uses, and the impact of the new conception of cochlear mechanical responses. *Hear. Res.* **362**, 38–47 (2018).

10. Rasmussen, G. L. Further observations of the efferent cochlear bundle. *J. Comp. Neurol.* **99**, 61–74 (1953).

11. Rasmussen, G. L. The olivary peduncle and other fiber projections of the superior olivary complex. *J. Comp. Neurol.* **84**, 141–219 (1946).

12. Kujawa, S. G. & Liberman, M. C. Conditioning-Related Protection From Acoustic Injury: Effects of Chronic Deefferentation and Sham Surgery. *J. Neurophysiol.* **78**, 3095–3106 (1997).

13. Darrow, K. N., Maison, S. F. & Liberman, M. C. Selective Removal of Lateral Olivocochlear Efferents Increases Vulnerability to Acute Acoustic Injury. *J. Neurophysiol.* **97**, 1775–1785 (2007).

14. Maison, S. F., Usubuchi, H. & Liberman, M. C. Efferent Feedback Minimizes Cochlear Neuropathy from Moderate Noise Exposure. *J. Neurosci.* **33**, 5542–5552 (2013).

15. Fuente, A. The olivocochlear system and protection from acoustic trauma: A mini literature review. *Front. Syst. Neurosci.* **9**, 1–6 (2015).

16. Handrock, M. & Zeisberg, J. The Influence of the Efferent System on Adaptation, Temporary and Permanent Threshold Shift. *Arch. Otorhinolaryngol.* **234**, 191–195 (1982).

17. Giraud, A. L. *et al.* Auditory efferents involved in speech-in-noise intelligibility. *Neuroreport* **8**, 1779–1783 (1997).

18. Dewson, J. H. Olivocochlear Bundle: Relationships to Signal Discrimination in Noise. *J. Acoust. Soc. Am.* **42**, 1189–1189 (1967).

19. Darrow, K. N., Maison, S. F. & Liberman, M. C. Cochlear efferent feedback balances interaural sensitivity. *Nat. Neurosci.* **9**, 1474–1476 (2006).

20. Larsen, E. & Liberman, M. C. Contralateral cochlear effects of ipsilateral damage: No evidence for interaural coupling. *Hear. Res.* **260**, 70–80 (2010).

21. Irving, S., Moore, D. R., Liberman, M. C. & Sumner, C. J. Olivocochlear Efferent Control in Sound Localization and Experience-Dependent Learning. *J. Neurosci.* **31**, 2493–2501 (2011).

22. Guinan, J. J. Cochlear efferent innervation and function. *Curr. Opin. Otolaryngol. Head Neck Surg.* **18**, 447–453 (2010).

23. Guinan, J. J. Olivocochlear Efferents: Anatomy, Physiology, Function, and the Measurement of Efferent Effects in Humans. *Ear Hear.* **27**, 589–607 (2006).

24. Warr, W. B. & Guinan, J. J. Efferent innervation of the organ of corti: two separate systems. *Brain Res.* **173**, 152–155 (1979).

25. White, J. S. & Warr, B. W. The dual origins of the olivocochlear bundle in the albino rat. *J. Comp. Neurol.* **219**, 203–214 (1983).

26. Roberts, B. L. & Meredith, G. E. The Efferent Innervation of the Ear: Variations on an Enigma. in *The Evolutionary Biology of Hearing* (eds. Webster, D. B., Popper, A. N. & Fay, R. R.) 185–210 (Springer, 1992). doi:10.1007/978-1-4612-2784-7_16

27. Brown, M. C. Anatomy of olivocochlear neurons. in *Auditory and Vestibular Efferents* (eds. Ryugo, D. K. & Fay, R. R.) **38**, 17–37 (Springer New York, 2011).

28. Robertson, D., Harvey, A. R. & Cole, K. S. Postnatal development of the efferent innervation of the rat cochlea. *Dev. Brain Res.* **47**, 197–207 (1989).

29. Guinan, J. J., Norris, B. E. & Guinan, S. S. Single Auditory Units in the Superior Olivary Complex: II: Locations of Unit Categories and Tonotopic Organization. *Int. J. Neurosci.* **4**, 147–166 (1972).

30. Sanes, D. H., Merickel, M. & Rubel, E. W. Evidence for an alteration of the tonotopic map in the gerbil cochlea during development. *J. Comp. Neurol.* **279**, 436–444 (1989).

31. Robertson, D., Anderson, C.-J. & Cole, K. S. Segregation of efferent projections to different turns of the guinea pig cochlea. *Hear. Res.* **25**, 69–76 (1987).

32. Elgoyhen, A. B., Johnson, D. S., Boulter, J., Vetter, D. E. & Heinemann, S. α9: An acetylcholine receptor with novel pharmacological properties expressed in rat cochlear hair

cells. *Cell* **79**, 705–715 (1994).

33. Elgoyhen, A. B. *et al.* α10: A determinant of nicotinic cholinergic receptor function in mammalian vestibular and cochlear mechanosensory hair cells. *Proc. Natl. Acad. Sci.* **98**, 3501–3506 (2001).

34. Elgoyhen, A. B. & Katz, E. The efferent medial olivocochlear-hair cell synapse. *J. Physiol.* **106**, 47–56 (2012).

35. Wersinger, E., McLean, W. J., Fuchs, P. A. & Pyott, S. J. BK Channels Mediate Cholinergic Inhibition of High Frequency Cochlear Hair Cells. *PLoS One* **5**, e13836 (2010).

36. Maison, S. F., Pyott, S. J., Meredith, A. L. & Liberman, M. C. Olivocochlear suppression of outer hair cells in vivo: evidence for combined action of BK and SK2 channels throughout the cochlea. *J. Neurophysiol.* **109**, 1525–1534 (2013).

37. Maison, S. F., Adams, J. C. & Liberman, M. C. Olivocochlear innervation in the mouse: Immunocytochemical maps, crossed versus uncrossed contributions, and transmitter colocalization. *J. Comp. Neurol.* **455**, 406–416 (2003).

38. Saunders, A., Granger, A. J. & Sabatini, B. L. Corelease of acetylcholine and GABA from cholinergic forebrain neurons. *Elife* **4**, 1–13 (2015).

39. Froud, K. E. *et al.* Type II spiral ganglion afferent neurons drive medial olivocochlear reflex suppression of the cochlear amplifier. *Nat. Commun.* **6**, 7115 (2015).

40. Maison, S., Liberman, L. D. & Liberman, M. C. Type II Cochlear Ganglion Neurons Do Not Drive the Olivocochlear Reflex: Re-Examination of the Cochlear Phenotype in Peripherin Knock-Out Mice. *eNeuro* **3**, 1–11 (2016).

41. Eybalin, M. Neurotransmitters and neuromodulators of the mammalian cochlea. *Physiol. Rev.* **73**, 309–373 (1993).

42. Sewell, W. F. Pharmacology and Neurochemistry of Olivocochlear Efferents. in *Auditory and Vestibular Efferents* (eds. Ryugo, D. K., Fay, R. R. & Popper, A. N.) 83–101 (Springer, 2011). doi:10.1007/978-1-4419-7070-1_4

43. Kaiser, A., Alexandrova, O. & Grothe, B. Urocortin-expressing olivocochlear neurons exhibit tonotopic and developmental changes in the auditory brainstem and in the innervation of the cochlea. *J. Comp. Neurol.* **519**, 2758–2778 (2011).

44. Darrow, K. N., Simons, E. J., Dodds, L. & Liberman, M. C. Dopaminergic innervation of the mouse inner ear: Evidence for a separate cytochemical group of cochlear efferent fibers. *J. Comp. Neurol.* **498**, 403–414 (2006).

45. Mulders, W. H. A. . & Robertson, D. Dopaminergic olivocochlear neurons originate in the high frequency region of the lateral superior olive of guinea pigs. *Hear. Res.* **187**, 122–130 (2004).

46. Niu, X. & Canlon, B. Activation of tyrosine hydroxylase in the lateral efferent terminals by sound conditioning. *Hear. Res.* **174**, 124–132 (2002).

47. Spitzer, N. C. Neurotransmitter Switching in the Developing and Adult Brain. *Annu. Rev.*

Neurosci. **40**, 1–19 (2017).

48. Wu, J. S. *et al.* Sound exposure dynamically induces dopamine synthesis in cholinergic LOC efferents for feedback to auditory nerve fibers. *Elife* **9**, 1–27 (2020).

49. Warr, W. B., Beck Boche, J. & Neely, S. T. Efferent innervation of the inner hair cell region: origins and terminations of two lateral olivocochlear systems. *Hear. Res.* **108**, 89–111 (1997).

50. Vetter, D. E. & Mugnaini, E. Distribution and dendritic features of three groups of rat olivocochlear neurons. *Anat. Embryol. (Berl).* **185**, 1–16 (1992).

51. Groff, J. A. & Liberman, M. C. Modulation of Cochlear Afferent Response by the Lateral Olivocochlear System: Activation Via Electrical Stimulation of the Inferior Colliculus. *J. Neurophysiol.* **90**, 3178–3200 (2003).

52. Fritzsch, B. & Nichols, D. H. DiI reveals a prenatal arrival of efferents at the differentiating otocyst of mice. *Hear. Res.* **65**, 51–60 (1993).

53. Bruce, L. L., Kingsley, J., Nichols, D. H. & Fritzsch, B. The development of vestibulocochlear efferents and cochlear afferents in mice. *Int. J. Dev. Neurosci.* **15**, 671–692 (1997).

54. Boord, R. L. The efferent cochlear bundle in the caiman and pigeon. *Exp. Neurol.* **3**, 225–239 (1961).

55. Köppl, C. Birds – same thing, but different? Convergent evolution in the avian and mammalian auditory systems provides informative comparative models. *Hear. Res.* **273**, 65–71 (2011).

56. Fritzsch, B., Christensen, M. A. & Nichols, D. H. Fiber pathways and positional changes in efferent perikarya of 2.5-to 7-day chick embryos as revealed with dil and dextran amiens. *J. Neurobiol.* **24**, 1481–1499 (1993).

57. Simon, H. & Lumsden, A. Rhombomere-specific origin of the contralateral vestibulo-acoustic efferent neurons and their migration across the embryonic midline. *Neuron* **11**, 209–220 (1993).

58. Fritzsch, B. & Elliott, K. L. Evolution and Development of the Inner Ear Efferent System: Transforming a Motor Neuron Population to Connect to the Most Unusual Motor Protein via Ancient Nicotinic Receptors. *Front. Cell. Neurosci.* **11**, 1–9 (2017).

59. Di Bonito, M. & Studer, M. Cellular and Molecular Underpinnings of Neuronal Assembly in the Central Auditory System during Mouse Development. *Front. Neural Circuits* **11**, (2017).

60. Lumsden, A. & Keynes, R. Segmental patterns of neuronal development in the chick hindbrain. *Nature* **337**, 424–428 (1989).

61. Fraser, S., Keynes, R. & Lumsden, A. Segmentation in the chick embryo hindbrain is defined by cell lineage restrictions. *Nature* **344**, 431–435 (1990).

62. Wilkinson, D. G., Bhatt, S., Cook, M., Boncinelli, E. & Krumlauf, R. Segmental expression of Hox-2 homoeobox-containing genes in the developing mouse hindbrain. *Nature* **341**,

405–409 (1989).

63. Wilkinson, D. G., Bhatt, S., Chavrier, P., Bravo, R. & Charnay, P. Segment-specific expression of a zinc-finger gene in the developing nervous system of the mouse. *Nature* **337**, 461–464 (1989).

64. Guthrie, S. Patterning and axon guidance of cranial motor neurons. *Nat. Rev. Neurosci.* **8**, 859–871 (2007).

65. Kiecker, C. & Lumsden, A. Compartments and their boundaries in vertebrate brain development. *Nat. Rev. Neurosci.* **6**, 553–564 (2005).

66. Parker, H. J. & Krumlauf, R. Segmental arithmetic: summing up the Hox gene regulatory network for hindbrain development in chordates. *Wiley Interdiscip. Rev. Dev. Biol.* **6**, e286 (2017).

67. Briscoe, J., Pierani, A., Jessell, T. M. & Ericson, J. A Homeodomain Protein Code Specifies Progenitor Cell Identity and Neuronal Fate in the Ventral Neural Tube. *Cell* **101**, 435–445 (2000).

68. Dessaud, E., McMahon, A. P. & Briscoe, J. Pattern formation in the vertebrate neural tube: a sonic hedgehog morphogen-regulated transcriptional network. *Development* **135**, 2489–2503 (2008).

69. Nothwang, H. G., Ebbers, L., Schlüter, T. & Willaredt, M. A. The emerging framework of mammalian auditory hindbrain development. *Cell Tissue Res.* **361**, 33–48 (2015).

70. Pierce, E. T. Time of Origin of Neurons in the Brain Stem of the Mouse. *Prog. Brain Res.* **40**, 53–65 (1973).

71. Pierce, E. T. Histogenesis of the dorsal and ventral cochlear nuclei in the mouse. An autoradiographic study. *J. Comp. Neurol.* **131**, 27–53 (1967).

72. Farago, A. F., Awatramani, R. B. & Dymecki, S. M. Assembly of the Brainstem Cochlear Nuclear Complex Is Revealed by Intersectional and Subtractive Genetic Fate Maps. *Neuron* **50**, 205–218 (2006).

73. Fujiyama, T. *et al.* Inhibitory and excitatory subtypes of cochlear nucleus neurons are defined by distinct bHLH transcription factors, Ptf1a and Atoh1. *Development* **136**, 2049–2058 (2009).

74. Rosengauer, E. *et al.* Egr2::Cre Mediated Conditional Ablation of Dicer Disrupts Histogenesis of Mammalian Central Auditory Nuclei. *PLoS One* **7**, e49503 (2012).

75. Marrs, G. S., Morgan, W. J., Howell, D. M., Spirou, G. A. & Mathers, P. H. Embryonic origins of the mouse superior olivary complex. *Dev. Neurobiol.* **73**, 384–398 (2013).

76. Di Bonito, M. *et al.* Assembly of the Auditory Circuitry by a Hox Genetic Network in the Mouse Brainstem. *PLoS Genet.* **9**, e1003249 (2013).

77. Maricich, S. M. *et al.* Atoh1-Lineal Neurons Are Required for Hearing and for the Survival of Neurons in the Spiral Ganglion and Brainstem Accessory Auditory Nuclei. *J. Neurosci.* **29**, 11123–11133 (2009).

78. Altieri, S. C., Jalabi, W., Zhao, T., Romito-DiGiacomo, R. R. & Maricich, S. M. En1 directs superior olivary complex neuron positioning, survival, and expression of FoxP1. *Dev. Biol.* **408**, 99–108 (2015).

79. Nichols, D. H. & Bruce, L. L. Migratory routes and fates of cells transcribing the Wnt-1 gene in the murine hindbrain. *Dev. Dyn.* **235**, 285–300 (2006).

80. Carney, P. R. & Silver, J. Studies on cell migration and axon guidance in the developing distal auditory system of the mouse. *J. Comp. Neurol.* **215**, 359–369 (1983).

81. Ma, Q., Chen, Z., Barrantes, I. D. B., Luis de la Pompa, J. & Anderson, D. J. neurogenin1 Is Essential for the Determination of Neuronal Precursors for Proximal Cranial Sensory Ganglia. *Neuron* **20**, 469–482 (1998).

82. Goodrich, L. V. *The Primary Auditory Neurons of the Mammalian Cochlea*. *The Primary Auditory Neurons of the Mammalian Cochlea* **52**, (Springer New York, 2016).

83. Appler, J. M. & Goodrich, L. V. Connecting the ear to the brain: Molecular mechanisms of auditory circuit assembly. *Prog. Neurobiol.* **93**, 488–508 (2011).

84. Lu, C. C., Appler, J. M., Houseman, E. A. & Goodrich, L. V. Developmental Profiling of Spiral Ganglion Neurons Reveals Insights into Auditory Circuit Assembly. *J. Neurosci.* **31**, 10903–10918 (2011).

85. Sandell, L. L., Butler Tjaden, N. E., Barlow, A. J. & Trainor, P. A. Cochleovestibular nerve development is integrated with migratory neural crest cells. *Dev. Biol.* **385**, 200–210 (2014).

86. Marrs, G. S. & Spirou, G. A. Embryonic assembly of auditory circuits: spiral ganglion and brainstem. *J. Physiol.* **590**, 2391–2408 (2012).

87. Higashijima, S., Hotta, Y. & Okamoto, H. Visualization of Cranial Motor Neurons in Live Transgenic Zebrafish Expressing Green Fluorescent Protein Under the Control of the Islet-1 Promoter/Enhancer. *J. Neurosci.* **20**, 206–218 (2000).

88. Jessell, T. M. Neuronal specification in the spinal cord: inductive signals and transcriptional codes. *Nat. Rev. Genet.* **1**, 20–29 (2000).

89. Ericson, J. *et al.* Pax6 Controls Progenitor Cell Identity and Neuronal Fate in Response to Graded Shh Signaling. *Cell* **90**, 169–180 (1997).

90. Murphy, P., Davidson, D. R. & Hill, R. E. Segment-specific expression of a homoeobox-containing gene in the mouse hindbrain. *Nature* **341**, 156–159 (1989).

91. Bell, E., Wingate, R. J. T. & Lumsden, A. Homeotic transformation of rhombomere identity after localized Hoxb1 misexpression. *Science (80-.).* **284**, 2168–71 (1999).

92. Jungbluth, S., Bell, E. & Lumsden, A. Specification of distinct motor neuron identities by the singular activities of individual Hox genes. *Development* **126**, 2751–8 (1999).

93. Studer, M. *et al.* Genetic interactions between Hoxa1 and Hoxb1 reveal new roles in regulation of early hindbrain patterning. *Development* **125**, 1025–36 (1998).

94. Studer, M., Lumsden, A., Ariza-McNaughton, L., Bradley, A. & Krumlauf, R. Altered

segmental identity and abnormal migration of motor neurons in mice lacking Hoxb-1. *Nature* **384**, 630–634 (1996).

95. Gaufo, G. O., Flodby, P. & Capecchi, M. R. Hoxb1 controls effectors of sonic hedgehog and Mash1 signaling pathways. *Development* **127**, 5343–54 (2000).

96. Goddard, J. M., Rossel, M., Manley, N. R. & Capecchi, M. R. Mice with targeted disruption of Hoxb-1 fail to form the motor nucleus of the VIIth nerve. *Development* **122**, 3217–28 (1996).

97. Ericson, J., Thor, S., Edlund, T., Jessell, T. & Yamada, T. Early stages of motor neuron differentiation revealed by expression of homeobox gene Islet-1. *Science (80-.).* **256**, 1555–1560 (1992).

98. Varela-Echavarría, A., Pfaff, S. L. & Guthrie, S. Differential Expression of LIM Homeobox Genes among Motor Neuron Subpopulations in the Developing Chick Brain Stem. *Mol. Cell. Neurosci.* **8**, 242–257 (1996).

99. Coppola, E., Pattyn, A., Guthrie, S. C., Goridis, C. & Studer, M. Reciprocal gene replacements reveal unique functions for Phox2 genes during neural differentiation. *EMBO J.* **24**, 4392–4403 (2005).

100. Pattyn, A. *et al.* Coordinated temporal and spatial control of motor neuron and serotonergic neuron generation from a common pool of CNS progenitors. *Genes Dev.* **17**, 729–737 (2003).

101. Tiveron, M.-C., Pattyn, A., Hirsch, M.-R. & Brunet, J.-F. Role of Phox2b and Mash1 in the generation of the vestibular efferent nucleus. *Dev. Biol.* **260**, 46–57 (2003).

102. Briscoe, J. *et al.* Homeobox gene Nkx2.2 and specification of neuronal identity by graded Sonic hedgehog signalling. *Nature* **398**, 622–627 (1999).

103. Müller, M., Jabs, N., Lorke, D. E., Fritzsch, B. & Sander, M. Nkx6.1 controls migration and axon pathfinding of cranial branchio-motoneurons. *Development* **130**, 5815–5826 (2003).

104. Pattyn, A., Vallstedt, A., Dias, J. M., Sander, M. & Ericson, J. Complementary roles for Nkx6 and Nkx2 class proteins in the establishment of motoneuron identity in the hindbrain. *Development* **130**, 4149–4159 (2003).

105. Jarrar, W., Dias, J. M., Ericson, J., Arnold, H.-H. & Holz, A. Nkx2.2 and Nkx2.9 Are the Key Regulators to Determine Cell Fate of Branchial and Visceral Motor Neurons in Caudal Hindbrain. *PLoS One* **10**, e0124408 (2015).

106. Song, M.-R. *et al.* T-Box transcription factor Tbx20 regulates a genetic program for cranial motor neuron cell body migration. *Development* **133**, 4945–4955 (2006).

107. Ahn, D., Ruvinsky, I., Oates, A. C., Silver, L. M. & Ho, R. K. tbx20 , a new vertebrate T-box gene expressed in the cranial motor neurons and developing cardiovascular structures in zebrafish. *Mech. Dev.* **95**, 253–258 (2000).

108. Kraus, F., Haenig, B. & Kispert, A. Cloning and expression analysis of the mouse T-box gene Tbx20. *Mech. Dev.* **100**, 87–91 (2001).

109. Pattyn, A., Hirsch, M.-R., Goridis, C. & Brunet, J.-F. Control of hindbrain motor neuron differentiation by the homeobox gene Phox2b. *Development* **127**, 1349–58 (2000).

110. Jacob, J. *et al.* Transcriptional repression coordinates the temporal switch from motor to serotonergic neurogenesis. *Nat. Neurosci.* **10**, 1433–1439 (2007).

111. Dubreuil, V., Hirsch, M.-R., Jouve, C., Brunet, J.-F. & Goridis, C. The role of Phox2b in synchronizing pan-neuronal and type-specific aspects of neurogenesis. *Development* **129**, 5241–53 (2002).

112. Dubreuil, V., Hirsch, M. R., Pattyn, A., Brunet, J. F. & Goridis, C. The Phox2b transcription factor coordinately regulates neuronal cell cycle exit and identity. *Development* **127**, 5191–201 (2000).

113. Samad, O. A. *et al.* Integration of anteroposterior and dorsoventral regulation of Phox2b transcription in cranial motoneuron progenitors by homeodomain proteins. *Development* **131**, 4071–4083 (2004).

114. Bingham, S., Higashijima, S., Okamoto, H. & Chandrasekhar, A. The Zebrafish trilobite Gene Is Essential for Tangential Migration of Branchiomotor Neurons. *Dev. Biol.* **242**, 149–160 (2002).

115. Chandrasekhar, A. Turning heads: Development of vertebrate branchiomotor neurons. *Dev. Dyn.* **229**, 143–161 (2004).

116. Pata, I. *et al.* The transcription factor GATA3 is a downstream effector of Hoxb1 specification in rhombomere 4. *Development* **126**, 5523–31 (1999).

117. Karis, A. *et al.* Transcription factor GATA-3 alters pathway selection of olivocochlear neurons and affects morphogenesis of the ear. *J. Comp. Neurol.* **429**, 615–630 (2001).

118. Bell, E., Lumsden, A. & Graham, A. Expression of GATA-2 in the developing avian rhombencephalon. *Mech. Dev.* **84**, 173–176 (1999).

119. Nardelli, J., Thiesson, D., Fujiwara, Y., Tsai, F.-Y. & Orkin, S. H. Expression and Genetic Interaction of Transcription Factors GATA-2 and GATA-3 during Development of the Mouse Central Nervous System. *Dev. Biol.* **210**, 305–321 (1999).

120. Wan, Y. Y. GATA3: a master of many trades in immune regulation. *Trends Immunol.* **35**, 233–242 (2014).

121. Garel, S., Garcia-Dominguez, M. & Charnay, P. Control of the migratory pathway of facial branchiomotor neurones. *Development* **127**, 5297–307 (2000).

122. Rossel, M., Loulier, K., Feuillet, C., Alonso, S. & Carroll, P. Reelin signaling is necessary for a specific step in the migration of hindbrain efferent neurons. *Development* **132**, 1175–85 (2005).

123. McKay, I. J., Lewis, J. & Lumsden, A. Organization and Development of Facial Motor Neurons in the Kreisler Mutant Mouse. *Eur. J. Neurosci.* **9**, 1499–1506 (1997).

124. Goffinet, A. M. Abnormal development of the facial nerve nucleus in reeler mutant mice. *J. Anat.* **138**, 207–15 (1984).

125. Auclair, F., Valdés, N. & Marchand, R. Rhombomere-specific origin of branchial and visceral motoneurons of the facial nerve in the rat embryo. *J. Comp. Neurol.* **369**, 451–461 (1996).

126. Campbell, J. . & Henson, M. . Olivocochlear neurons in the brainstem of the mouse. *Hear. Res.* **35**, 271–274 (1988).

127. Brown, M. C. & Levine, J. L. Dendrites of medial olivocochlear neurons in mouse. *Neuroscience* **154**, 147–159 (2008).

128. Simmons, D., Duncan, J., de Caprona, D. C. & Fritzsch, B. Development of the Inner Ear Efferent System. in *Auditory and Vestibular Efferents* (eds. Ryugo, D. K., Fay, R. R. & Popper, A. N.) 187–216 (Springer, 2011). doi:10.1007/978-1-4419-7070-1_7

129. Cowan, C. A., Yokoyama, N., Bianchi, L. M., Henkemeyer, M. & Fritzsch, B. EphB2 Guides Axons at the Midline and Is Necessary for Normal Vestibular Function. *Neuron* **26**, 417–430 (2000).

130. Hammond, R. *et al.* Slit-mediated repulsion is a key regulator of motor axon pathfinding inthe hindbrain. *Development* **132**, 4483–4495 (2005).

131. Kim, M. *et al.* Motor neuron cell bodies are actively positioned by Slit/Robo repulsion and Netrin/DCC attraction. *Dev. Biol.* **399**, 68–79 (2015).

132. Kim, K.-T. *et al.* ISL1-based LIM complexes control Slit2 transcription in developing cranial motor neurons. *Sci. Rep.* **6**, 36491 (2016).

133. Davey, C. F., Mathewson, A. W. & Moens, C. B. PCP Signaling between Migrating Neurons and their Planar-Polarized Neuroepithelial Environment Controls Filopodial Dynamics and Directional Migration. *PLoS Genet.* **12**, e1005934 (2016).

134. Wada, H. *et al.* Dual roles of zygotic and maternal Scribble1 in neural migration and convergent extension movements in zebrafish embryos. *Development* **132**, 2273–2285 (2005).

135. Qu, Y. *et al.* Atypical Cadherins Celsr1-3 Differentially Regulate Migration of Facial Branchiomotor Neurons in Mice. *J. Neurosci.* **30**, 9392–9401 (2010).

136. Vivancos, V. *et al.* Wnt activity guides facial branchiomotor neuron migration, and involves the PCP pathway and JNK and ROCK kinases. *Neural Dev.* **4**, 7 (2009).

137. Yang, T., Bassuk, A. G., Stricker, S. & Fritzsch, B. Prickle1 is necessary for the caudal migration of murine facial branchiomotor neurons. *Cell Tissue Res.* **357**, 549–561 (2014).

138. Davey, C. F. & Moens, C. B. Planar cell polarity in moving cells: think globally, act locally. *Development* **144**, 187–200 (2017).

139. Glasco, D. M. *et al.* The mouse Wnt/PCP protein Vangl2 is necessary for migration of facial branchiomotor neurons, and functions independently of Dishevelled. *Dev. Biol.* **369**, 211–222 (2012).

140. Glasco, D. M. *et al.* The atypical cadherin Celsr1 functions non-cell autonomously to block rostral migration of facial branchiomotor neurons in mice. *Dev. Biol.* **417**, 40–49 (2016).

141. Jessen, J. R. *et al.* Zebrafish trilobite identifies new roles for Strabismus in gastrulation and neuronal movements. *Nat. Cell Biol.* **4**, 610–615 (2002).

142. Mapp, O. M., Wanner, S. J., Rohrschneider, M. R. & Prince, V. E. Prickle1b mediates interpretation of migratory cues during zebrafish facial branchiomotor neuron migration. *Dev. Dyn.* **239**, 1596–1608 (2010).

143. Mapp, O. M., Walsh, G. S., Moens, C. B., Tada, M. & Prince, V. E. Zebrafish Prickle1b mediates facial branchiomotor neuron migration via a farnesylation-dependent nuclear activity. *Development* **138**, 2121–2132 (2011).

144. Bingham, S. M. *et al.* Multiple mechanisms mediate motor neuron migration in the zebrafish hindbrain. *Dev. Neurobiol.* **70**, 87–99 (2009).

145. Wada, H., Tanaka, H., Nakayama, S., Iwasaki, M. & Okamoto, H. Frizzled3a and Celsr2 function in the neuroepithelium to regulate migration of facial motor neurons in the developing zebrafish hindbrain. *Development* **133**, 4749–4759 (2006).

146. Ohsawa, R., Ohtsuka, T. & Kageyama, R. Mash1 and Math3 are required for development of branchiomotor neurons and maintenance of neural progenitors. *J. Neurosci.* **25**, 5857–65 (2005).

147. Ohshima, T. *et al.* Cyclin-Dependent Kinase 5/p35 Contributes Synergistically with Reelin/Dab1 to the Positioning of Facial Branchiomotor and Inferior Olive Neurons in the Developing Mouse Hindbrain. *J. Neurosci.* **22**, 4036–4044 (2002).

148. Dennis, D. J., Han, S. & Schuurmans, C. bHLH transcription factors in neural development, disease, and reprogramming. *Brain Res.* (2018). doi:10.1016/j.brainres.2018.03.013

149. Pfaff, S. L., Mendelsohn, M., Stewart, C. L., Edlund, T. & Jessell, T. M. Requirement for LIM Homeobox Gene Isl1 in Motor Neuron Generation Reveals a Motor Neuron–Dependent Step in Interneuron Differentiation. *Cell* **84**, 309–320 (1996).

150. Duncan, J. S., Lim, K.-C., Engel, J. D. & Fritzsch, B. Limited inner ear morphogenesis and neurosensory development are possible in the absence of GATA3. *Int. J. Dev. Biol.* **55**, 297–303 (2011).

151. Duncan, J. S. & Fritzsch, B. Continued Expression of GATA3 Is Necessary for Cochlear Neurosensory Development. *PLoS One* **8**, e62046 (2013).

152. Appler, J. M. *et al.* Gata3 Is a Critical Regulator of Cochlear Wiring. *J. Neurosci.* **33**, 3679–3691 (2013).

153. Nakamura, P. A. & Cramer, K. S. Formation and maturation of the calyx of Held. *Hear. Res.* **276**, 70–78 (2011).

154. Elliott, K. L., Houston, D. W. & Fritzsch, B. Transplantation of Xenopus laevis Tissues to Determine the Ability of Motor Neurons to Acquire a Novel Target. *PLoS One* **8**, e55541 (2013).

155. Elliott, K. L. & Fritzsch, B. Transplantation of Xenopus laevis ears reveals the ability to form afferent and efferent connections with the spinal cord. *Int. J. Dev. Biol.* **54**, 1443–1451 (2010).

156. Ma, Q., Anderson, D. J. & Fritzsch, B. Neurogenin 1 Null Mutant Ears Develop Fewer, Morphologically Normal Hair Cells in Smaller Sensory Epithelia Devoid of Innervation. *J. Assoc. Res. Otolaryngol.* **1**, 129–143 (2000).

157. Simmons, D. D. Development of the inner ear efferent system across vertebrate species. *J. Neurobiol.* **53**, 228–250 (2002).

158. Fritzsch, B. Development of the labyrinthine efferent system. *Ann. N. Y. Acad. Sci.* **781**, 21–33 (1996).

159. Huang, E. J. *et al.* Brn3a is a transcriptional regulator of soma size, target field innervation and axon pathfinding of inner ear sensory neurons. *Development* **128**, 2421–32 (2001).

160. Katayama, K. *et al.* Disorganized Innervation and Neuronal Loss in the Inner Ear of Slitrk6-Deficient Mice. *PLoS One* **4**, e7786 (2009).

161. Fritzsch, B., Barbacid, M. & Silos-Santiago, I. The combined effects of trkB and trkC mutations on the innervation of the inner ear. *Int. J. Dev. Neurosci.* **16**, 493–505 (1998).

162. Sapède, D., Rossel, M., Dambly-Chaudière, C. & Ghysen, A. Role of SDF1 chemokine in the development of lateral line efferent and facial motor neurons. *Proc. Natl. Acad. Sci.* **102**, 1714–8 (2005).

163. Wang, L., Klein, R., Zheng, B. & Marquardt, T. Anatomical Coupling of Sensory and Motor Nerve Trajectory via Axon Tracking. *Neuron* **71**, 263–277 (2011).

164. Gallarda, B. W. *et al.* Segregation of Axial Motor and Sensory Pathways via Heterotypic Trans-Axonal Signaling. *Science (80-.).* **320**, 233–236 (2008).

165. Cramer, K. S. & Gabriele, M. L. Axon guidance in the auditory system: Multiple functions of Eph receptors. *Neuroscience* **277**, 152–162 (2014).

166. Ernfors, P., Van De Water, T., Loring, J. & Jaenisch, R. Complementary roles of BDNF and NT-3 in vestibular and auditory development. *Neuron* **14**, 1153–1164 (1995).

167. Wiechers, B. *et al.* A Changing Pattern of Brain-Derived Neurotrophic Factor Expression Correlates with the Rearrangement of Fibers during Cochlear Development of Rats and Mice. *J. Neurosci.* **19**, 3033–3042 (1999).

168. Shnerson, A., Devigne, C. & Pujol, R. Age-related changes in the C57BL/6J mouse cochlea. II. Ultrastructural findings. *Dev. Brain Res.* **2**, 77–88 (1981).

169. Delacroix, L. & Malgrange, B. Cochlear afferent innervation development. *Hear. Res.* **330**, 157–169 (2015).

170. Blankenship, A. G. & Feller, M. B. Mechanisms underlying spontaneous patterned activity in developing neural circuits. *Nat. Rev. Neurosci.* **11**, 18–29 (2010).

171. Ehret, G. Development of absolute auditory thresholds in the house mouse (Mus musculus). *J. Am. Audiol. Soc.* **1**, 179–84 (1976).

172. Tritsch, N. X., Yi, E., Gale, J. E., Glowatzki, E. & Bergles, D. E. The origin of spontaneous activity in the developing auditory system. *Nature* **450**, 50–55 (2007).

173. Tritsch, N. X. *et al.* Calcium action potentials in hair cells pattern auditory neuron activity before hearing onset. *Nat. Neurosci.* **13**, 1050–1052 (2010).

174. Tritsch, N. X. & Bergles, D. E. Developmental Regulation of Spontaneous Activity in the Mammalian Cochlea. *J. Neurosci.* **30**, 1539–1550 (2010).

175. Gummer, A. W. & Mark, R. F. Patterned neural activity in brain stem auditory areas of a prehearing mammal, the tammar wallaby (Macropus eugenii). *Neuroreport* **5**, 685–8 (1994).

176. Beutner, D. & Moser, T. The Presynaptic Function of Mouse Cochlear Inner Hair Cells during Development of Hearing. *J. Neurosci.* **21**, 4593–4599 (2001).

177. Brandt, N. *et al.* Thyroid Hormone Deficiency Affects Postnatal Spiking Activity and Expression of Ca2+ and K+ Channels in Rodent Inner Hair Cells. *J. Neurosci.* **27**, 3174–3186 (2007).

178. Marcotti, W., Johnson, S. L., Holley, M. C. & Kros, C. J. Developmental changes in the expression of potassium currents of embryonic, neonatal and mature mouse inner hair cells. *J. Physiol.* **548**, 383–400 (2003).

179. Marcotti, W., Johnson, S. L., Rüsch, A. & Kros, C. J. Sodium and calcium currents shape action potentials in immature mouse inner hair cells. *J. Physiol.* **552**, 743–761 (2003).

180. Kros, C. J., Ruppersberg, J. P. & Rüsch, A. Expression of a potassium current in inner hair cells during development of hearing in mice. *Nature* **394**, 281–284 (1998).

181. Clause, A. *et al.* The Precise Temporal Pattern of Prehearing Spontaneous Activity Is Necessary for Tonotopic Map Refinement. *Neuron* **82**, 822–835 (2014).

182. Cole, K. S. & Robertson, D. Early efferent innervation of the developing rat cochlea studied with a carbocyanine dye. *Brain Res.* **575**, 223–230 (1992).

183. Bruce, L. L., Christensen, M. A. & Warr, W. B. Postnatal development of efferent synapses in the rat cochlea. *J. Comp. Neurol.* **423**, 532–548 (2000).

184. Simmons, D. D., Mansdorf, N. B. & Kim, J. H. Olivocochlear innervation of inner and outer hair cells during postnatal maturation: Evidence for a waiting period. *J. Comp. Neurol.* **370**, 551–562 (1996).

185. Rontal, D. A. & Echteler, S. M. Developmental segregation in the efferent projections to auditory hair cells in the gerbil. *J. Comp. Neurol.* **467**, 509–520 (2003).

186. Sobkowicz, H. M. & Emmerling, M. R. Development of acetylcholinesterase-positive neuronal pathways in the cochlea of the mouse. *J. Neurocytol.* **18**, 209–224 (1989).

187. Simmons, D. D., Bertolotto, C., Kim, J., Raji-Kubba, J. & Mansdorf, N. Choline acetyltransferase expression during a putative developmental waiting period. *J. Comp. Neurol.* **397**, 281–295 (1998).

188. Merchán Pérez, A., Gil-Loyzaga, P., Eybalin, M., Fernández Mateos, P. & Bartolomé, M. V. Choline-acetyltransferase-like immunoreactivitity in the organ of Corti of the rat during postnatal development. *Dev. Brain Res.* **82**, 29–34 (1994).

189. Simmons, D. D. & Morley, B. J. Differential expression of the α9 nicotinic acetylcholine receptor subunit in neonatal and adult cochlear hair cells. *Mol. Brain Res.* **56**, 287–292 (1998).

190. Simmons, D. D. & Morley, B. J. Spatial and temporal expression patterns of nicotinic acetylcholine alpha 9 and alpha 10 subunits in the embryonic and early postnatal inner ear. *Neuroscience* **194**, 326–336 (2011).

191. Kanold, P. O. Transient microcircuits formed by subplate neurons and their role in functional development of thalamocortical connections. *Neuroreport* **15**, 2149–2153 (2004).

192. McConnell, S., Ghosh, A. & Shatz, C. Subplate neurons pioneer the first axon pathway from the cerebral cortex. *Science (80-.).* **245**, 978–982 (1989).

193. Ghosh, A., Antonini, A., McConnell, S. K. & Shatz, C. J. Requirement for subplate neurons in the formation of thalamocortical connections. *Nature* **347**, 179–181 (1990).

194. Glowatzki, E. & Fuchs, P. A. Cholinergic synaptic inhibition of inner hair cells in the neonatal mammalian cochlea. *Science (80-.).* **288**, 2366–2368 (2000).

195. Goutman, J. D., Fuchs, P. A. & Glowatzki, E. Facilitating efferent inhibition of inner hair cells in the cochlea of the neonatal rat. *J. Physiol.* **566**, 49–59 (2005).

196. Marcotti, W., Johnson, S. L. & Kros, C. J. A transiently expressed SK current sustains and modulates action potential activity in immature mouse inner hair cells. *J. Physiol.* **560**, 691–708 (2004).

197. Sendin, G., Bourien, J., Rassendren, F., Puel, J.-L. & Nouvian, R. Spatiotemporal pattern of action potential firing in developing inner hair cells of the mouse cochlea. *Proc. Natl. Acad. Sci.* **111**, 1999–2004 (2014).

198. Johnson, S. L. *et al.* Position-dependent patterning of spontaneous action potentials in immature cochlear inner hair cells. *Nat. Neurosci.* **14**, 711–717 (2011).

199. Katz, E. *et al.* Developmental regulation of nicotinic synapses on cochlear inner hair cells. *J. Neurosci.* **24**, 7814–7820 (2004).

200. Roux, I., Wersinger, E., McIntosh, J. M., Fuchs, P. A. & Glowatzki, E. Onset of Cholinergic Efferent Synaptic Function in Sensory Hair Cells of the Rat Cochlea. *J. Neurosci.* **31**, 15092–15101 (2011).

201. Roux, I., Wu, J. S., McIntosh, J. M. & Glowatzki, E. Assessment of the expression and role of the α 1-nAChR subunit in efferent cholinergic function during the development of the mammalian cochlea. *J. Neurophysiol.* **116**, 479–492 (2016).

202. Kearney, G. *et al.* Developmental synaptic changes at the transient olivocochlear-inner hair cell synapse. *J. Neurosci.* **39**, 3360–3375 (2019).

203. Brown, M. C. & Nuttall, A. L. Efferent control of cochlear inner hair cell responses in the guinea-pig. *J. Physiol.* **354**, 625–46 (1984).

204. Vetter, D. E. *et al.* Role of α9 Nicotinic ACh Receptor Subunits in the Development and Function of Cochlear Efferent Innervation. *Neuron* **23**, 93–103 (1999).

205. Vetter, D. E. *et al.* The α10 nicotinic acetylcholine receptor subunit is required for normal synaptic function and integrity of the olivocochlear system. *Proc. Natl. Acad. Sci.* **104**, 20594–20599 (2007).

206. Clause, A., Lauer, A. M. & Kandler, K. Mice Lacking the Alpha9 Subunit of the Nicotinic Acetylcholine Receptor Exhibit Deficits in Frequency Difference Limens and Sound Localization. *Front. Cell. Neurosci.* **11**, 1–12 (2017).

207. Taranda, J. *et al.* A point mutation in the hair cell nicotinic cholinergic receptor prolongs cochlear inhibition and enhances noise protection. *PLoS Biol.* **7**, e1000018 (2009).

208. Di Guilmi, M. N. *et al.* Strengthening of the Efferent Olivocochlear System Leads to Synaptic Dysfunction and Tonotopy Disruption of a Central Auditory Nucleus. *J. Neurosci.* **39**, 7037–7048 (2019).

209. Johnson, S. L. *et al.* Cholinergic efferent synaptic transmission regulates the maturation of auditory hair cell ribbon synapses. *Open Biol.* **3**, 130163–130163 (2013).

210. Gómez-Casati, M. E. *et al.* Electrical Properties and Functional Expression of Ionic Channels in Cochlear Inner Hair Cells of Mice Lacking the α10 Nicotinic Cholinergic Receptor Subunit. *J. Assoc. Res. Otolaryngol.* **10**, 221–232 (2009).

211. Dulon, D., Luo, L., Zhang, C. & Ryan, A. F. Expression of small-conductance calcium-activated potassium channels (SK) in outer hair cells of the rat cochlea. *Eur. J. Neurosci.* **10**, 907–915 (1998).

212. Dulon, D. & Lenoir, M. Cholinergic Responses in Developing Outer Hair Cells of the Rat Cochlea. *Eur. J. Neurosci.* **8**, 1945–1952 (1996).

213. Pujol, R., Carlier, E. & Devigne, C. Significance of presynaptic formations in early stages of cochlear synaptogenesis. *Neurosci. Lett.* **15**, 97–102 (1979).

214. Lenoir, M., Shnerson, A. & Pujol, R. Cochlear receptor development in the rat with emphasis on synaptogenesis. *Anat. Embryol. (Berl).* **160**, 253–262 (1980).

215. Simmons, D. ., Manson-Gieseke, L., Hendrix, T. . & McCarter, S. Reconstructions of efferent fibers in the postnatal hamster cochlea. *Hear. Res.* **49**, 127–139 (1990).

216. Echteler, S. M. Developmental segregation in the afferent projections to mammalian auditory hair cells. *Proc. Natl. Acad. Sci.* **89**, 6324–6327 (1992).

217. He, D. Z. Z., Evans, B. N. & Dallos, P. First appearance and development of electromotility in neonatal gerbil outer hair cells. *Hear. Res.* **78**, 77–90 (1994).

218. Pujol, R. Morphology, Synaptology and Electrophysiology of the Developing Cochlea. *Acta Otolaryngol.* **99**, 5–9 (1985).

219. Pujol, R. & Carlier, E. Cochlear synaptogenesis after sectioning the efferent bundle. *Dev. Brain Res.* **3**, 151–154 (1982).

220. He, D. Z. Z. Relationship between the Development of Outer Hair Cell Electromotility and Efferent Innervation: A Study in Cultured Organ of Corti of Neonatal Gerbils. *J. Neurosci.* **17**, 3634–3643 (1997).

221. He, D. Z. Z., Cheatham, M. A., Pearce, M. & Vetter, D. E. Mouse outer hair cells lacking the α9 ACh receptor are motile. *Dev. Brain Res.* **148**, 19–25 (2004).

222. Liberman, M. C., O'Grady, D. F., Dodds, L. W., Mcgee, J. & Walsh, E. J. Afferent innervation of outer and inner hair cells is normal in neonatally de-efferented cats. *J. Comp. Neurol.* **423**, 132–139 (2000).

223. Liberman, M. C. Auditory-nerve response from cats raised in a low-noise chamber. *J. Acoust. Soc. Am.* **63**, 442–455 (1978).

224. Wu, J. S., Young, E. D. & Glowatzki, E. Maturation of Spontaneous Firing Properties after Hearing Onset in Rat Auditory Nerve Fibers: Spontaneous Rates, Refractoriness, and Interfiber Correlations. *J. Neurosci.* **36**, 10584–10597 (2016).

225. Liberman, M. C. Morphological differences among radial afferent fibers in the cat cochlea: An electron-microscopic study of serial sections. *Hear. Res.* **3**, 45–63 (1980).

226. Liberman, M. C. Efferent synapses in the inner hair cell area of the cat cochlea: An electron microscopic study of serial sections. *Hear. Res.* **3**, 189–204 (1980).

227. Liberman, M. C. Effects of chronic cochlear de-efferentation on auditory-nerve response. *Hear. Res.* **49**, 209–223 (1990).

228. Yin, Y., Liberman, L. D., Maison, S. F. & Liberman, M. C. Olivocochlear Innervation Maintains the Normal Modiolar-Pillar and Habenular-Cuticular Gradients in Cochlear Synaptic Morphology. *J. Assoc. Res. Otolaryngol.* **15**, 571–583 (2014).

229. Hickman, T. T., Liberman, M. C. & Jacob, M. H. Adenomatous Polyposis Coli Protein Deletion in Efferent Olivocochlear Neurons Perturbs Afferent Synaptic Maturation and Reduces the Dynamic Range of Hearing. *J. Neurosci.* **35**, 9236–9245 (2015).

230. Liberman, L. D., Wang, H. & Liberman, M. C. Opposing Gradients of Ribbon Size and AMPA Receptor Expression Underlie Sensitivity Differences among Cochlear-Nerve/Hair-Cell Synapses. *J. Neurosci.* **31**, 801–808 (2011).

231. Kumar, U. A. & Vanaja, C. S. Functioning of Olivocochlear Bundle and Speech Perception in Noise. *Ear Hear.* **25**, 142–146 (2004).

232. Lauer, A. M. & May, B. J. The Medial Olivocochlear System Attenuates the Developmental Impact of Early Noise Exposure. *J. Assoc. Res. Otolaryngol.* **12**, 329–343 (2011).

233. May, B. J., Lauer, A. M. & Roos, M. J. Impairments of the Medial Olivocochlear System Increase the Risk of Noise-Induced Auditory Neuropathy in Laboratory Mice. *Otol. Neurotol.* **32**, 1568–1578 (2011).

234. Kulesza, R. J. & Mangunay, K. Morphological features of the medial superior olive in autism. *Brain Res.* **1200**, 132–137 (2008).

235. Kulesza, R. J., Lukose, R. & Stevens, L. V. Malformation of the human superior olive in autistic spectrum disorders. *Brain Res.* **1367**, 360–371 (2011).

236. Khalfa, S. *et al.* Peripheral auditory asymmetry in infantile autism. *Eur. J. Neurosci.* **13**, 628–632 (2001).

237. Collet, L. *et al.* Objective auditory dysfunction in infantile autism. *Lancet* **342**, 923–924 (1993).

238. Veuillet, E. *et al.* Abnormal peripheral auditory asymmetry in schizophrenia. *J. Neurol. Neurosurg. Psychiatry* **70**, 88–94 (2001).

239. Abdul Wahab, N. A., Wahab, S., Abdul Rahman, A. H., Sidek, D. & Zakaria, M. N. The Hyperactivity of Efferent Auditory System in Patients with Schizophrenia: A Transient Evoked Otoacoustic Emissions Study. *Psychiatry Investig.* **13**, 82 (2016).

240. Bennetto, L., Keith, J. M., Allen, P. D. & Luebke, A. E. Children with autism spectrum disorder have reduced otoacoustic emissions at the 1 kHz mid-frequency region. *Autism Res.* **10**, 337–345 (2017).

241. Kaf, W. A. & Danesh, A. A. Distortion-product otoacoustic emissions and contralateral suppression findings in children with Asperger's Syndrome. *Int. J. Pediatr. Otorhinolaryngol.* **77**, 947–954 (2013).

242. Knudson, I. M., Shera, C. A. & Melcher, J. R. Increased contralateral suppression of otoacoustic emissions indicates a hyperresponsive medial olivocochlear system in humans with tinnitus and hyperacusis. *J. Neurophysiol.* **112**, 3197–3208 (2014).

243. Fu, B. *et al.* Age-related synaptic loss of the medial olivocochlear efferent innervation. *Mol. Neurodegener.* **5**, 53 (2010).

244. Lauer, A. M., Fuchs, P. A., Ryugo, D. K. & Francis, H. W. Efferent synapses return to inner hair cells in the aging cochlea. *Neurobiol. Aging* **33**, 2892–2902 (2012).

245. Zachary, S. P. & Fuchs, P. A. Re-Emergent Inhibition of Cochlear Inner Hair Cells in a Mouse Model of Hearing Loss. *J. Neurosci.* **35**, 9701–9706 (2015).

246. Liberman, M. C., Liberman, L. D. & Maison, S. F. Efferent Feedback Slows Cochlear Aging. *J. Neurosci.* **34**, 4599–4607 (2014).

247. Bakken, T. E. *et al.* Single-nucleus and single-cell transcriptomes compared in matched cortical cell types. *PLoS One* **13**, e0209648 (2018).

248. Mo, A. *et al.* Epigenomic Signatures of Neuronal Diversity in the Mammalian Brain. *Neuron* **86**, 1369–1384 (2015).

249. Tenney, A. P. *et al.* Etv1 Controls the Establishment of Non-overlapping Motor Innervation of Neighboring Facial Muscles during Development. *Cell Rep.* **29**, 437-452.e4 (2019).

250. Astick, M., Tubby, K., Mubarak, W. M., Guthrie, S. & Price, S. R. Central Topography of Cranial Motor Nuclei Controlled by Differential Cadherin Expression. *Curr. Biol.* **24**, 2541–2547 (2014).

251. Hanley, O. *et al.* Parallel Pbx -Dependent Pathways Govern the Coalescence and Fate of Motor Columns. *Neuron* **91**, 1005–1020 (2016).

252. Cooper, K. L., Leisenring, W. M. & Moens, C. B. Autonomous and nonautonomous functions for Hox/Pbx in branchiomotor neuron development. *Dev. Biol.* **253**, 200–213 (2003).

253. Dasen, J. S., Tice, B. C., Brenner-Morton, S. & Jessell, T. M. A Hox regulatory network establishes motor neuron pool identity and target-muscle connectivity. *Cell* **123**, 477–491 (2005).

254. Parrish, M. *et al.* Loss of the Sall3 Gene Leads to Palate Deficiency, Abnormalities in Cranial Nerves, and Perinatal Lethality. *Mol. Cell. Biol.* **24**, 7102–7112 (2004).

255. Horvath, M. *et al.* Intracochlear injection of pseudorabies virus labels descending auditory and monoaminerg projections to olivocochlear cells in guinea pig. *Eur. J. Neurosci.* **18**, 1439–1447 (2003).

256. Wang, X. & Robertson, D. Effects of bioamines and peptides on neurones in the ventral nucleus of trapezoid body and rostral periolivary regions of the rat superior olivary complex: An in vitro investigation. *Hear. Res.* **106**, 20–28 (1997).

257. Lein, E. S. *et al.* Genome-wide atlas of gene expression in the adult mouse brain. *Nature* **445**, 168–176 (2007).

258. McLean, W. J., Smith, K. A., Glowatzki, E. & Pyott, S. J. Distribution of the Na,K-ATPase α subunit in the rat spiral ganglion and organ of corti. *JARO - J. Assoc. Res. Otolaryngol.* **10**, 37–49 (2009).

259. Vetter, D. E. *et al.* Urocortin-deficient mice show hearing impairment and increased anxiety-like behavior. *Nat. Genet.* **31**, 363–369 (2002).

260. Brown, M. C., Mukerji, S., Drottar, M., Windsor, A. M. & Lee, D. J. Identification of Inputs to Olivocochlear Neurons Using Transneuronal Labeling with Pseudorabies Virus (PRV). *J. Assoc. Res. Otolaryngol.* **14**, 703–717 (2013).

261. Cadenas, L. T., Fischl, M. J. & Weisz, C. J. C. Synaptic inhibition of medial olivocochlear efferent neurons by neurons of the medial nucleus of the trapezoid body. *J. Neurosci.* **40**, 509–525 (2020).

262. Nagahara, T. *et al.* Design and Synthesis of Non-Peptide, Selective Orexin Receptor 2 Agonists. *J. Med. Chem.* **58**, 7931–7937 (2015).

263. Chowdhury, S. *et al.* Dissociating orexin-dependent and - independent functions of orexin neurons using novel orexin-flp knock-in mice. *Elife* **8**, 1–25 (2019).

264. Brown, E. N., Purdon, P. L. & Van Dort, C. J. General anesthesia and altered states of arousal: a systems neuroscience analysis. *Annu. Rev. Neurosci.* **34**, 601–628 (2011).

265. Cadwell, C. R. *et al.* Electrophysiological, transcriptomic and morphologic profiling of single neurons using Patch-seq. *Nat. Biotechnol.* **34**, 199–203 (2016).

266. Frank, M. M. & Goodrich, L. V. Talking back: Development of the olivocochlear efferent system. *Wiley Interdiscip. Rev. Dev. Biol.* **7**, 1–20 (2018).

267. Korada, S. & Schwartz, I. R. Development of GABA, glycine, and their receptors in the auditory brainstem of gerbil: A light and electron microscopic study. *J. Comp. Neurol.* **409**, 664–681 (1999).

268. Kotak, V. C., Korada, S., Schwartz, I. R. & Sanes, D. H. A developmental shift from

GABAergic to glycinergic transmission in the central auditory system. *J. Neurosci.* **18**, 4646–55 (1998).

269. Kandler, K. & Friauf, E. Development of glycinergic and glutamatergic synaptic transmission in the auditory brainstem of perinatal rats. *J. Neurosci.* **15**, 6890–6904 (1995).

270. Ehrlich, I., Löhrke, S. & Friauf, E. Shift from depolarizing to hyperpolarizing glycine action in rat auditory neurones is due to age-dependent Cl- regulation. *J. Physiol.* **520**, 121–137 (1999).

271. Kakazu, Y., Akaike, N., Komiyama, S. & Nabekura, J. Regulation of intracellular chloride by cotransporters in developing lateral superior olive neurons. *J. Neurosci.* **19**, 2843–2851 (1999).

272. Jenkins, S. A. & Simmons, D. D. GABAergic neurons in the lateral superior olive of the hamster are distinguished by differential expression of gad isoforms during development. *Brain Res.* **1111**, 12–25 (2006).

273. Finck, A., Schneck, C. D. & Hartman, A. F. Development of cochlear function in the neonate Mongolian gerbil (Meriones unguiculatus). *J. Comp. Physiol. Psychol.* **78**, 375–380 (1972).

274. Woolf, N. K. & Ryan, A. F. The development of auditory function in the cochlea of the mongolian gerbil. *Hear. Res.* **13**, 277–283 (1984).

275. Stuart, T. *et al.* Comprehensive Integration of Single-Cell Data. *Cell* **177**, 1888-1902.e21 (2019).

276. Hafemeister, C. & Satija, R. Normalization and variance stabilization of single-cell RNA-seq data using regularized negative binomial regression. *Genome Biol.* **20**, 1–15 (2019).

277. Waltman, L. & van Eck, N. J. A smart local moving algorithm for large-scale modularity-based community detection. *Eur. Phys. J. B* **86**, 471 (2013).

278. Paul, A. *et al.* Transcriptional Architecture of Synaptic Communication Delineates GABAergic Neuron Identity. *Cell* **171**, 522-539.e20 (2017).

279. Shrestha, B. R. *et al.* Sensory Neuron Diversity in the Inner Ear Is Shaped by Activity. *Cell* **174**, 1229-1246.e17 (2018).

280. Choi, H. M. T. *et al.* Third-generation in situ hybridization chain reaction: Multiplexed, quantitative, sensitive, versatile, robust. *Dev.* **145**, (2018).

281. Madisen, L. *et al.* A robust and high-throughput Cre reporting and characterization system for the whole mouse brain. *Nat. Neurosci.* **13**, 133–140 (2010).

282. Daigle, T. L. *et al.* A Suite of Transgenic Driver and Reporter Mouse Lines with Enhanced Brain-Cell-Type Targeting and Functionality. *Cell* **174**, 465-480.e22 (2018).

283. Rossi, J. *et al.* Melanocortin-4 Receptors Expressed by Cholinergic Neurons Regulate Energy Balance and Glucose Homeostasis. *Cell Metab.* **13**, 195–204 (2011).

284. Rasmussen, G. L. American association of anatomists. *Anat. Rec.* **82**, 441 (1942).

285. Morin, S. M., Ling, N., Liu, X. J., Kahl, S. D. & Gehlert, D. R. Differential distribution of urocortin- and corticotropin-releasing factor-like immunoreactivities in the rat brain. *Neuroscience* **92**, 281–291 (1999).

286. Skelton, K. H., Owens, M. J. & Nemeroff, C. B. The neurobiology of urocortin. *Regul. Pept.* **93**, 85–92 (2000).

287. Zhao, W. & Dhar, S. The Effect of Contralateral Acoustic Stimulation on Spontaneous Otoacoustic Emissions. *J. Assoc. Res. Otolaryngol.* **11**, 53–67 (2010).

288. Madisen, L. *et al.* Transgenic mice for intersectional targeting of neural sensors and effectors with high specificity and performance. *Neuron* **85**, 942–958 (2015).

289. Plummer, N. W. *et al.* Expanding the power of recombinase-based labeling to uncover cellular diversity. *Development* **142**, 4385–4393 (2015).

290. Quadros, R. M. *et al.* Easi-CRISPR: A robust method for one-step generation of mice carrying conditional and insertion alleles using long ssDNA donors and CRISPR ribonucleoproteins. *Genome Biol.* **18**, 1–15 (2017).

291. Miura, H., Quadros, R. M., Gurumurthy, C. B. & Ohtsuka, M. Easi-CRISPR for creating knock-in and conditional knockout mouse models using long ssDNA donors. *Nat. Protoc.* **13**, 195–215 (2018).

292. Raymond, C. S. & Soriano, P. High-Efficiency FLP and ΦC31 Site-Specific Recombination in Mammalian Cells. *PLoS One* **2**, e162 (2007).

293. Gu, H., Zou, Y.-R. & Rajewsky, K. Independent control of immunoglobulin switch recombination at individual switch regions evidenced through Cre-loxP-mediated gene targeting. *Cell* **73**, 1155–1164 (1993).

294. Ran, F. A. *et al.* Genome engineering using the CRISPR-Cas9 system. *Nat. Protoc.* **8**, 2281–2308 (2013).

295. Irving, S., Moore, D. R., Liberman, M. C. & Sumner, C. J. Olivocochlear Efferent Control in Sound Localization and Experience-Dependent Learning. *J. Neurosci.* **31**, 2493–2501 (2011).

296. Delano, P. H., Elgueda, D., Hamame, C. M. & Robles, L. Selective attention to visual stimuli reduces cochlear sensitivity in chinchillas. *J. Neurosci.* **27**, 4146–53 (2007).

297. Terreros, G., Jorratt, P., Aedo, C., Elgoyhen, A. B. & Delano, P. H. Selective Attention to Visual Stimuli Using Auditory Distractors Is Altered in Alpha-9 Nicotinic Receptor Subunit Knock-Out Mice. *J. Neurosci.* **36**, 7198–7209 (2016).

298. Wimmer, R. D. *et al.* Thalamic control of sensory selection in divided attention. *Nature* (2015). doi:10.1038/nature15398

299. Beim, J. A., Oxenham, A. J. & Wojtczak, M. Examining replicability of an otoacoustic measure of cochlear function during selective attention. *J. Acoust. Soc. Am.* **144**, 2882–2895 (2018).

300. Liberman, L. D. & Liberman, M. C. Cochlear Efferent Innervation Is Sparse in Humans and

Decreases with Age. *J. Neurosci.* **39**, 9560–9569 (2019).

301. Saper, C. B., Chou, T. C. & Scammell, T. E. The sleep switch: Hypothalamic control of sleep and wakefulness. *Trends Neurosci.* **24**, 726–731 (2001).

302. Alexandre, C., Andermann, M. L. & Scammell, T. E. Control of arousal by the orexin neurons. *Curr. Opin. Neurobiol.* **23**, 752–759 (2013).

303. Highstein, S. M. & Baker, R. Action of the efferent vestibular system on primary afferents in the toadfish, Opsanus tau. *J. Neurophysiol.* **54**, 370–384 (1985).

304. Mathews, M. A., Camp, A. J. & Murray, A. J. Reviewing the role of the efferent vestibular system in motor and vestibular circuits. *Front. Physiol.* **8**, 1–15 (2017).

305. Peyron, C. *et al.* Neurons containing hypocretin (orexin) project to multiple neuronal systems. *J. Neurosci.* **18**, 9996–10015 (1998).

306. Nambu, T. *et al.* Distribution of orexin neurons in the adult rat brain. *Brain Res.* **827**, 243–260 (1999).

307. Scammell, T. E. & Winrow, C. J. Orexin Receptors: Pharmacology and Therapeutic Opportunities. *Annu. Rev. Pharmacol. Toxicol.* **51**, 243–266 (2011).

308. Sun, S. *et al.* Hair Cell Mechanotransduction Regulates Spontaneous Activity and Spiral Ganglion Subtype Specification in the Auditory System. *Cell* **174**, 1247-1263.e15 (2018).

309. Petitpré, C. *et al.* Neuronal heterogeneity and stereotyped connectivity in the auditory afferent system. *Nat. Commun.* **9**, (2018).

310. Wang, Y., Hirose, K. & Liberman, M. C. Dynamics of Noise-Induced Cellular Injury and Repair in the Mouse Cochlea. *J. Assoc. Res. Otolaryngol.* **3**, 248–268 (2002).

311. Kujawa, S. G. & Liberman, M. C. Translating animal models to human therapeutics in noise-induced and age-related hearing loss. *Hear. Res.* **377**, 44–52 (2019).

312. Kirk, E. C. & Smith, D. W. Protection from Acoustic Trauma Is Not a Primary Function of the Medial Olivocochlear Efferent System. *J. Assoc. Res. Otolaryngol.* **4**, 445–465 (2003).

313. Graham, C. E., Basappa, J., Turcan, S. & Vetter, D. E. The Cochlear CRF Signaling Systems and their Mechanisms of Action in Modulating Cochlear Sensitivity and Protection Against Trauma. *Mol. Neurobiol.* 1–24 (2011). doi:10.1007/s12035-011-8203-3

314. Maison, S. F., Luebke, A. E., Liberman, M. C. & Zuo, J. Efferent protection from acoustic injury is mediated via alpha9 nicotinic acetylcholine receptors on outer hair cells. *J. Neurosci.* **22**, 10838–46 (2002).

315. Wang, Y. & Liberman, M. C. Restraint stress and protection from acoustic injury in mice. *Hear. Res.* **165**, 96–102 (2002).

316. Harley, R. J. *et al.* Neuronal cell adhesion molecule (NrCAM) is expressed by sensory cells in the cochlea and is necessary for proper cochlear innervation and sensory domain patterning during development. *Dev. Dyn.* **247**, 934–950 (2018).

317. Ranum, P. T. *et al.* Insights into the Biology of Hearing and Deafness Revealed by Single-Cell RNA Sequencing. *Cell Rep.* **26**, 3160-3171.e3 (2019).

318. Khoshnoodi, J., Pedchenko, V. & Hudson, B. G. Mammalian collagen IV. *Microsc. Res. Tech.* **71**, 357–370 (2008).

319. Heino, J. The collagen family members as cell adhesion proteins. *BioEssays* **29**, 1001–1010 (2007).

320. Kruegel, J., Rubel, D. & Gross, O. Alport syndrome - Insights from basic and clinical research. *Nat. Rev. Nephrol.* **9**, 170–178 (2013).

321. Hudson, B. G., Tryggvason, K., Sundaramoorthy, M. & Neilson, E. G. Alport's syndrome, Goodpasture's syndrome, and type IV collagen. *N. Engl. J. Med.* **348**, 2543–2556 (2003).

322. Zehnder, A. F. *et al.* Distribution of type IV collagen in the cochlea in Alport syndrome. *Arch. Otolaryngol. - Head Neck Surg.* **131**, 1007–1013 (2005).

323. Johnsson, L. G. & Arenberg, I. K. Cochlear Abnormalities in Alport's Syndrome. *Arch. Otolaryngol.* **107**, 340–349 (1981).

324. Ungar, O. J., Nadol, J. B. & Santos, F. Temporal Bone Histopathology of X-linked Inherited Alport Syndrome. *Laryngoscope Investig. Otolaryngol.* **3**, 311–314 (2018).

325. Kandler, K. & Gillespie, D. C. Developmental refinement of inhibitory sound-localization circuits. *Trends Neurosci.* **28**, 290–296 (2005).

326. Kujawa, S. G. & Liberman, M. C. Adding Insult to Injurt: Cochlear Nerve Degeneration after 'Temporary' Noise- Induced Hearing Loss. *J. Neurosci.* **29**, 14077- (2009).

327. Kujawa, S. G. & Liberman, M. C. Synaptopathy in the noise-exposed and aging cochlea: Primary neural degeneration in acquired sensorineural hearing loss. *Hear. Res.* **330**, 191–199 (2015).

328. Wu, P. Z. *et al.* Primary Neural Degeneration in the Human Cochlea: Evidence for Hidden Hearing Loss in the Aging Ear. *Neuroscience* **407**, 8–20 (2019).

329. Suzuki, J., Corfas, G. & Liberman, M. C. Round-window delivery of neurotrophin 3 regenerates cochlear synapses after acoustic overexposure. *Sci. Rep.* **6**, 1–11 (2016).

330. Hashimoto, K. *et al.* Protection from noise-induced cochlear synaptopathy by virally mediated overexpression of NT3. *Sci. Rep.* **9**, 1–12 (2019).